An Overview of the Large-Magnitude (VEI 4) Eruption of Merapi in 2010

12

Subandriyo, Ralf Gertisser, Nurnaning Aisyah, Hanik Humaida, Katie Preece, Sylvain Charbonnier, Agus Budi-Santoso, Heather Handley, Sri Sumarti, Dewi Sri Sayudi, I Gusti Made Agung Nandaka, and Haryo Edi Wibowo

Abstract

The VEI 4 eruption in 2010 was the worst volcanic disaster at Merapi in 80 years.The unusual size and dynamics of the eruption, the rapid acceleration of events and the large number of evacuees posed significant challenges for the management of the volcanic crisis and post-eruption recovery. The first indications of Merapi's reawakening were observed in the seismic monitoring record about one year before the eruption. The eruption commenced on 26 October 2010, with initial explosions and associated pyroclastic density currents (PDCs) directed towards the south flank of Merapi. Subsequently, the intensity of the eruption accelerated with rapid lava dome growth and increasing PDC runout, culminating in a climactic eruption phase on 5 November, where blast-like, high-energy PDCs destroyed areas on Merapi's south flank and PDCs reached ~16 km in the Gendol valley. After 5 November, the eruption waned, leading to reductions of the exclusion zone from mid-November 2010 and successive lowering of the alert level from early December 2010. The 2010 eruption was fed by basaltic andesite magma similar to other recent Merapi eruptions, but was driven by a larger than normal influx of deep, volatile-rich magma that replenished the shallower magma system within the carbonate-dominated upper crust beneath Merapi at relatively short timescales. During and after the eruption, lahars swept down almost all major valleys, causing considerably larger impact than after previous eruptions. As a result of the eruption, nearly 400,000 people were displaced from their

Subandriyo (✉) · N. Aisyah · H. Humaida · A. Budi-Santoso · S. Sumarti · D. S. Sayudi · I G. M. A. Nandaka
Balai Penyelidikan Dan Pengembangan Teknologi Kebencanaan Geologi (BPPTKG), Jl. Cendana 15, Yogyakarta 55166, Indonesia
e-mail: jsubandriyo@gmail.com

R. Gertisser (✉)
School of Geography, Geology and the Environment, Keele University, Keele ST5 5BG, UK
e-mail: r.gertisser@keele.ac.uk

K. Preece
Department of Geography, Swansea University, Swansea SA2 8PP, UK

S. Charbonnier
School of Geosciences, University of South Florida, Tampa, FL 33620-5201, USA

H. Handley
Department of Applied Earth Sciences, University of Twente, 7514 AE Enschede, The Netherlands

School of Earth, Atmosphere and Environment, Monash University, Clayton, VIC 3800, Australia

H. E. Wibowo
Department of Geological Engineering, Faculty of Engineering, Universitas Gadjah Mada, Yogyakarta 55281, Indonesia

Center for Disaster Studies, Universitas Gadjah Mada, Yogyakarta 55281, Indonesia

R. Gertisser et al. (eds.), *Merapi Volcano*, Active Volcanoes of the World,
https://doi.org/10.1007/978-3-031-15040-1_12

homes and accommodated in temporary or permanent residences. Tourist activities and sand quarrying of PDC and lahar deposits facilitated post-eruption recovery. Mitigation measures, including strengthening of the volcano monitoring system, establishment of a disaster risk reduction forum, strengthening of community capacity, and preparation of contingency plans for local governments based on hazard scenarios, were all part of the disaster risk reduction strategy that saved many lives during the 2010 eruption crisis.

Keywords

2010 eruption · Eruption chronology · Pyroclastic density currents · Geochemistry · Petrology · Eruption impact · Recovery · Disaster management · Risk reduction strategy

12.1 Introduction

With a Volcano Explosivity Index (VEI) of 4, the catastrophic eruption in 2010 was the largest eruption of Merapi since 1872 and the deadliest since 1930 (Siebert et al. 2011; Surono et al. 2012; Jousset et al. 2013a), causing 398 casualties. The eruption had a significant impact on the natural environment, built infrastructures and the population in the vicinity of Merapi (Fig. 12.1), and posed major challenges during crisis management and post-disaster recovery. Compared with Merapi's activity in the past few decades (e.g. Voight et al. 2000), the 2010 eruption was unusual in many respects. Following a rapid increase in seismicity and ground deformation, the eruption began on 26 October with partially laterally directed explosions at the summit. These were not preceded by lava dome extrusion, which frequently characterised previous Merapi eruptions. A few days later, a dome extruded within the newly formed summit crater over a period of less than a week, growing at unprecedented rates of 25 m^3 s^{-1} (Surono et al. 2012; Pallister et al. 2013). During the climactic eruption phase on 5 November, this dome was rapidly destroyed in a series of explosions generating blast-like, high-energy pyroclastic density currents (PDCs) and contemporaneous valley-confined PDCs, of which at least one travelled ~16 km beyond the summit along the Gendol valley, more than twice the distance of the largest flows in 2006 and other recent eruptions (Voight et al. 2000; Charbonnier and Gertisser 2008; Charbonnier et al. 2013; Komorowski et al. 2013). Both phenomena, as well as associated valley-derived, unconfined (overbank) flows and accompanying ash-cloud surges, caused widespread devastation on Merapi's south flank and the large number of casualties (Surono et al. 2012; Charbonnier et al. 2013; Cronin et al. 2013; Jenkins et al. 2013; Komorowski et al. 2013; Lerner et al. 2021). In a later phase on 5 November, collapse of a sub-plinian convective eruption column produced PDCs rich in pumice and scoria. This was followed by renewed lava dome extrusion, at a rate of 35 m^3 s^{-1} (Pallister et al. 2013), exceeding the already unusually high rates of the previous (pre-climax) dome extrusion phase. The eruption intensity declined on 8 November (Surono et al. 2012; Komorowski et al. 2013; Pallister et al. 2013).

This chapter provides an overview of the 2010 eruption compiled by an international team of experts who worked on various aspects of the eruption and its crisis management. After a summary of the chronology of the 2010 eruption crisis (Sect. 12.2), the chapter reviews the volcano monitoring record (Sect. 12.3) and the volcanic deposits of the eruption (Sect. 12.4). The petrology and geochemistry of the eruptive products are described in Sect. 12.5 and used to shed light on the pre-eruptive magma plumbing system and the magmatic processes leading up to the eruption. This is followed by a description of the eruption's impact on the environment, infrastructures and population as well as the recovery after the disaster (Sect. 12.6). The management and disaster risk reduction strategy of the 2010 volcanic crisis is covered in Sect. 12.7, followed by a conclusion section (Sect. 12.8).

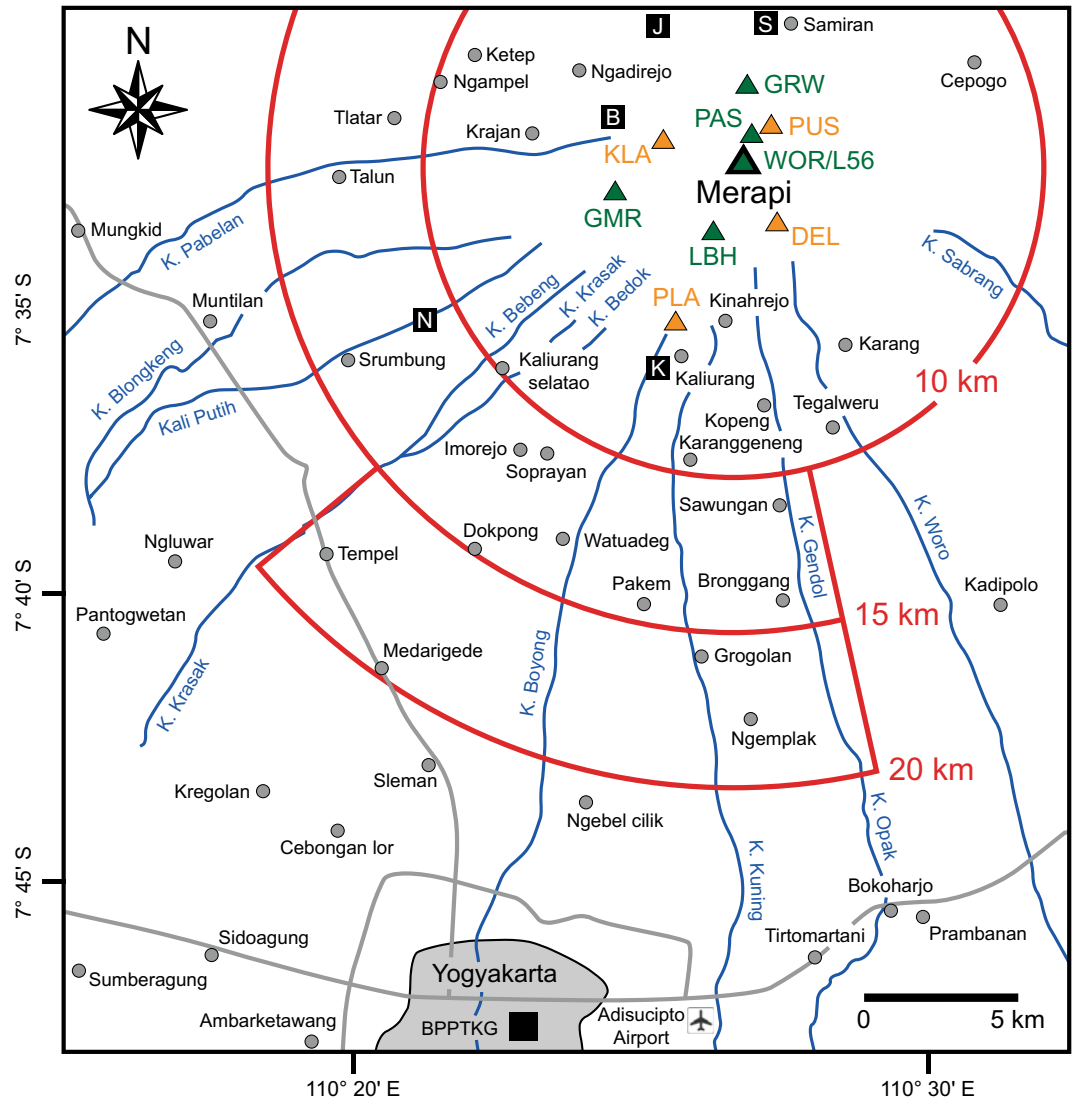

Fig. 12.1 Map of Merapi volcano and its surroundings, showing some of the larger towns and villages (grey circles), the city of Yogyakarta (grey area) and Adisucipto Interntional Airport, the BPPTKG head office in Yogyakarta (black square), volcano observation posts (labelled black squares: K = Kaliurang; N = Ngepos; B = Babadan; J = Jrakah; S = Selo), main river valleys (blue), and major roads (light grey). Permanent short-period seismic stations are shown by orange triangles (PUS; DEL; PLA; KLA) and temporary broadband seismic stations are indicated by green triangles (LBH; GMR; GRW; PAS; WOR/L56). The red arcs at distances of 10, 15 and 20 km from the summit of Merapi show evacuation zones in effect at different times during the 2010 eruption crisis. See text for details. After Surono et al. (2012) and Jousset et al. (2013a)

12.2 Eruption Chronology

For the purpose of this chapter, the chronology and main phenomena of the 2010 eruption are grouped into four phases: (1) Reawakening of Merapi and volcanic unrest, (2) Beginning of the eruption and pre-climactic activity, (3) Climactic eruption phase, and (4) Post-climactic activity and end of the eruption (Fig. 12.2). These are closely aligned with the eruption phases proposed by Surono et al. (2012) and the eruption stages put forward by Komorowski et al. (2013) (Fig. 12.2). The latter provides a detailed framework for linking the volcanic deposits to eruption chronology (see Sect. 12.4).

12.2.1 Reawakening of Merapi and Volcanic Unrest

After the 2006 eruption, Merapi stayed in a resting phase for 42 months until signs of renewed activity began in October 2009 (Fig. 12.2). As in previous eruptions, the first substantial indication of Merapi's reawakening and continuing unrest was increased seismic activity, with various seismic signals, as previously identified at Merapi, associated with different processes and events, including (1) volcano-tectonic (VT—VTA = deeper VT earthquakes, 2.5–5 km below the summit; VTB = shallower VT earthquakes, <1.5 km below the summit), (2) multiphase (MP), (3) low-frequency (LF) or long period (LP), (4) very-long period (VLP), (5) tremor, (6) rockfall (RF), and (7) pyroclastic flow (PF) types (e.g. Ratdomopurbo 1995; Ratdomopurbo and Poupinet 2000; Jousset et al. 2013b). The rise in activity leading up to the 2010 eruption was signalled by the appearance of a swarm of shallow VT earthquakes (<1 km depth) on 31 October 2009. The largest VT events had a magnitude of 3.0 on the Richter Scale and were felt by the inhabitants around Merapi; further VT earthquakes were detected on 31 October 2009, 9 December 2009, 1 February 2010, and 10 June 2010 (Fig. 12.2). In September 2010, the seismic activity increased significantly, marking the start of the 2010 eruption crisis phase (Fig. 12.2). The increase in VT earthquakes was accompanied by shortening of the slope distances (i.e. the distance between a base station on the lower slopes of the volcano and a reflector at the summit, as determined by electronic distance measurements (EDM)), particularly on the southern baselines from Kaliurang (see Aisyah et al. 2018). Felt VT earthquakes with a magnitude 2.5 and 2.2 on the Richter scale occurred on 12 and 13 September 2010, respectively. The first of the two earthquakes was followed by a large rockfall that was heard from several volcano observation posts. The daily number of MP and VT earthquakes increased sharply on 19 September 2010, and shortening of the southern baselines reached up to 0.5 m from 3 April 2009 to 19 September 2010, and 3 cm on 20 September alone. Considering the increase in seismicity and the gradual shortening of the slope distance, the alert level was upgraded on 21 September 2010 from level I (NORMAL) to level II (WASPADA; Engl.: Advisory) on the four-level alert system (Fig. 12.2).

From mid-October 2010, all monitoring data revealed a significant increase in volcanic activity. The daily numbers of VT and MP earthquakes increased to 56 and 579, respectively on 17 October, while the cumulative energy of both types of earthquakes reached 27.9×10^9 J on 20 October. On that day, rockfall activity increased to 87 events per day. This number was still relatively low compared to earlier eruptions between the 1990s and 2006, which involved rockfalls from the destruction of older domes. By 21 October, the southern baselines had contracted by up to 1.643 m since 3 April 2009. The concentration of CO_2 gas in the summit fumaroles also increased significantly, reflecting accumulation of high magmatic pressure in the upper conduit, and raising the possibility that the expected eruption could be explosive and not preceded by lava dome extrusion. The further increase in volcanic unrest prompted the Center of Volcanology and Geological Hazard Mitigation (CVGHM) to raise the alert level to level III (SIAGA; Engl.: Watch) on 21 October 2010 (Fig. 12.2).

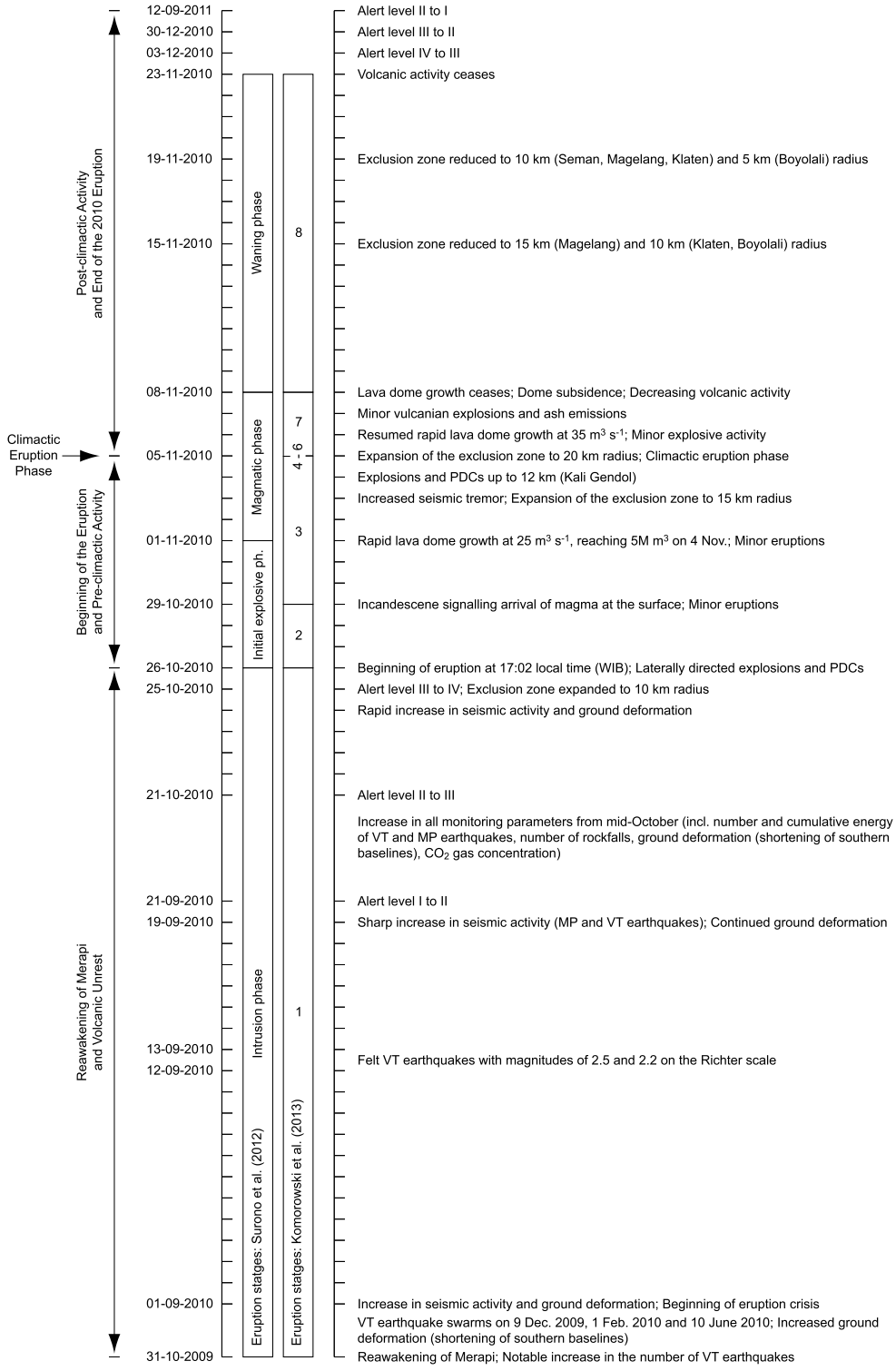

Fig. 12.2 Chronology and main phenomena of the 2010 eruption from the first signs of reawakening in October 2009 to September 2011, when the alert level was lowered to level I (NORMAL). Also shown are the eruption phases and stages proposed by Surono et al. (2012) and Komorowski et al. (2013)

On 24 October, the number of VT and MP earthquakes significantly increased to 80 and 588, respectively, and the cumulative energy of VT and MP earthquakes reached 62.5 × 10^9 J. Rockfalls occurred frequently, with 194 events recorded, suggesting that the old 2006 lava dome became unstable. The concentration of CO_2 gas in the summit fumaroles also continued to increase. The following day, on 25 October, the numbers of VT, MP and rock-fall events continued to increase to 222, 624 and 454, respectively, and the cumulative seismic energy of VT and MP earthquakes reached 75.8 × 10^9 J. The southern baselines shortened by up to 0.551 m in only one day since 24 October, suggesting that at this point, the activity of Merapi was at a critical phase where an eruption could occur any time. Therefore, at 06:00 local time (WIB) on 25 October, CVGHM decided to raise the alert to the highest level IV (AWAS; Engl.: Warning). A restricted zone with a radius of 10 km from the summit was recommended, and 70,000 residents had to be evacuated from the restricted zone (Figs. 12.1, and 12.2).

High seismicity and rapid shortening of the southern baselines continued on 26 October. The number of VT, MP and rockfall events were 232, 397 and 269, respectively, and the total energy reached 94.8 × 10^9 J until the onset of the eruption. The shortening of the southern baselines was rapid at up to 0.744 m in only 4 h.

12.2.2 Beginning of the Eruption and Pre-Climactic Activity

The eruption began at 17:02 (local time (WIB) = UTC + 7 h) on 26 October (Fig. 12.1). The initial explosive phase, which was categorised as a magmatic eruption, lasted for about two hours (Table 12.1). It destroyed the 2006 lava dome and the southern rim of the summit, forming a large crater open to the south (Fig. 12.3a, b). Pyroclastic density currents from laterally directed explosions reached up to 6.8 km in Kali Gendol and Kali Kuning and caused as many as 35 casualties in the restricted zone in Kinahrejo, including Mbah Marijan, a local traditional figure.

The number of VT and MP events decreased after the initial explosions, and the quiescence continued until 28 October. As all the EDM reflectors were broken as a result of the 26 October events, ground deformation data could no longer be obtained along the established baselines. Further smaller eruptions occurred on 29 October, 31 October and 1 November. Incandescence, signalling arrival of magma at the surface, was initially observed on 29 October (Komorowski et al. 2013). Growth of a new lava dome within the 26 October summit crater was first detected by Interferometry Satellite Aperture

Table 12.1 Eruptive activity and phenomena observed at the beginning of the 2010 eruption on 26 October

Time (WIB)	Eruptive activity and phenomena	Duration
17:02	Pyroclastic flow (PDC[a])	9 min
17:18	Pyroclastic flow (PDC)	4 min
17:23	Pyroclastic flow (PDC)	5 min
17:30	Pyroclastic flow (PDC)	2 min
17:37	Pyroclastic flow (PDC)	2 min
17:42	Large pyroclastic flow (PDC)	33 min
18:00–18:45	Loud noise heard at the Jrakah and Selo volcano observation posts	45 min
18:10, 18:15, 18:25	Thumping sounds occurred 3 times	< 1 min
18:16	Pyroclastic flow (PDC)	5 min
18:21	Large pyroclastic flow (PDC); 'flames' and an ash column up to 1.5 km above Merapi observed from the Selo volcano observation post	33 min
18:54	Activity begins to decline	–

[a] PDC—Pyroclastic density current

Radar (InSAR) on 1 November (Pallister et al. 2013; Kubanek et al. 2015; Kelfoun et al. 2017). Partial collapse of the growing dome led to several PDCs over the next few days.

At 11:00 local time (WIB) on 3 November, the amplitude of seismic tremors suddenly increased, marking the beginning of a short sub-Plinian eruption phase. With PDCs reaching more than 10 km runout distance, the restricted zone was enlarged to 15 km radius from the summit at 16:05 (WIB) on that day (Figs. 12.1, and 12.2). At 18:46 (WIB), further large PDCs occurred in the Gendol valley, reaching 9 km from the summit. At that time, the KLA (Klatakan) seismic station, located 2 km west of Merapi's summit (Fig. 12.1), was damaged by PDCs or falling rocks and stopped transmitting a signal. With PDCs reaching distances of up to 12 km in Kali Gendol on 4 November, CVGHM expanded the radius of the danger zone to 20 km that evening (Figs. 12.1 and 12.2). At that time, the volume of the lava dome had increased to ~5 million m^3 (Fig. 12.3c), suggesting a time-averaged growth rate of ~25 $m^3\ s^{-1}$ (2.160×10^6 m^3/day) since 1 November (Surono et al. 2012; Pallister et al. 2013). This significantly exceeded the highest extrusion rates observed during the previous dome-forming eruption in 2006 (0.285×10^6 m^3/day) (Ratdomopurbo et al. 2013) and Merapi's long-term (100 year) average (0.003×10^6 m^3/day (Siswowidjoyo et al. 1995).

12.2.3 Climactic Eruption Phase

The eruptive activity reached its peak on 5 November (Fig. 12.2). The largest pyroclastic events occurred at 00:01 (WIB) and lasted for about 27 min. It included a sequence of several laterally directed dome explosions that produced high-energy PDCs and retrogressive gravitational dome collapses that removed the growing and older lava domes at the summit, and generated PDCs reaching a distance of ~16 km in the Gendol valley (Surono et al. 2012; Budi-Santoso et al. 2013; Charbonnier et al. 2013; Komorowski et al. 2013) (Fig. 12.3d). An unsustained convective column reached a height of 17 km above the summit, producing PDCs rich in scoria and pumice clasts. A cumulative SO_2 emission of ~0.44 Tg (Surono et al. 2012), obtained by satellite observation, was used to estimate a volume of ~120 million m^3 of degassing magma at depth. The events at the peak of the eruption caused damage to the DEL (Deles) and PUS (Pusunglondon) seismic stations (Fig. 12.1). Due to the magnitude of the eruption and seismic energy, the vibrations were also recorded by the IMG (Imogiri) seismic station ~40 km south of Merapi (see Budi-Santoso et al. 2023, Chap. 13). The sound of the eruption could be heard more than 60 km away.

12.2.4 Post-Climactic Activity and End of the 2010 Eruption

The eruptive activity gradually decreased after 5 November (Fig. 12.2). Rapid lava dome extrusion resumed over a period of ~11 h on 6–7 November at an unprecedented rate of 35 $m^3\ s^{-1}$ and was accompanied by minor explosive activity. When dome growth ceased on 8 November, the new lava dome had a volume of $\sim 1.5 \times 10^6$ m^3 (Pallister et al. 2013) (Fig. 12.3e). Subsequent activity was characterised by dome subsidence, and minor vulcanian explosions and ash emissions.

On 15 November, CVGHM recommended reducing the radius of the restricted zone to 15 km from the summit in the Magelang district and to 10 km in the Klaten and Boyolali districts, while the zone for the Sleman district, as the most impacted area, was kept at 20 km radius from the summit (Fig. 12.2). Reduction of the radius of the restricted zone continued on 19 November, with the hazard zone reduced to 10 km from the summit in the Sleman, Magelang and Klaten districts, and to 5 km in the Boyolali district (Fig. 12.2). With continued waning of the eruptive activity, as indicated by decreasing seismicity, the alert level was downgraded to level III on 3 December 2010, and subsequently to level II on 30 December 2010 (Fig. 12.2).

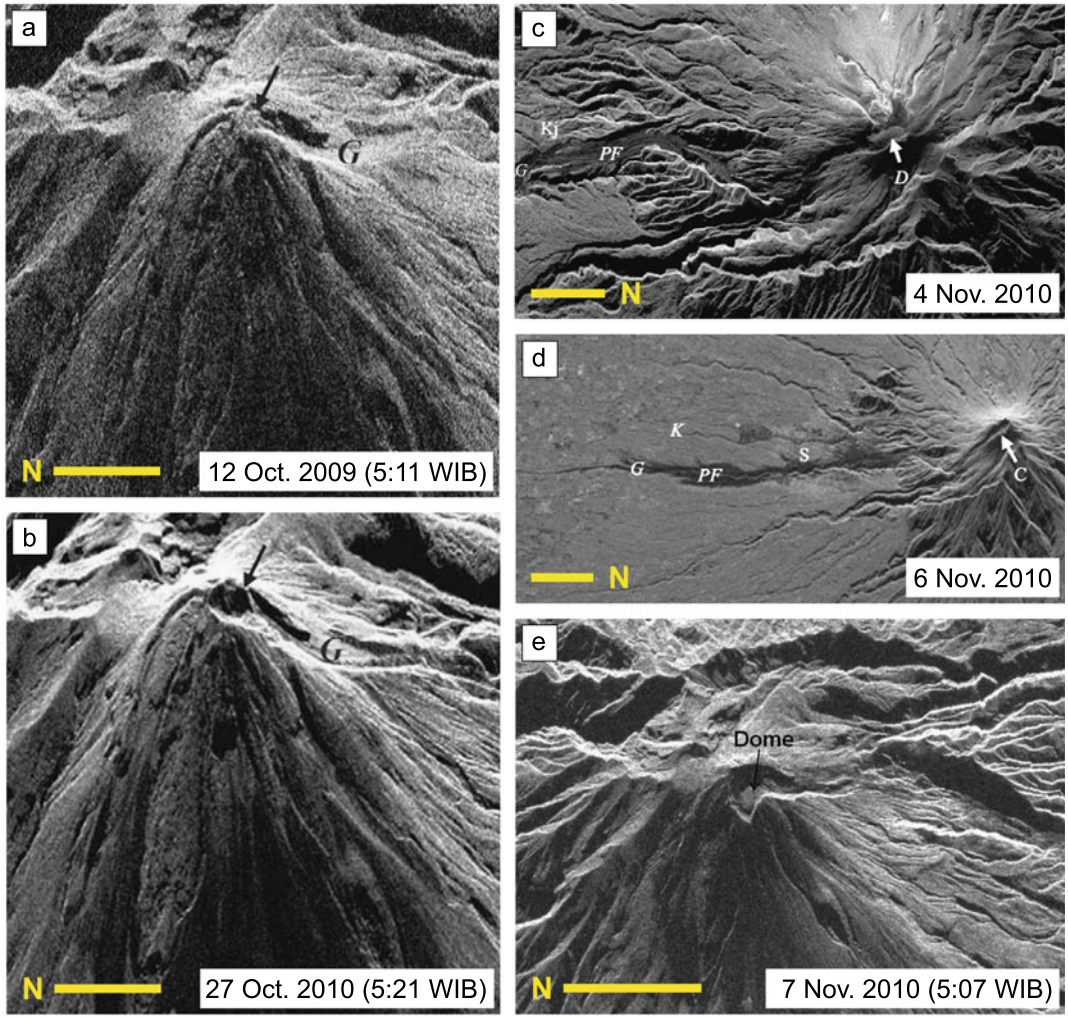

Fig. 12.3 **a** RADARSAT-2 Synthetic Aperture Radar (SAR) base reflectivity image of 12 October 2009 at 5:11 (WIB), with arrow indicating the remnants of the 2006 lava dome and 'G' denoting Kali Gendol. **b** TerraSAR-X image from 27 October 2010 at 5:21 (WIB), with arrow showing the deepened summit crater produced by the initial explosions of the 2010 eruption on 26 October. 'G' indicates Kali Gendol. **c** TerraSAR-X image from 4 November 2010. 'D' marks the large ($\sim 5 \times 10^6$ m^3) lava dome, first detected on 1 November, 'PF' denotes pyroclastic flow (PDC) deposits from the 26 October to 4 November activity, and 'Kj' shows the location of Kinahrejo. **d** RADARSAT-2 SAR base reflectivity image from 6 November 2010. 'C' indicates the empty summit crater, 'PF' shows channelised and overbank pyroclastic flow (PDC) deposits and 'S' are dilute PDC (surge) deposits in and around Kali Gendol ('G'), both formed during the climactic eruption phase on 5 November. 'K' shows the location of Kali Kuning. **e** RADARSAT-2 SAR base reflectivity image from 7 November 2010 at 5:07 (WIB), showing the new lava dome that had grown to $\sim 1.5 \times 10^6$ m^3 in the previous 11 h. In each image, the scale bar (yellow) is 2 km; the north direction is indicated by the position of 'N' relative to the scale bar. After Surono et al. (2012) and Pallister et al. (2013)

These decisions were crucial, given that the large number of refugees reached nearly 400,000 people (Mei and Lavigne 2013; Mei et al. 2013). After lowering of the alert level, some of the refugees were able to return to their homes, except for people whose houses were severely damaged by the eruption. Lahars occurred continuously in all of the rivers around the flanks

during the rainy season from November 2010 to April 2011 (de Bélizal et al. 2013). The alert level was downgraded to level I on 12 September 2011 after most of the lahar events had finished (Fig. 12.2). This means that from the first early warning issued on 20 September 2010 to the return to normal conditions, the 2010 Merapi disaster crisis lasted for about 1 year.

12.3 The Volcano Monitoring Record of the 2010 Eruption

As outlined in the previous section, indications of the eruption were clearly shown by the monitoring data. The daily seismicity gradually increased and was accompanied by felt earthquakes from 8 months prior to the eruption on 26 October 2010. The deformation of the summit area, which had been monitored by EDM, showed shortening of the slope distance for one year prior to eruption, and significantly accelerated about 2 weeks before the eruption. About five days before the eruption, volcanic gas concentrations increased. Below, the main characteristics of the seismic, deformation and gas-geochemical monitoring data of the 2010 eruption are presented and discussed.

12.3.1 Seismicity

The most prominent seismic features leading up to the 2010 eruption were the high seismic intensity and energy (Fig. 12.4). The maximum daily number of VT, MP, and RF earthquakes reached 242, 624 and 454, respectively. Excluding RF earthquakes, these numbers exceeded what occurred during previous eruptions. Leading up to the 2010 eruption, the maximum number of VT earthquakes was around 6 times higher, and the number of MP earthquakes was around 3 times higher, compared to the period prior to the 2006 eruption. Similarly, the value of seismic energy of the 2010 eruption was greater than the previous eruption in 2006 (Fig. 12.5). The cumulative seismic energy released through VT and MP earthquakes during the year prior to the 2010 eruption reached 7.5×10^{10} J. Compared to previous eruptions, the energy from 1992 to 2006 never exceeded 2.5×10^{10} J. This considerably higher amount of energy was the most important seismic feature of the 2010 eruption, consistent with its highly explosive character. Along with deformation and gas emission measurements, this observation gave an early identification of the impending large eruption and underpinned the decision making for the evacuation of a larger than usual area. An increase was also observed in the continuous seismic signals (Fig. 12.4). The accelerated rate of seismic energy was clearly reflected in the RSAM and MRSAM values for the frequency bands other than 1–3 Hz, and offered an opportunity to test the Failure Forecasting Method (Voight 1988) used to predict volcanic eruptions. MRSAM values of the 3–5 Hz frequency band gave the best results, where during the six days before the onset of eruption, the model consistently pointed to the eruption time with an accuracy of $\sim$4 h (Budi-Santoso et al. 2013).

Rapid magma migration from depth was a further important feature in the lead-up to the eruption. Most deep VT events with focal depths from 2.5 to 5 km occurred before 17 October 2010, the date when VLP events were also recorded at the summit and at several distal broadband seismic stations and linked to inertial displacement of material such as magma or gas (Jousset et al. 2013b). After this date, deep VT events diminished, while shallow activity (<1.5 km) increased (Fig. 12.6). This indicated migration of magma towards the surface, with calculated ascent rates of 1 mm/s or 86 m/day during deep intrusion, 6 mm/s or 520 m/day during aseismic intrusion, and 3 mm/s or 260 m/day during shallow intrusion. These values were considered plausible given the different stress constraints corresponding to these different zones. According to Hidayat et al. (2000), the average magma ascent velocity ranged from 0.2 to 0.5 mm/s or 17 to 43 m/day during pre-eruptive activity of Merapi in the 1990s.

An additional important feature of the 2010 seismic data was the emergence of large LF earthquakes at a depth of several hundred metres below the summit on 23–24 October, about three

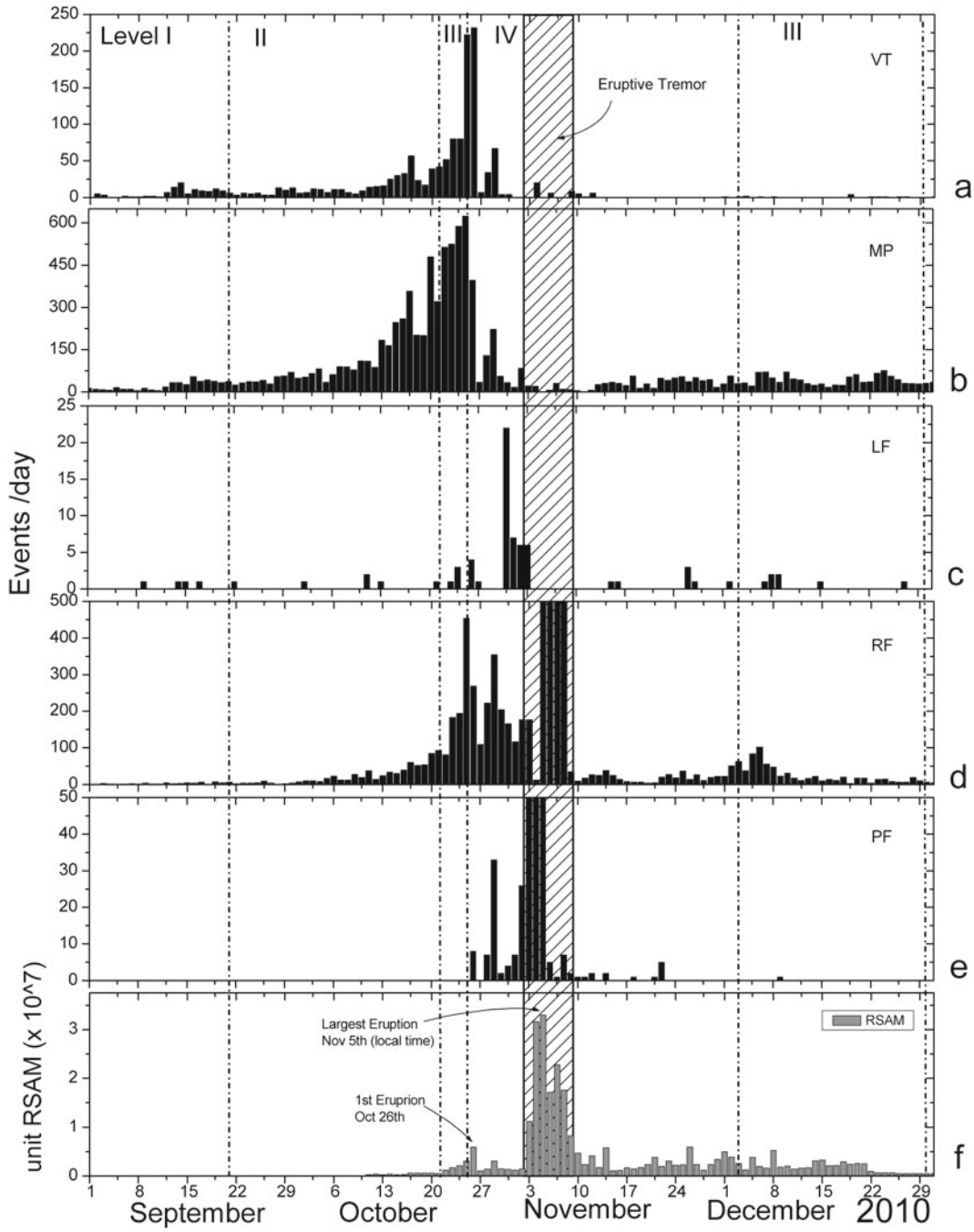

Fig. 12.4 Seismicity at Merapi from September to December 2010. **a** Volcano-tectonic (VT) earthquakes. **b** Multiphase (MP) earthquakes. **c** Low-frequency (LF) earthquakes. **d** Rockfalls (RF). **e** Pyroclastic flows (PF). **f** Real-time seismic amplitude measurements (RSAM). After Surono et al. (2012)

days before the eruption (Figs. 12.4 and 12.6), which confirmed that a large bulk volume of gas was involved in the eruption. However, these events were saturated on the short period stations and therefore not considered as LF events by the observers at the time.

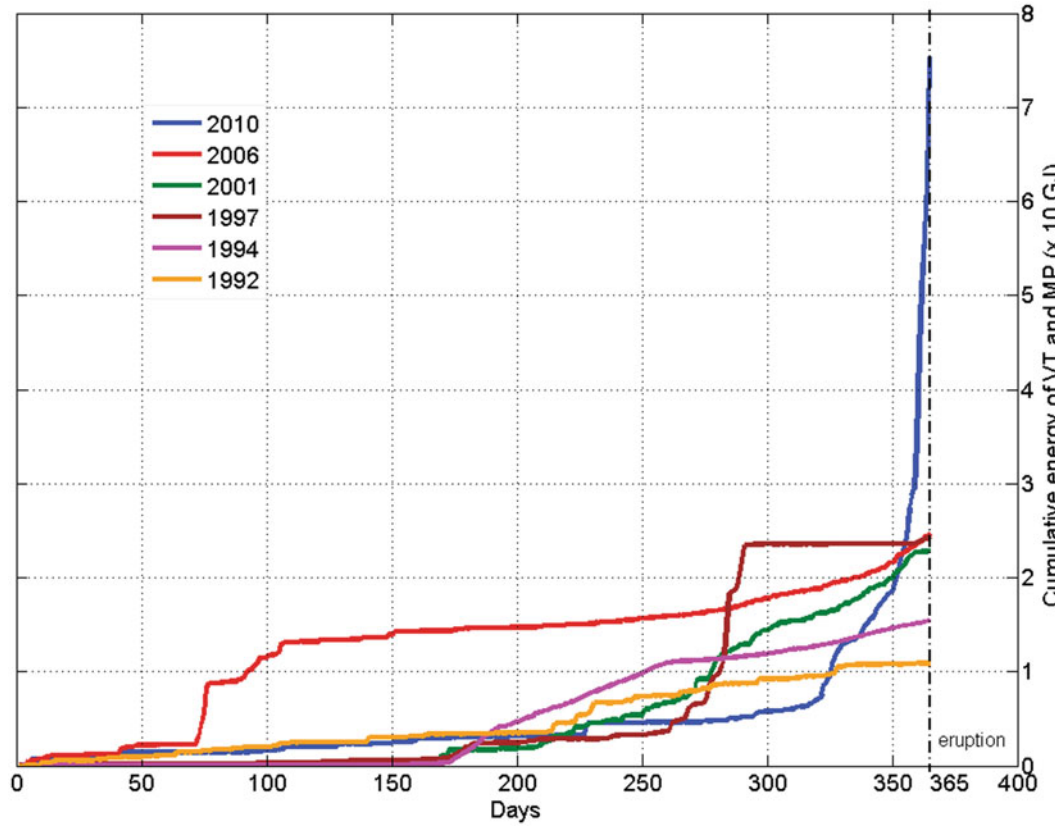

Fig. 12.5 Comparison of the cumulative energy release of VT and MP earthquakes in the year prior to the eruptions from 1992–2010. After Budi-Santoso et al. (2013)

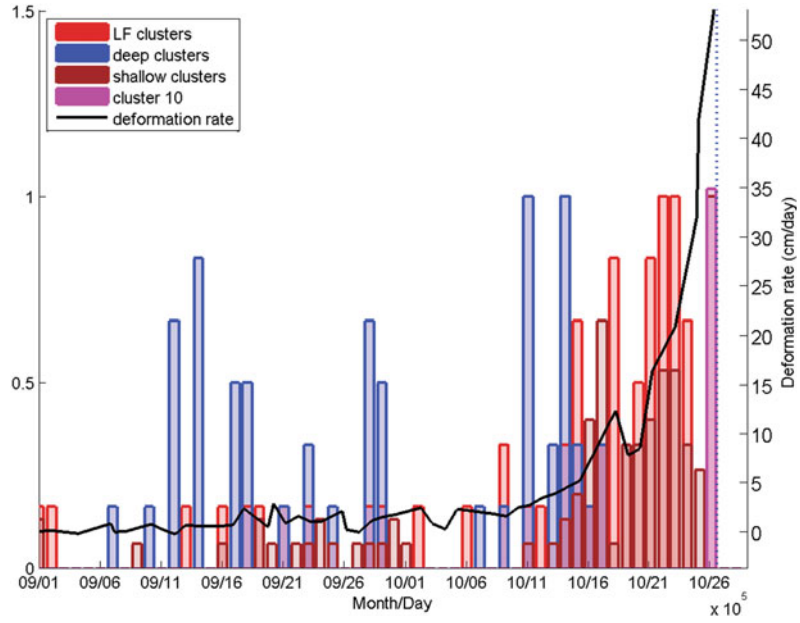

Fig. 12.6 Daily number of events for each group of earthquake clusters during September and October 2010. The values (left axis) are normalised by their maximum. The deformation rate of reflector RK4 obtained by EDM is superimposed as a black line. The rapid increase in the deformation rate approximately on 18 October 2010 corresponds to the strong increase of shallow earthquake events and the vanishing of deep earthquakes

12.3.2 Ground Deformation

Ground deformation prior to the 2010 eruption was characterised by uniaxial displacement and long-term creep (Aisyah et al. 2018). A large change of slope distance was detected by daily distance measurements using EDM only from the southern volcano observation post (Kaliurang) to the south summit area; changes of slope distance from the other directions were minimal (Surono et al. 2012; Aisyah et al. 2018). The rate of contraction of the southern baselines accelerated up to the first explosions on 26 October.

Changes of slope distance of the baselines from April 2009 are shown in Fig. 12.7. The change of slope distance data was divided into 11 (T1 to T11) periods based on the contraction rate of the southern baseline Rk4-KAL (Kaliurang) (Fig. 12.7a), the slope distance of which decreased by 1.64 m from April 2009 to 21 October 2010. By contrast, shortening of baselines from the Babadan post (BAB) amounted to only 0.02 to 0.05 m for the same period (Fig. 12.7a, b). Larger contractions were observed using the reflectors closer to the summit, with a much larger contraction of baseline Rk4-KAL, compared to the other flanks. Baselines Rk1-KAL, Rk2-KAL, and Rk3-KAL on the south flank also exhibited significant contractions (−1.43 m, −0.58 m, and −0.59 m, respectively). Contractions of EDM lines accelerated from 21 to 26 October 2010, when baseline Rk4-KAL was shortened by 3.73 m on 26 October, while baselines Rk3-KAL, Rk2-KAL, and Rk1-KAL decreased by 3.23 m, 2.07 m, and 1.10 m, respectively. Unlike the contraction of the southern and north-western baselines, baselines Rj1-JRK (Jrakah) and Rb5-BAB were shortened only from April 2009 to August 2010 (T1 and T2), changing to extension from August to October 2010 (T3 to T7; Fig. 12.7b). Measurements at the Rs1-SEL (Selo) baseline indicated shortening until April 2010, after which no measurements were documented (Fig. 12.7b).

The contraction rate increased linearly during periods T4 to T6, from 0.03 m/day between 24 September and 15 October (T4 and T5) to 0.05 m/day between 15 and 20 October (T6) (Fig. 12.7). On 20 October, the contraction rate increased exponentially, reaching 0.95 m/day on 26 October, the start date of the eruption. As before, the contraction of the north-western baseline Rb5-BAB was considerably less than that of the southern baseline Rk4-KAL, although the contraction rate gradually increased from T2 to T7 (Fig. 12.7). The CVGHM upgraded the alert level from level II to level III on 21 October and distance measurements of the north-western and northern baselines using EDM were discontinued. The dominant contraction of the southern baselines indicated surface deformation in an asymmetrical pattern, with a large movement of the summit area towards the south flank and minor movement of the summit area in other directions.

12.3.3 Gas Geochemistry

One of the manifestations of the activity of Merapi is the presence of solfataras or fumaroles in the summit area. The concentration of solfatara or fumarole gas emissions changes during an increase in activity. Merapi is a H_2O-rich volcano, with the volcanic gases mainly composed of H_2O—a typical feature of subduction zone volcanoes (Shinohara et al. 2008)—followed by CO_2, SO_2, H_2S and the minor gaseous components hydrogen (H_2), carbon monoxide (CO), hydrogen chloride (HCl), hydrogen fluoride (HF), and helium (He) (Le Guern et al. 1982; Sumarti and Suryono 1994; Delmelle and Stix 2000). The characteristics of the volcanic gas emissions of the explosive 2010 eruption were different from previous effusive eruptions, with the most significant changes prior to the 2010 eruption observed in the volcanic gas concentrations of H_2O and CO_2 (Fig. 12.8). During the repose period between the 2006 eruption and 2009, volcanic gas compositions fluctuated. In November 2007, the concentration of H_2O dropped to 75 mol.% from >90 mol.% and was accompanied by increases in other gas species, such as CO_2 and SO_2, which reached concentrations of 19.2 mol.% and 3.0 mol.%, respectively. After 2009, the composition returned to

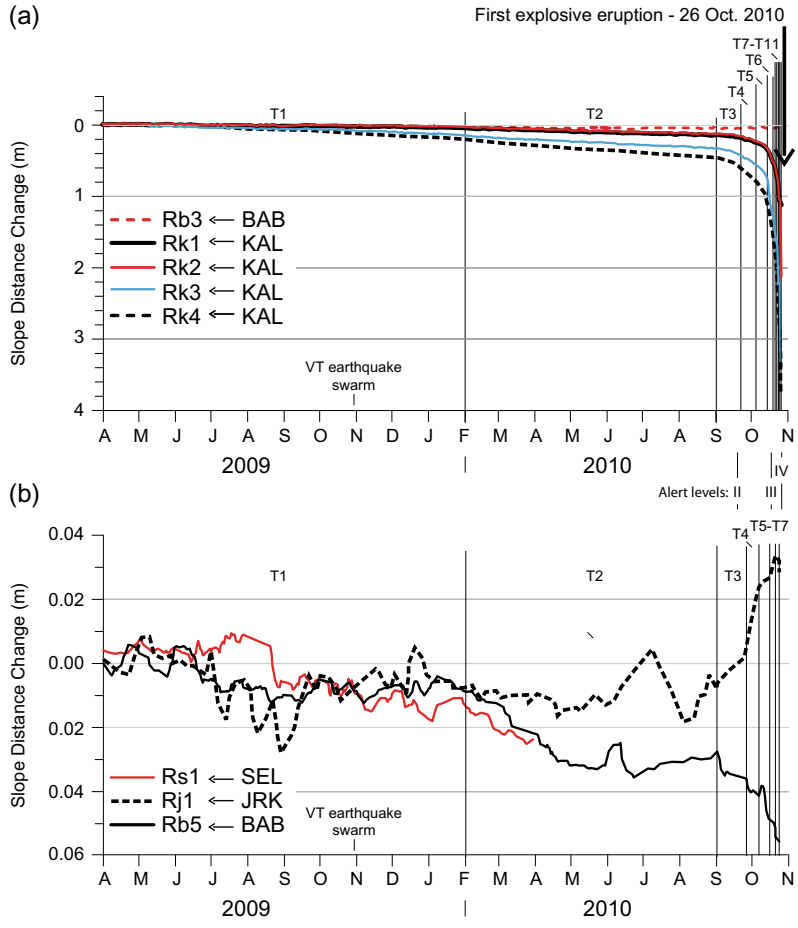

Fig. 12.7 **a** Change of slope distance (i.e. the distance between a base station on the lower slopes of the volcano and a reflector (R) at the summit, as determined by EDM) at the southern baselines (Rk1/Rk2/Rk3/Rk4-KAL), and the north-western baseline (Rb3-BAB) between April 2009 and October 2010. **b** Change of slope distance at the north-western (Rb5-BAB), northern (Rj1-JRK) and north-eastern (Rs1-SEL) baselines. For the configuration of the EDM network in 2010, see Aisyah et al. (2018). Deformation changes, observed since the beginning of 2009, were divided into 11 (T1 through T11) periods based on the contraction rate of the Rk4-KAL baseline. The volcano-tectonic (VT) earthquake swarm on 31 October 2009 and the dates of alert level changes are also shown. Abbreviations: BAB = Babadan; JRK = Jrakah; KAL = Kaliurang; SEL = Selo. After Aisyah et al. (2018)

normal (background) levels until March 2010. In April 2010, the concentration of H_2O decreased, and CO_2 increased, before the gas emissions returned to normal levels in March 2010. In June 2010, H_2O levels decreased again to 77.7 mol.% and CO_2 rose to 14.2 mol.%, and gas concentrations remained at a higher-than-normal level afterwards. Significant changes in gas concentrations were observed in October 2010, when H_2O concentrations were as low as 59 mol.%, and CO_2 and H_2S increased to 35 mol.% and 2.5 mol.%, respectively (Fig. 12.8).

During the 2010 eruption, explosive eruption phases were characterised by a significant increase in H_2S/H_2O ratios, which were not detected during the effusive eruption phase. This observation was due to the dominance of H_2S among the sulphur compounds (Fig. 12.9a). As H_2S is a stable sulphur compound at higher pressure and temperature (Delmelle and

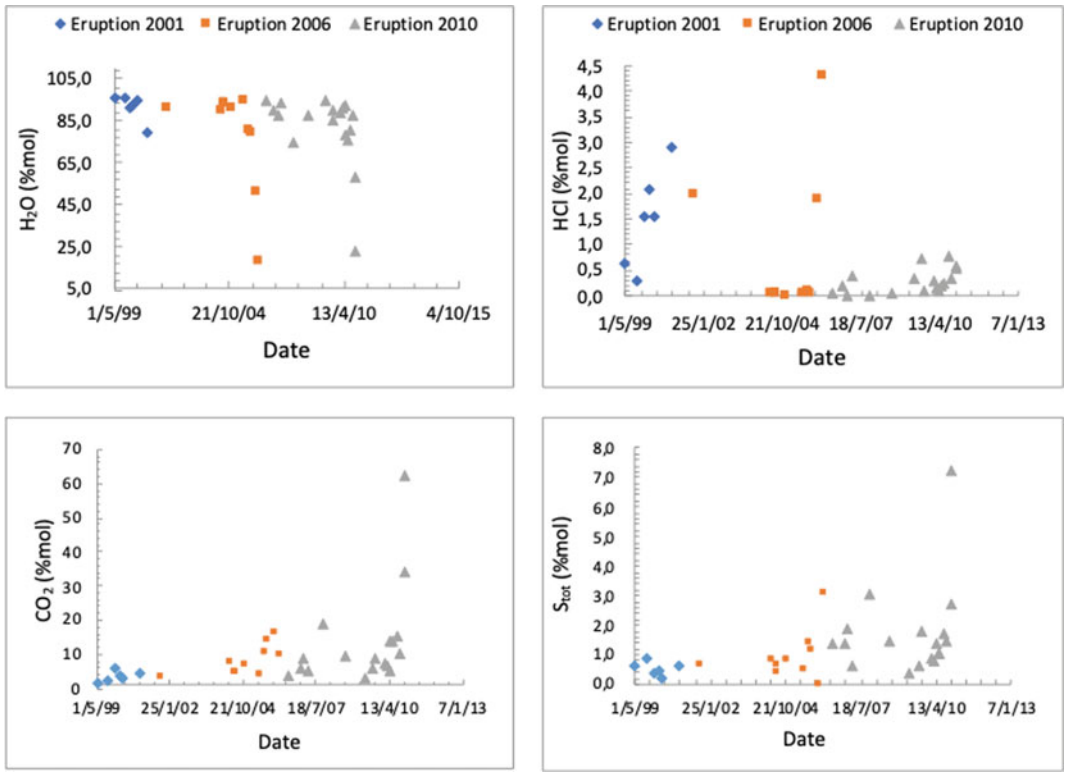

Fig. 12.8 Changes in gas composition at the Woro fumarole field at Merapi's summit prior the 2001 and 2006 effusive eruptions and the explosive eruption of 2010

Stix 2000), the higher observed H_2S/H_2O ratios during explosive eruption phases likely reflects fresh magma input from depth characterised by higher H_2S (and CO_2) concentrations (relative to SO_2, HCl and H_2O) compared to magma stored in a shallower part of the magma plumbing system. The large variation in SO_2/H_2O may have been due to different gas sources in general (Shinohara et al. 2011), including deep as well as shallow magma sources, which release gas generally dominated by SO_2 (Delmelle and Stix 2000). Emitted CO_2/H_2O ratios, which are proportional to the bubble fraction in the melt (e.g. Botcharnikov et al. 2004), also significantly increased during the 2010 explosive eruption compared to the effusive eruptions in 2001 and 2006. The strong increase in the CO_2 emission prior to the 2010 eruption is distinctly negatively correlated with the emission of H_2O and a CO_2/H_2O ratio of 0.83, while the effusive eruptions in 2001 and 2006 were characterised by CO_2/H_2O ratios of 0.14 and 0.11, respectively (Fig. 12.9b).

Changes in gas ratios leading up to the 2010 eruption were observed from August/September 2010 to October 2010. CO_2/SO_2 increased from 9.4–19.0 to 24.1–115.6, CO_2/HCl from 20.8–31.0 to 52.8–115.7, and CO_2/H_2O from 0.1–0.2 to 0.6–2.7. Combined, these changes in gas concentrations indicated migration of magmatic fluid to shallower levels in October 2010. Such an interpretation is in line with seismic, particularly LP, events (Jousset et al. 2013b) and decreasing CO_2/H_2S ratios from 16.8–26.4 to 13.4–13.9, which suggested that the new magma from depth carried a volatile-rich phase of CO_2 and H_2S (relative to SO_2 and HCl) that was rapidly released at the surface.

During the effusive eruption phase in 2010, the growth rate of the lava dome showed a positive correlation with the CO_2/H_2O ratio and HCl

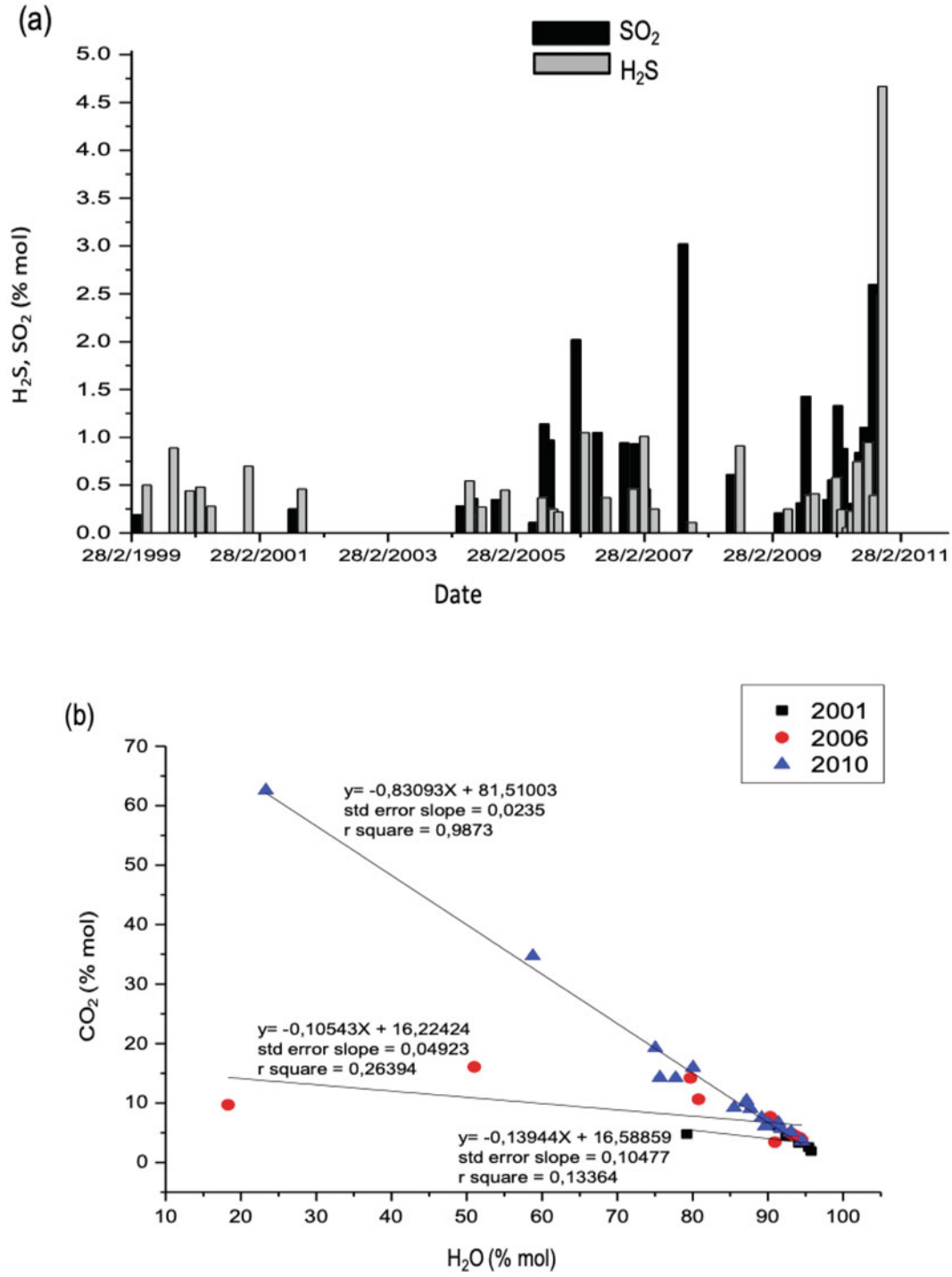

Fig. 12.9 **a** Merapi gas H_2S and SO_2 concentrations (mol.%) prior to the 2001 and 2006 effusive eruptions, and the explosive eruption in 2010. **b** Concentrations (mol.%) of CO_2 and H_2O prior to the 2001, 2006 and 2010 eruptions

concentration of the emitted gases. Typically, the HCl concentration during dome extrusion is higher than during explosive eruptions or eruption phases due to the complexity of the Cl degassing behaviour of the melt as magma rises towards to the surface, and other factors, including differentiation of the magma, melt composition, temperature and pressure (e.g. Carroll and Webster 1994).

SO_2 emissions and their variations that have been routinely measured at Merapi provide insights into the behaviour of the volcano over longer periods of time. Since 1991, monitoring of SO_2 emissions was conducted from the fumaroles in the summit area and the former Gendol and Woro fumarole fields, using a correlation spectrometer (COSPEC) and differential optical absorption spectroscopy (DOAS), complemented by satellite remote sensing during explosive activity. Measurements were made almost daily when the weather permitted, especially in the dry season. Results indicate that SO_2 emissions averaging >100 tons/day coincide with an increase of activity at Merapi and that before every eruption, the SO_2 gas emission of Merapi increases (Fig. 12.10). Prior to the eruption in early 1992, a sharp increase from an average of 50 tons/day to >200 tons/day was observed, with a maximum SO_2 gas emission >300 tons/day, similar to the eruptions in November 1994, January 1997 and July 1998. Long-term variations in the SO_2 concentration at Merapi are noticed, for example, between 1991 and 1998, when the SO_2 concentration decreased slightly. By contrast, from 1999 to 2010, the trend changed to a significant increase of the SO_2 concentration in the emitted gases (Fig. 12.10).

12.3.4 Physical Processes Prior to the Eruption

The topography of the summit area of Merapi prior to the 2010 eruption was dominated by the lava dome that extruded after the large dome collapse events in June 2006 (Ratdomopurbo et al. 2013). Therefore, the state of a shallow part of the conduit allowed higher pressure to build up than during the 2006 eruption (Aisyah et al. 2018). The location of the pressure source was estimated at 2 km beneath the crater (see Aisyah et al. 2018). Magma began to inject into the shallow reservoir at a depth of 2 km below the summit in April 2009, and the pressure of the reservoir increased to 150–200 MPa on 15 October 2010 (Fig. 12.11a). VT earthquakes were clustered (Budi-Santoso et al. 2013) below and above the shallow magma reservoir. The

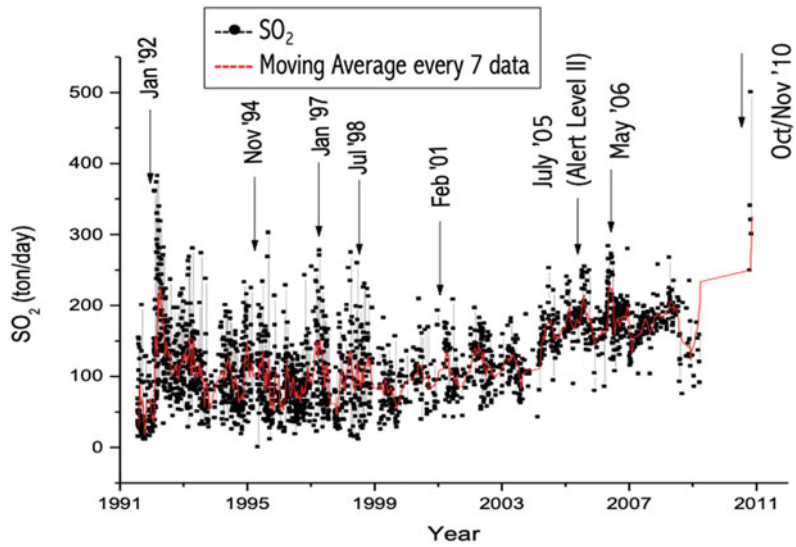

Fig. 12.10 SO_2 emissions of Merapi from 1991 to 2010

increase in VT earthquakes was reflected by an increase in pressure of the shallow reservoir, causing inflation of the ground around the summit and movement of a block south-eastward. The block corresponds to one of the biggest lava domes which filled the east part of the large Mesdjidanlama crater in 1911 (East Dome). Inflation of the shallow reservoir increased the instability of the East Dome, the base of which corresponded to a deeper discontinuity.

Magma injection continued on 15 to 20 October 2010, increasing the pressure of the shallow reservoir to 200–250 MPa (Fig. 12.11b), and causing inflation of the ground around the summit and south-eastward movement of the 1911 lava dome. Magma injection accelerated on 20 October 2010 resulting in an estimated increase in pressure to 400–450 MPa (Fig. 12.11c). The acceleration continued until immediately before the onset of the explosive eruption on 26 October (Fig. 12.11d), when the pressure reached 450–500 MPa, about 4 times higher than in 2006. The explosivity of the 26 October events at the onset of the eruption, with ballistic bombs ejected up to 2 km and PDCs reaching 6.8 km from the summit, is therefore inferred to have been caused by a highly pressurised shallow magma reservoir (Aisyah et al. 2018).

12.4 Volcanic Deposits of the 2010 Eruption

During the multistage 2010 eruption, distinct volcanic deposit types were formed as the eruption progressed (Fig. 12.12). Following a description of types, volume and distribution of the 2010 volcanic deposits, we use the detailed framework of eruption stages proposed by Komorowski et al. (2013) to link the volcanic deposits to the eruption chronology, before discussing the generation, dynamics and significance of high-energy PDCs, which may well represent the first, well-documented examples of blast-like PDCs at Merapi (Komorowski et al. 2013; see Gertisser et al. 2023a, Chap. 1).

12.4.1 Types, Volume and Distribution of the 2010 Volcanic Deposits

Volcanic deposits of the 2010 eruption were associated with a range of volcanic phenomena, including vertical and directed explosions, eruption column or fountain collapse, lava dome extrusion, dome explosion, dome collapse, rockfalls and tephra (ash) fall (Surono et al.

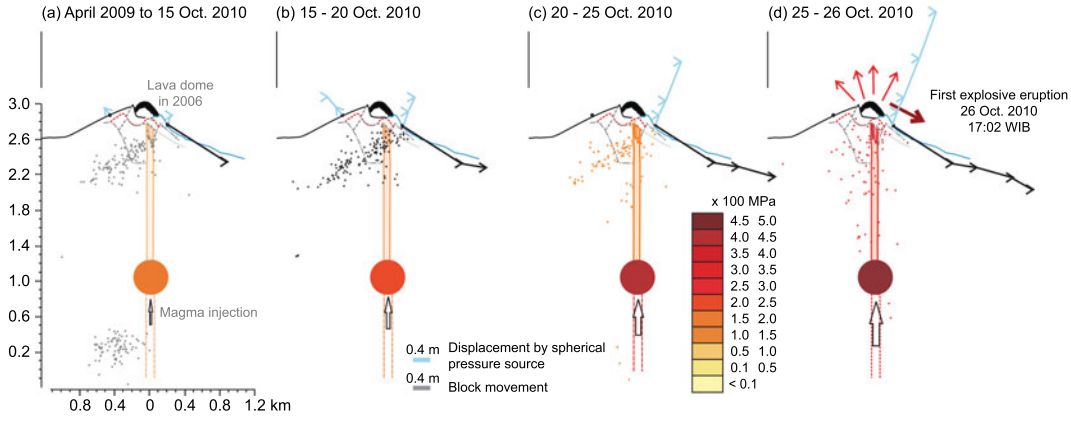

Fig. 12.11 Ascent and storage of magma and block movement prior to the 2010 eruption. Dots represent hypocentres of volcano-tectonic (VT) earthquakes, light blue vectors show displacement caused by a spherical pressure source and black vectors display southward block movement. The thick dark red arrow shows the southward directed explosions on 26 October 2010, while the thinner red arrows indicate explosive eruption phases between 26 October and 5 November 2010

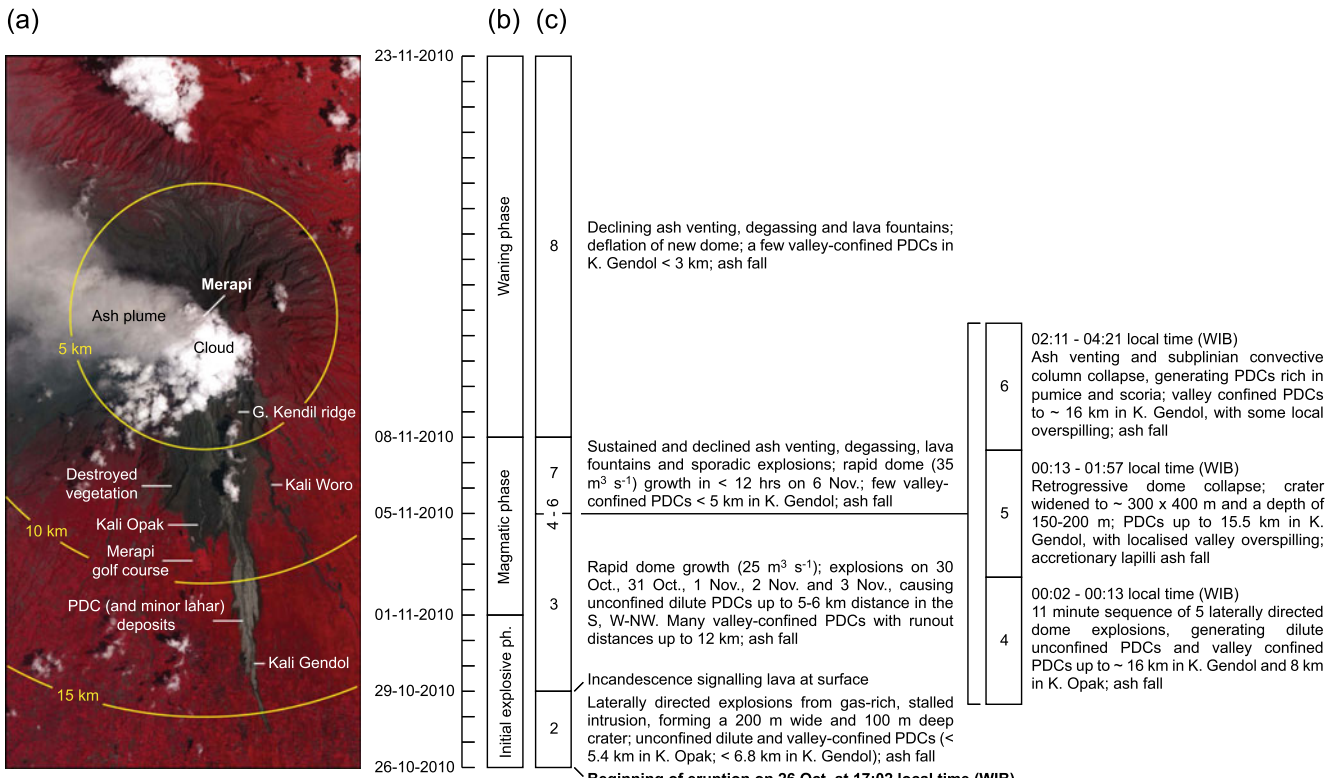

Fig. 12.12 **a** ASTER false-colour satellite image from 15 November 2010, showing pyroclastic density current (PDC) deposits filling the valleys of Kali Gendol and Kali Opak on Merapi's south flank (light grey). Fluvial erosion of the deposits in Kali Gendol had already set in, producing lahars. The dark grey area north of the Merapi Golf course was affected by dilute unconfined PDCs, causing almost total devastation. PDCs also fill the valley of Kali Woro. The bright red areas were unaffected by PDCs and consist of healthy vegetation. An ash plume is drifting away from the volcano to the west, causing ash fall in the dull red to grey area on Merapi's western slopes. *Source* NASA Earth Observatory (Digital Globe—November 2010). **b-c** Eruption timeline, with eruption stages since the beginning of the eruption on 26 October 2010 based on (**b**) Surono et al. (2012) and (**c**) Komorowski et al. (2013). The latter includes a description of the eruptive activity and deposits at each stage

2012; Charbonnier et al. 2013; Cronin et al. 2013; Komorowski et al. 2013; Preece 2014; Preece et al. 2016). Lahars occurred during and immediately after the eruption from remobilisation of primary pyroclastic deposits mainly during Indonesia's rainy season and continued for several years (de Bélizal 2013).

As during other recent Merapi eruptions, generation of PDCs was ubiquitous, with PDCs having been produced during all eruption stages (Charbonnier et al. 2013; Cronin et al. 2013; Komorowski et al. 2013; Preece 2014; Preece et al. 2016). However, due to the complexity of the 2010 eruption, the PDCs were characterised by marked differences in deposit characteristics, distribution and dynamics, and included: (1) massive, concentrated and block-rich valley-confined PDCs or block-and-ash flows (BAFs) that formed by gravitational lava dome failure, (2) lobate overbank PDC deposits resulting from overspilling of the massive, concentrated and block-rich valley-confined PDCs onto interfluve areas and into adjacent valleys (fast and slow overspill flows; Lerner et al. 2021), (3) dilute unconfined PDCs or surges that formed by detachment from valley-confined massive, concentrated and block-rich PDCs and by laterally directed explosions from a gas-rich, shallow intrusion or cryptodome (low-energy detached surges; Lerner et al. 2021), (4) pumice-rich PDCs generated by the collapse of explosive, pumice-rich eruption columns, and (5) unconfined, turbulent high-energy PDCs, distinct from the dilute unconfined PDCs or surges described above, which were among the most striking volcanic phenomena of the eruption (high-energy surges; Lerner et al. 2021).

The 2010 eruption was considerably larger than other recent and historical Merapi eruptions. Initial estimates (Surono et al. 2012) suggested a bulk deposit volume of $\sim$40–80 $\times$ 10^6 m^3, consisting of $\sim$30–60 $\times$ 10^6 m^3 of juvenile material and an additional $\sim$10–20 $\times$ 10^6 m^3 of non-juvenile material derived from the summit. Based on field studies and a multi-temporal dataset of high-resolution satellite imagery, Charbonnier et al. (2013) determined a bulk PDC deposit volume of $\sim$36.3 $\times$ 10^6 m^3, which is at the lower end of the range proposed by Surono et al. (2012) and similar to the $\sim$40 $\times$ 10^6 m^3 estimated by Bignami et al. (2013), based on synthetic aperture radar (SAR) data. Both estimates do not include deposits other than those on the south flank and must therefore be regarded as minimum values. They are slightly lower than the PDC bulk volume estimates of $\sim$41 $\times$ 10^6 m^3 (Komorowski et al. 2013) and 48.6 $\times$ 10^6 m^3 (Cronin et al. 2013). According to Charbonnier et al. (2013), the total volume is distributed between valley-confined deposits (50.2%), overbank deposits (39.3%), as well as surges and fallout tephra (10.5%). An estimated >70% of the deposits were generated on 4–5 November, and only 28.1% and 0.9% formed prior to and after 5 November, respectively. Solikhin et al. (2015) proposed a bulk PDC deposit volume of $\sim$45 $\times$ 10^6 m^3 in the south, south-west, west and north-west sectors, and a bulk tephra-fall deposit volume of $\sim$18–21 $\times$ 10^6 m^3. The authors estimated that the Gendol and Opak catchments on the south flank contained about 10–15% of the total tephra-fall and 65–70% of the PDC deposit bulk volume. Overall, the published estimates of the bulk volume of the 2010 deposits range from $\sim$36.3–80 $\times$ 10^6 m^3. These estimates indicate a bulk deposit volume at least $\sim$4 times (and possibly up to $\sim$9 times) larger than, for example, that of the preceding eruption in 2006 ($\sim$8.7 $\times$ 10^6 m^3; Charbonnier and Gertisser 2011). About 5 $\times$ 10^6 m^3 of the juvenile material erupted in 2010 was derived from the main 2010 lava dome that formed over several days prior to its destruction on 5 November (Surono et al. 2012; Komorowski et al. 2013; Pallister et al. 2013).

With the significantly larger bulk deposit volume compared to previous eruptions has come a much wider distribution of the 2010 pyroclastic deposits (Fig. 12.13). The 2010 PDC deposits covered an estimated area between $\sim$22.3 km^2 (Charbonnier et al. 2013) and $\sim$33.9 km^2 (Cronin et al. 2013) or, when areas outside the south flank are considered, $\sim$35 km^2 (Solikhin et al. 2015). The high-energy PDCs generated on 5 November spread over $\sim$22 km^2 with a runout distance of $\sim$8.4

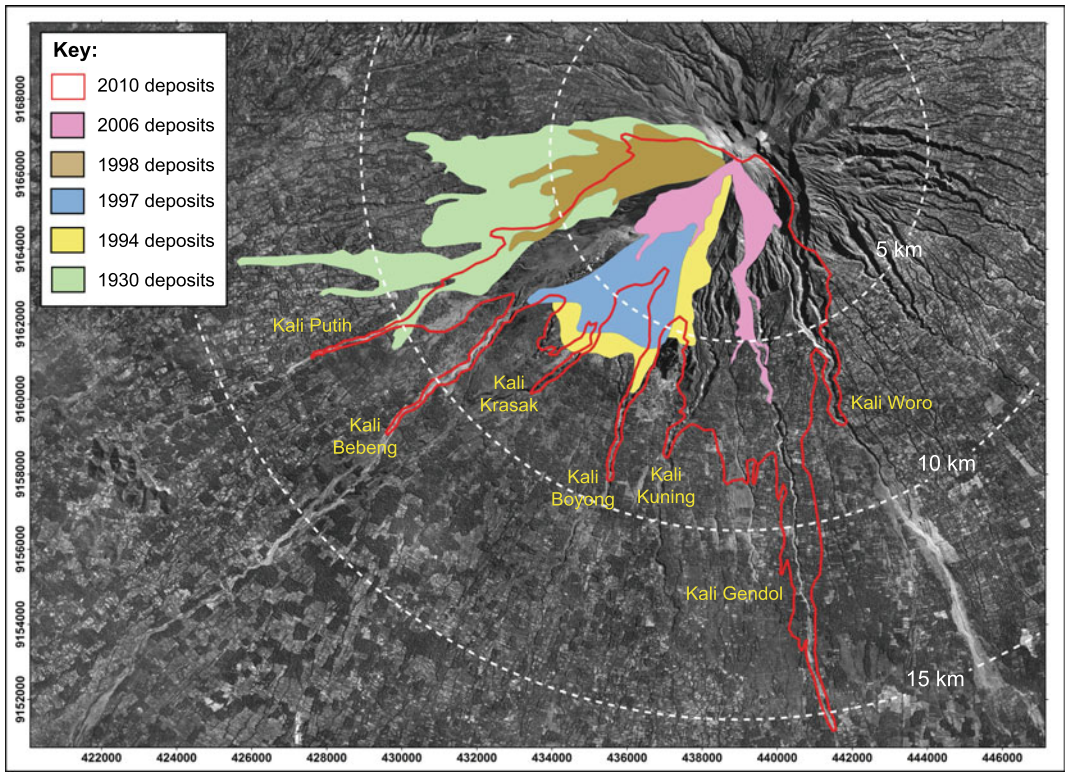

Fig. 12.13 Areas covered by PDC deposits from the 2010 and other recent Merapi eruptions since 1994 as well as from the most devastating historical eruption in 1930. Circles mark areas within 5, 10 and 15 km radius from the summit of Merapi. The map coordinates are in UTM metres. After Gertisser et al. (2011)

km (Komorowski et al. 2013), while tephra fall deposits covered an area of 1300 km^2 (Solikhin et al. 2015). The majority of the PDC deposits inundated areas on Merapi's south flank, where they reached a runout distance of ~15.5 to 16.1 km in Kali Gendol on 5 November (Charbonnier et al. 2013; Cronin et al. 2013; Komorowski et al. 2013), approximately twice as long as during the previous eruption in 2006 (Charbonnier and Gertisser 2008). In other valleys, such as Kali Opak, PDC runout distances were typically <10 km. The large volume, significantly exceeding that of previous recent and historical Merapi BAFs, has been regarded as one of the controlling factors explaining the long runout distances reached by the 2010 PDCs (Cronin et al. 2013), although other causes, such as previous valley infilling and reduction in channel capacity, PDC generation mechanisms at the source or the transport regime, where currents produce a near-frictionless basal region by air lubrication (Lube et al. 2019), may have also played a role.

12.4.2 Volcanic Deposits Linked to Eruption Chronology

Most of the deposits described in this section are from the most affected area on Merapi's south flank. Correlated stratigraphic sections of the 2010 deposits, linked to the eruption stages of Komorowski et al. (2013) (Fig. 12.12), are shown in Fig. 12.14.

The first eruption deposits were related to partially laterally (southward) directed explosions on 26 October, which generated dilute PDCs (surges) that spilled over the upper Gendol valley and propagated towards Kinahrejo (Gertisser et al. 2011; Charbonnier et al. 2013; Cronin

(a)

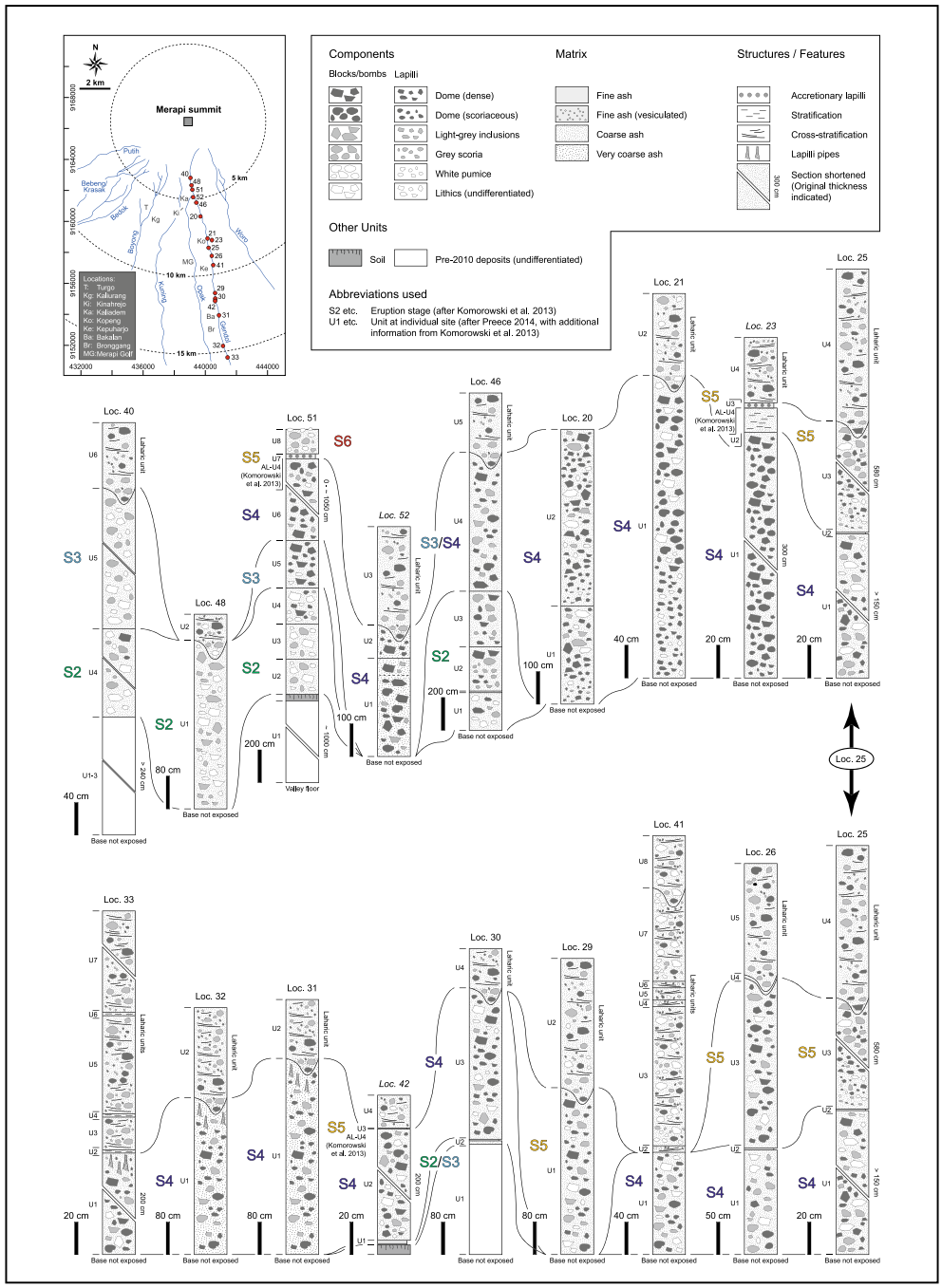

Fig. 12.14 **a** Correlated stratigraphic sections of the 2010 eruption deposits in the Gendol river valley (Kali Gendol), arranged from N (locality 40) to S (locality 33). Stratigraphic sections on interfluve areas adjacent to the main valley are indicated in italics. **b** Correlated stratigraphic sections of predominantly unconfined 2010 Merapi deposits in the southwestern and southern sector of the volcano, arranged from W (locality 49) to E (locality 22). Eruption stages (e.g. S4) after Komorowski et al. (2013). Detailed descriptions of the stratigraphic sections (including individual units; U) can be found in Preece (2014). After Preece et al. (2016)

(b)

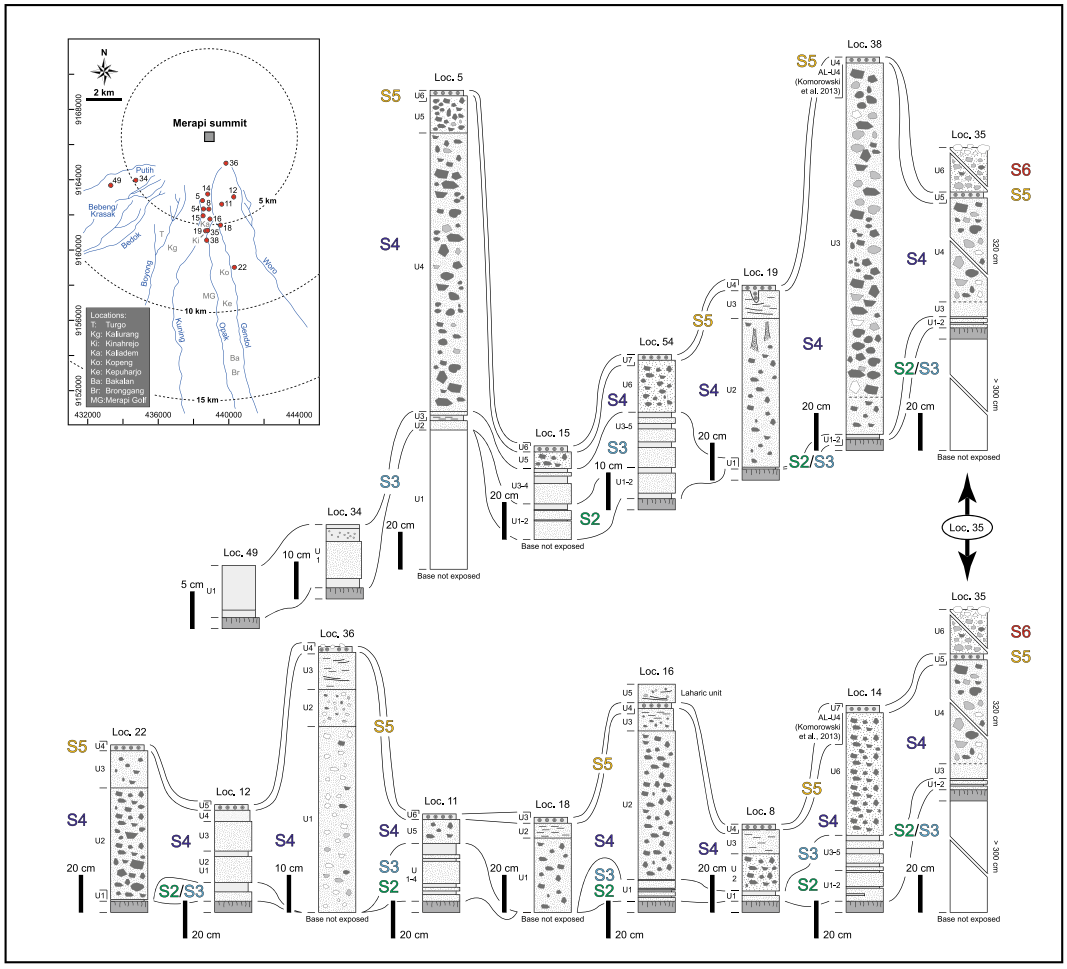

Fig. 12.14 (continued)

et al. 2013; Komorowski et al. 2013), and to subsequent explosive activity and partial lava dome collapse prior to the eruption climax on 5 November that affected a similar area (eruption stages 2 and 3; Komorowski et al. 2013). In and around Kinahrejo, up to 5 dilute PDCs occurred during these two stages, with each of these emplacing a unit consisting of two layers (Fig. 12.15). Typically, the lower layer is composed of massive, grey-coloured or 'salt and pepper' coarse ash to fine lapilli, comprised of scoriaceous, pumiceous or dense clasts (Charbonnier et al. 2013; Cronin et al. 2013; Komorowski et al. 2013; Preece 2014; Drignon et al. 2016; Preece et al. 2016). The upper layer is usually a brown-orange or grey coloured fine ash, which is often stratified. The coarser basal layer is interpreted to have formed via emplacement of the dilute PDC, with the upper fine ash layer emplaced due to ash settling from the accompanying ash cloud. Although valley-confined stage 2 and stage 3 PDCs or BAFs, such as those in the Gendol river valley (Kali Gendol), were buried by subsequent flows, some were already exposed a few weeks after the eruption due to fluvial erosion (Fig. 12.16). Correlation between valley-confined and unconfined PDC deposits (Fig. 12.14) was aided by

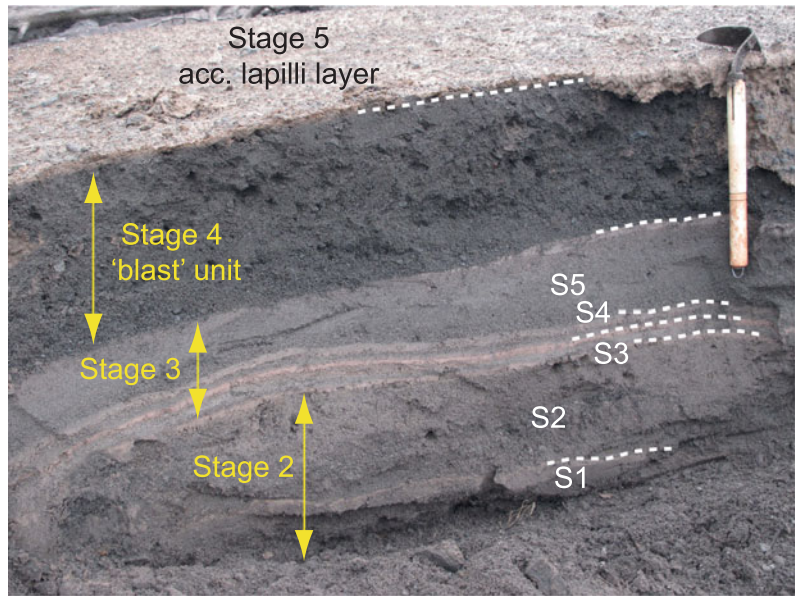

Fig. 12.15 Section on Merapi's south flank north of Kinahrejo (see Fig. 12.13) composed of 5 surge units formed during stages 2 and 3, all with a coarser lower layer and a fine ash upper layer. Above the surges is the stage 4 high energy PDC unit, topped by stage 5 accretionary lapilli-bearing ash. Scraper for scale (length: 35 cm). See text for further details. After Preece (2014)

stratigraphic position and comparable clast componentry, including the presence of non-juvenile, hydrothermally altered and accidental lithics, as well as light grey dense crystalline clasts, abundant grey scoria and occasional white pumice. The presence of scoriaceous and pumiceous clasts in at least two depositional units related to the 26 October deposits and pumice levees in unconfined and valley-confined PDC deposits near the base of the 2010 eruption sequence (Charbonnier et al. 2013; Komorowski et al. 2013; Preece 2014; Drignon et al. 2016; Preece et al. 2016), and the energetic nature of the surges (Cronin et al. 2013), suggests that fresh (juvenile) magma had already been involved in the initial explosions.

At the climax of the eruption, a series of deposits was produced over a period of a few hours in the early hours (local time; WIB) of 5 November (eruption stages 4, 5 and 6; Komorowski et al. 2013). During the most intense eruption phase, corresponding to eruption stage 4 (Komorowski et al. 2013), a series of paroxysmal dome explosions and collapses occurred in a matter of minutes (Fig. 12.12). These produced high-energy, dilute PDC (surge) deposits, valley-confined BAFs and associated overbank deposits (Fig. 12.16), which were generated via the breakout of confined flows onto interfluve areas (Charbonnier et al. 2013; Cronin et al. 2013; Komorowski et al. 2013). The high-energy PDC deposits have bi-partite layering (Fig. 12.17a), with the lower layer coarser than the upper one. The lower layer is clast-supported, fines-depleted, consisting mostly of lapilli, but may also contain blocks or bombs, sometimes up to ~20 cm in diameter, replaced distally by coarse ash. The upper unit is composed of fine to coarse ash, which sometimes has wavy cross- and planar-stratification (Fig. 12.17b). Lapilli pipes are often present, originating from the top of the lower unit (Preece 2014). Komorowski et al. (2013) identified two high-energy PDC units (termed U1 and U2) produced by two paroxysmal explosions, both with bi-partite layering (U1-L1, U1-L2, U2-L1 and U2-L2). Both units are similar and were distributed over a similar area, although Unit 2 is typically finer grained, thinner, and outcrops are less abundant. While the two paroxysmal explosions generated these unconfined dilute PDC deposits, channelling of the basal, high particle concentration portion of the PDCs resulted in emplacement of valley-confined BAFs and unconfined (overbank) flows. The valley-confined BAFs are massive, poorly sorted and often reversely graded (Charbonnier et al. 2013). They

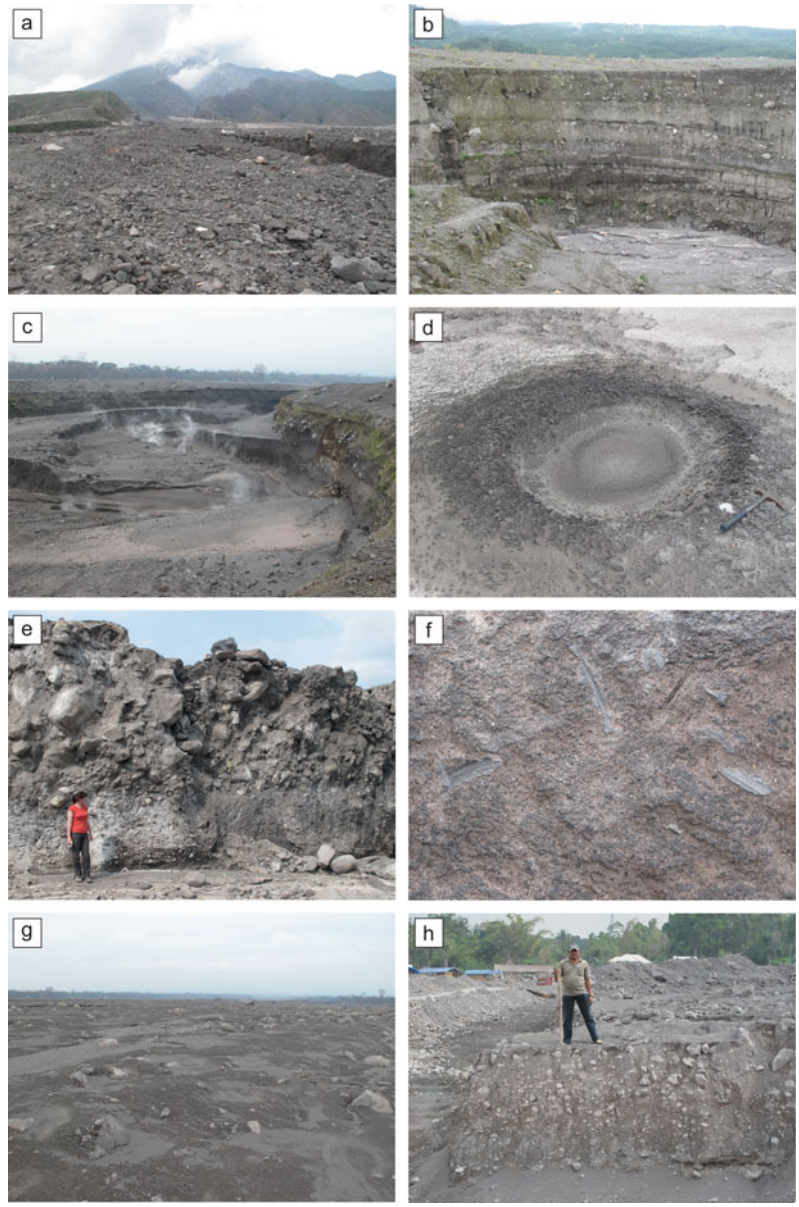

Fig. 12.16 Valley-confined and overbank PDC (block-and-ash flow; BAF) deposits and some of their features. **a** BAF deposits filling the Gendol river valley (Kali Gendol); view north from Kaliadem towards Merapi. **b** Buried by subsequent flows from stage 4/5, stage 2 and stage 3 BAF deposits were already exposed in Kali Gendol a few weeks after the eruption due to fluvial erosion. The valley side is approximately 15 m high. Photograph taken near Kaliadem. **c** Partly eroded and still hot BAF deposits in the medial reaches of Kali Gendol around Kepuharjo. **d** Fumarole pipe at the surface of a BAF deposit, formed from continued degassing of the hot deposit following emplacement. Hammer for scale. **e** Reversely graded BAF deposit from stage 4/5 near Kopeng. **f** Randomly orientated friction marks (Schwarzkopf et al. 2001) on a block within the 2010 BAF deposits, resulting from tumbling and sliding of blocks during flow transport. Field of view is 40 cm wide. **g** Vast area on the western side of Kali Gendol near Kepuharjo covered by overbank PDC deposits. **h** Close-up of overbank PDC deposits near Kepuharjo, illustrating their poorly sorted nature, with clasts up to a few decimetres in size. For locations, see Fig. 12.14. *Photo credit* R. Gertisser, K. Preece

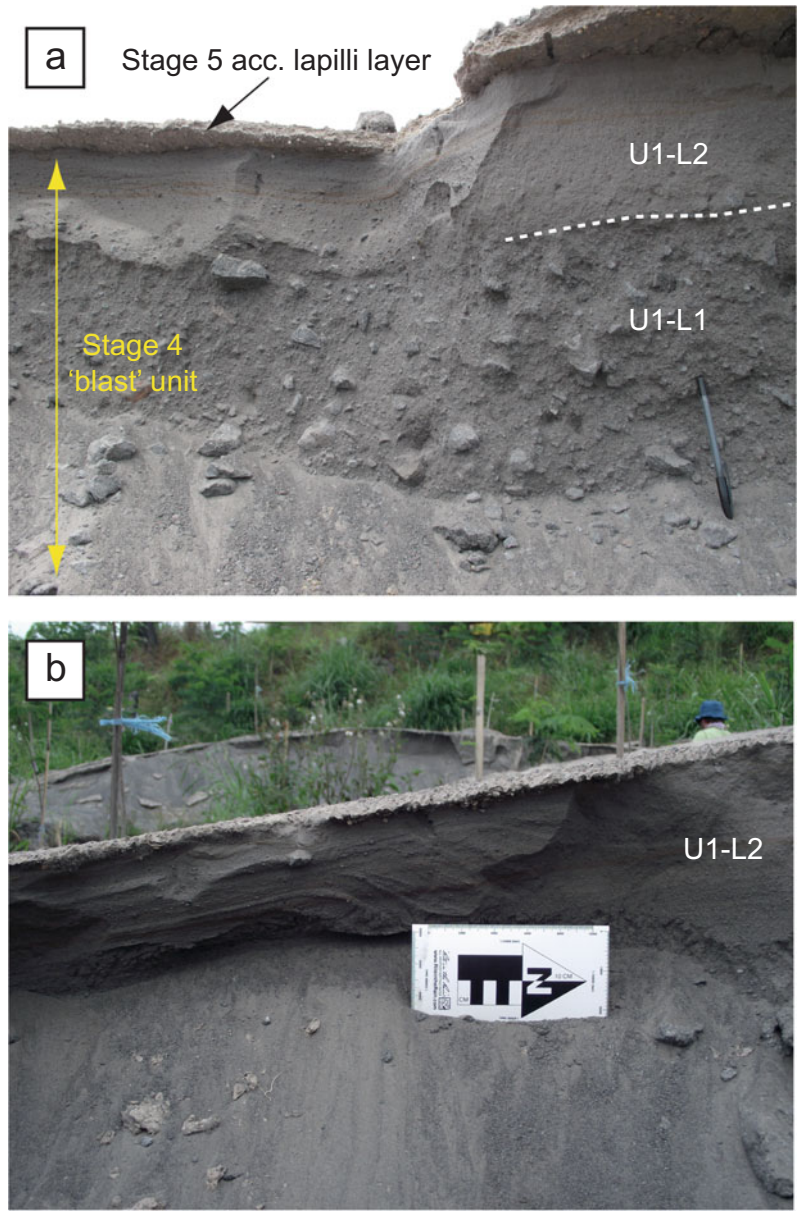

Fig. 12.17 **a** Stage 4 high-energy PDC unit with bi-partite layering, characterised by a coarse lower layer and a finer grained upper layer. The lower and upper layers correspond to units U1-L1 and U1-L2 of Komorowski et al. 2013. The unit is overlain by stage 5 accretionary lapilli-bearing ash. Pen for scale (length: 15 cm). **b** Upper layer of high-energy PDC deposit (unit U1-L2; Komorowski et al. 2013) showing cross stratification. Photo scale (length: 12 cm). Both photographs were taken around Kinahrejo. For location, see Figs. 12.1 and 12.14. *Photo credit* K. Preece

may contain lapilli pipes formed via post-depositional gas escape, carbonised plant material, are frequently encrusted with sublimates, and may be oxidised towards the top. The deposits from the climactic phase of the eruption are almost monolithological, in that their componentry is dominated by dark grey to black, dense fragments of the fast growing, pre-climax lava dome (Fig. 12.18a) that was destroyed by the cataclysmic explosions (stage 4; Komorowski et al.

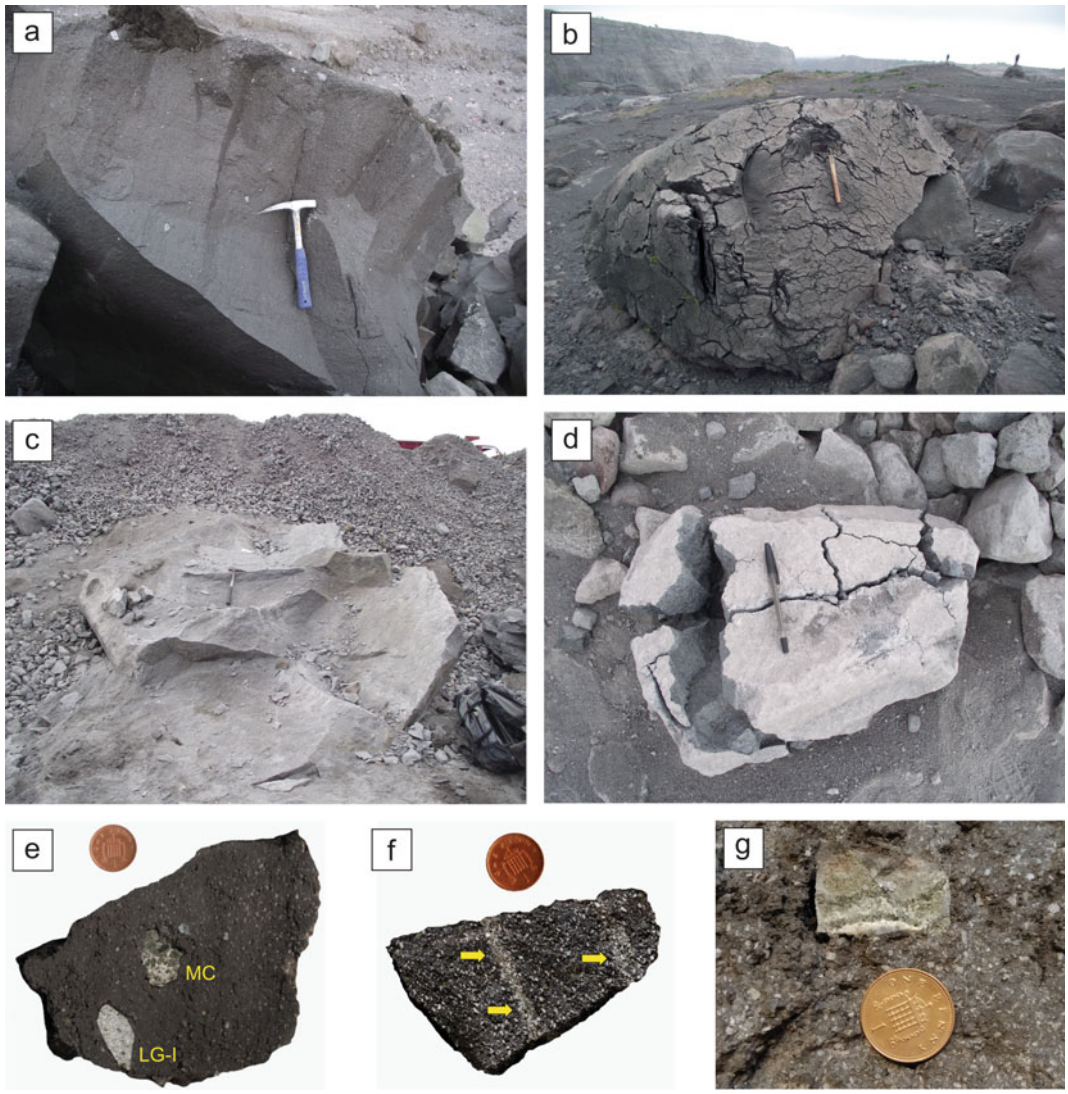

Fig. 12.18 Characteristic lithologies of stage 4 deposits in Kali Gendol and adjacent areas (see Fig. 12.14). **a** Dark dense fragment of the main 2010 lava dome, the principal component of stage 4 PDC deposits. Hammer for scale (length: 28 cm). **b** Rare lava dome block with breadcrust texture. Scraper for scale (length: 35 cm). **c** Highly crystalline block of light grey dense basaltic andesite. Hammer for scale (length: 40 cm). **d** Prismatically jointed block of light grey dense basaltic andesite. Pen for scale (length: 15 cm). The light grey dense basaltic andesite also occurs as **e** inclusions (LG-I), and **f** streaks or bands within the 2010 dome lava, along with inclusions of **e** plutonic xenoliths (magmatic cumulates; MC) and **g** crustal carbonate (calc-silicate) xenoliths. Coin for scale (diameter: 2 cm). *Photo credit* R. Gertisser, K. Preece

2013) on 5 November. Dark grey to black scoriaceous fragments and rare blocks with breadcrust texture from the same lava dome also occur within the stage 4 PDC deposits, along with blocks (up to several metres in diameter) of light grey dense rock fragments (Fig. 12.18b, c). Many of the latter are prismatically jointed, signifying that they were hot at the time of eruption, and therefore originate from the eruption (Fig. 12.18d). Light grey dense crystalline material has also been found as abundant inclusions within the juvenile dome material (Fig. 12.18e). These inclusions range in size from

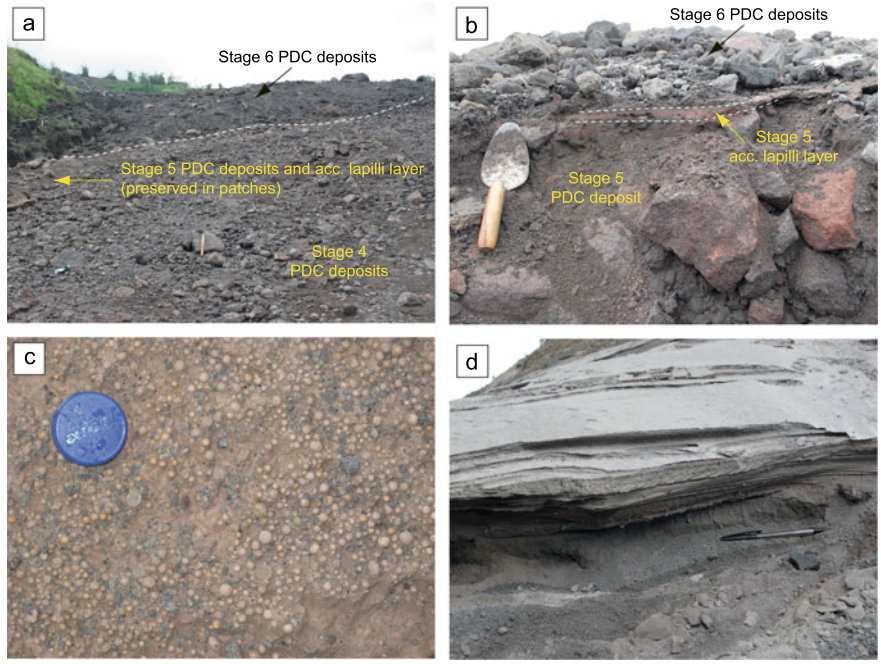

Fig. 12.19 Stage 5 and 6 deposits and their lithological characteristics. **a** Stage 5 and 6 deposits, emplaced stratigraphically above stage 4 flows around Kinahrejo. Scraper for scale (length: 35 cm). **b** Overbank deposits around Kinahrejo, including stage 5 red-pink PDC and accretionary lapilli-bearing ash layer below stage 6 PDC (scoriaceous and pumiceous flow) deposits. Trowel for scale (length: 20 cm). **c** Close-up of the distinctive orange accretionary lapilli-bearing ash layer stratigraphically above the stage 4 high-energy PDC deposits north of Kinahrejo. Bottle lid for scale (diameter: 4 cm). **d** Dilute PDC (surge) layers north of Gunung Kendil containing poorly vesicular pumice lapilli. Pen for scale (length: 15 cm). For locations, see Figs. 12.1, 12.12 and 12.14. *Photo credit* K. Preece

a few millimetres to a several centimetres and have angular shapes, indicating brittle deformation of the light grey material, although occasionally it forms wavy bands through the dome material, indicating ductile behaviour (Fig. 12.18f). The light grey dense material has been interpreted to originate from a 'plug' of cooled, rigid magma that resided at shallow depth within the magmatic system and was partially re-heated, fragmented and incorporated the juvenile 2010 magma (Preece 2014; Preece et al. 2016). Other inclusions within the 2010 dome rocks comprise plutonic xenoliths or magmatic cumulates (Fig. 12.18e), which are composed of coarse-grained plagioclase, amphibole and clinopyroxene and interpreted to originate deep within the Merapi system (see Troll and Deegan 2023, Chap. 8), along with calc-silicate xenoliths (e.g. Preece 2014; Whitley et al. 2019, 2020; Deegan et al. 2023, Chap. 10). Formed by interaction of the 2010 magma with the surrounding crustal carbonate rocks underlying the volcano, the calc-silicate inclusions are dominated by wollastonite and diopside, giving them a characteristic green and white colour (Fig. 12.18g).

Later on 5 November, during eruption stage 5 of Komorowski et al. (2013), the volcanic activity consisted of a series of retrogressive summit dome collapses followed by a brief eruptive lull of less than 15 min (Fig. 12.12). The summit collapses produced BAFs consisting of variable components, including dense and scoriaceous 2010 lava dome clasts, light grey dense clasts, as well as variable non-juvenile lithics (Fig. 12.19a, b). The deposits often have a distinctive reddish-pink colour. The eruptive lull at the end of stage 5 allowed for the deposition of a layer consisting of orange-pink coloured fine ash with abundant accretionary lapilli (Fig. 12.19b, c). This accretionary lapilli layer formed a distinctive marker

horizon across the southern flanks of Merapi either stratigraphically above the stage 5 BAFs in the valleys or above the stage 4 'directed blast' deposits on interfluve areas.

The last phase at the eruption climax on 5 November 2010 consisted of ash venting and recurrent fountain collapses (stage 6; Komorowski et al. 2013) (Fig. 12.12), generating PDCs rich in grey scoriaceous or white pumiceous clasts, deposited stratigraphically above stage 5 deposits in Kali Gendol and the adjacent interfluve areas (Fig. 12.19a, b) (Komorowski et al. 2013; Preece 2014; Preece et al. 2016). Stage 6 deposits related to fountain collapse also contain minor amounts of juvenile lava dome fragments as well as various non-juvenile lithics. Where the stage 5 orange-pink accretionary lapilli-rich ash layer had been preserved, stage 6 deposits were readily identified in the field above this distinct marker horizon. Scattered on the surface of the scoria-rich flow deposits in and around Kali Gendol are abundant conspicuous juvenile white pumice clasts, interpreted to be associated with stage 6 Vulcanian to sub-Plinian fountain-collapse pumice-rich PDCs on 5 November, some of which may have reached distances of up to ~16 km in the Gendol valley (Komorowski et al. 2013). Juvenile white pumice lapilli were also found on the ridges north of Kinahrejo, where it was dispersed on the surface of the stage 5 accretionary lapilli-rich ash layer, scattered around the surface near to the Kinahrejo 'Forest Gate', as well as being found in reworked deposits in Kali Putih on the southwest flank of Merapi. Another type of poorly vesicular and low-K (see below) white pumice lapilli were discovered distributed on top of proximal dilute PDC deposits on a ridge north of Gunung Kendil and in Kali Putih (Preece 2014) (Fig. 12.19d).

After the climactic eruption phase on 5 November, the activity was characterised by ash venting, sporadic explosions and lava fountains (eruption stages 7 and 8; Komorowski et al. 2013). Renewed rapid lava dome growth in less than 12 h on 6 November was associated with occasional valley-confined PDCs with runout distances up to 5 km, directed towards Kali Gendol (Komorowski et al. 2013). Declining ash venting, intermittent explosions and lava fountains, deflation of the new dome, and a few valley-confined PDCs with runout distances of less than 3 km in Kali Gendol continued until 23 November (Komorowski et al. 2013). Rain-triggered, syn-eruptive lahars also occurred during this period.

12.4.3 Generation, Dynamics and Significance of High-Energy Pyroclastic Density Currents

The recognition of high-energy PDCs is regarded as one of the most significant findings related to the 2010 volcanic deposits of Merapi. Interpreted as blast-like PDCs (Komorowski et al. 2013), the deposits of the high-energy PDCs generated during the peak of the eruption on 5 November and their impact on infrastructures, buildings and trees are strikingly similar to those from historical 'directed blasts' from Montagne Pelée, Martinique (1902), Mount Lamington, Papua New Guinea (1951), Bezymianny, Russia (1956), Mount St. Helens, USA (1980) and Soufrière Hills, Montserrat (1997) (e.g. Taylor 1958; Tanguy 1994, 2004; Clarke and Voight 2000; Sparks et al. 2002; Belousov et al. 2007, 2020). However, both the volume of magma (>5 × 10^6 m^3) and the devastated area of the Merapi high-energy PDCs (Fig. 12.20) were smaller than those of these historical volcanic blasts (Komorowski et al. 2013).

While the exact generation mechanism of the 2010 high-energy PDCs has been discussed controversially (Cronin et al. 2013; Komorowski et al. 2013), there is agreement that the high-energy PDCs on 5 November 2020 formed by explosive disintegration of a rapidly growing, unstable lava dome, favoured by rapid ascent of deeper, volatile-rich magma underneath a plugged conduit which limited degassing and induced significant pressurisation in the upper conduit prior to 5 November (Surono et al. 2012; Costa et al. 2013; Cronin et al. 2013; Jousset et al. 2013b; Komorowski et al. 2013; Preece 2014; Drignon et al. 2016; Kushnir et al. 2016, 2017;

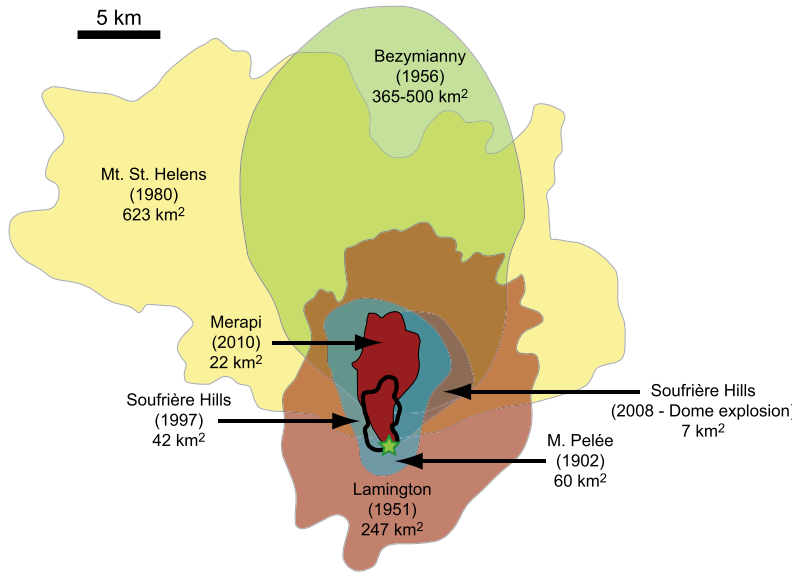

Fig. 12.20 Areas devastated by the 2010 Merapi high-energy PDCs, other historical directed blasts and a smaller directed lava dome explosion at Soufrière Hills volcano, Montserrat. After Komorowski et al. (2013)

Preece et al. 2016; Carr et al. 2020). According to Komorowski et al. (2013), the asymmetric collapse phase of the blast was short-lived and transformed into a channelised blast phase downslope, where the dynamics of the unsteady, stratified, gravity-driven currents was strongly influenced by the topography along the flow path. The currents reached heights of ~330 m and travelled at velocities of ~100 m/s within the first 3 km from the summit. Flow momentum was maintained by the morphology of the upper southeastern slopes, which led to channelling of the currents into a deep valley (Kali Gendol) towards a major constriction downslope leading to a venturi effect after the currents were deflected by the Gunung Kendil ridge (Fig. 12.12). This resulted in increased current velocities and high particle concentrations, promoting avulsion of the currents across ridges and interfluve areas into adjacent valleys, and generating high dynamic pressures (Jenkins et al. 2013; Komorowski et al. 2013). In total, a ~3–4 km wide area between Kali Kuning and Kali Woro, extending to the Merapi Golf course ~8.4 km from the summit, was affected by the 2010 high-energy PDCs (Komorowski et al. 2013).

The occurrence of high-energy PDCs related to directed explosions or blasts at the source are uncommon at Merapi. Grandjean (1931a, b, c) suggested that such currents, referred to as Peléean-type, occurred during the 1930 eruption, which wiped out villages on the volcano's western slopes and caused about 1369 fatalities (Siebert et al. 2011). The idea of directed blast-generated PDCs was not accepted indisputably though at the time (Kemmerling 1932; Escher; 1933; Neumann van Padang 1933) and, as such, the 2010 eruption is the first, where unequivocal blast-like, high-energy PDC deposits were identified in Merapi's recent history (Komorowski et al. 2013). Moreover, the 2010 high-energy PDC deposits were the first to be studied comprehensively immediately after deposition using a modern volcanological approach, providing unparalleled insights into generation, transport and depositional mechanisms as well as their impact on the surrounding area and environment (Jenkins et al. 2013; Komorowski et al. 2013). High-energy PDCs generated by laterally directed dome explosions, as observed in 2010, may be a hitherto underestimated hazard of future eruptions at Merapi that pose challenges for eruption forecasts and prediction. The events in 2010 have highlighted that such currents can be associated with rapidly growing or pressurised domes and may occur repeatedly during multistage eruptions (Komorowski et al. 2013).

12.5 Geochemistry and Petrology of the 2010 Eruptive Products

In this section, we classify the 2010 eruptive products based on bulk rock geochemistry, document their petrography and mineral chemistry, and discuss magma storage and the pre-eruptive magmatic processes and their timescales, based on a range of petrological, geochemical and isotopic data.

12.5.1 Rock Types and Classification

The 2010 deposits contain a range of juvenile lithologies, which formed at different stages of the eruption and include clasts of grey scoria lapilli, white pumice lapilli, volcanic ash and dark lapilli to block-size clasts of dense to scoriaceous dome rock of the pre-5 November lava dome (Charbonnier et al. 2013; Komorowski et al. 2013; Preece 2014; Drignon et al. 2016; Preece et al. 2016). The volumetrically most significant juvenile component in the 2010 deposits from the pre-5 November lava dome is macroscopically similar to other recent Merapi domes (Fig. 12.18a) and contains inclusions of various lithologies (Fig. 12.18e, g).

In the total alkali versus silica (TAS) diagram (Fig. 12.21a), the 2010 rocks are classed as basaltic trachyandesite and trachyandesite, while in the K_2O versus SiO_2 classification diagram (Fig. 12.21b), they fall into the high-K basaltic andesite and andesite fields. All 2010 eruptive products contain between 52.6 and 58.1 wt.% SiO_2, on a volatile-free basis (Preece 2014; Preece et al. 2016) (Fig. 12.21c). Most juvenile components have ~54.5–55.7 wt.% SiO_2, similar to the 2006 products and those from other twentieth century dome eruptions (Gertisser et al. 2012b) and fall within the high-K group that has dominated the eruptive products of Merapi since ~1900 ^{14}C y BP (Gertisser and Keller 2003; Gertisser et al. 2012b, 2023b, Chap. 6). The light grey dense inclusions in the dome rocks generally have less SiO_2-rich compositions (~52.6–55.0 wt% SiO_2) and the ash sampled from surge and fall deposits is generally more SiO_2-rich (55.1–58.1 wt.% SiO_2), extending into the trachyandesite and high-K andesite field, respectively (Fig. 12.21a). Selected bulk-rock major element analyses of the 2010 eruptive products are presented in Table 12.2.

12.5.2 Petrography and Mineral Chemistry

The magmatic products of the 2010 eruption, including the 2010 dome lava and light grey dense inclusions, are seriate to porphyritic, with phenocrysts (2000–500 μm; size range following Preece 2014) and microphenocrysts (500–50 μm) set in a groundmass that may be predominantly crystalline (microlites <50 μm) or contain abundant glass (Fig. 12.22a–c). The mineral cargo typically includes plagioclase (and alkali) feldspar, clinopyroxene, orthopyroxene, amphibole, which may be megacrystic, Fe-Ti oxides and accessory apatite. Coarse-grained plutonic xenoliths (magmatic cumulates) in the pre-5 November dome are dominated by plagioclase, clinopyroxene and amphibole (Fig. 12.22d). Additionally, cristobalite and biotite are present in the light grey inclusions in the 2010 lava dome (Fig. 12.22e, f) (Costa et al. 2013; Preece 2014). There are large variations in mineral size, textures and compositions as summarised below from Preece (2014), with additional data from Costa et al. (2013) and Li et al. (2021), as indicated.

Feldspar is always present as phenocrysts, microphenocrysts and microlites. Phenocrysts and microphenocrysts are wide ranging in composition between $An_{25}Ab_{70}Or_5$ and $An_{91}Ab_9Or_{<1}$ (Fig. 12.23a-I). Phenocrysts may be normally, reversely or oscillatory zoned, have sieve-textured cores or have very high-An (up to An_{91}) unzoned cores, with lower-An rims. Rims often contain ~40–50 mol.% An. Microlites are generally more albitic but may contain up to ~84 mol.% An. Plagioclase microlites are often mantled by alkali element-rich rims of anorthoclase and more K-rich alkali feldspar (sanidine). Microlite compositions range from $An_1Ab_{41}Or_{58}$ (alkali feldspar) to $An_{84}Ab_{16}Or_{<1}$ (plagioclase) (Fig. 12.23a-II). Microlites from all

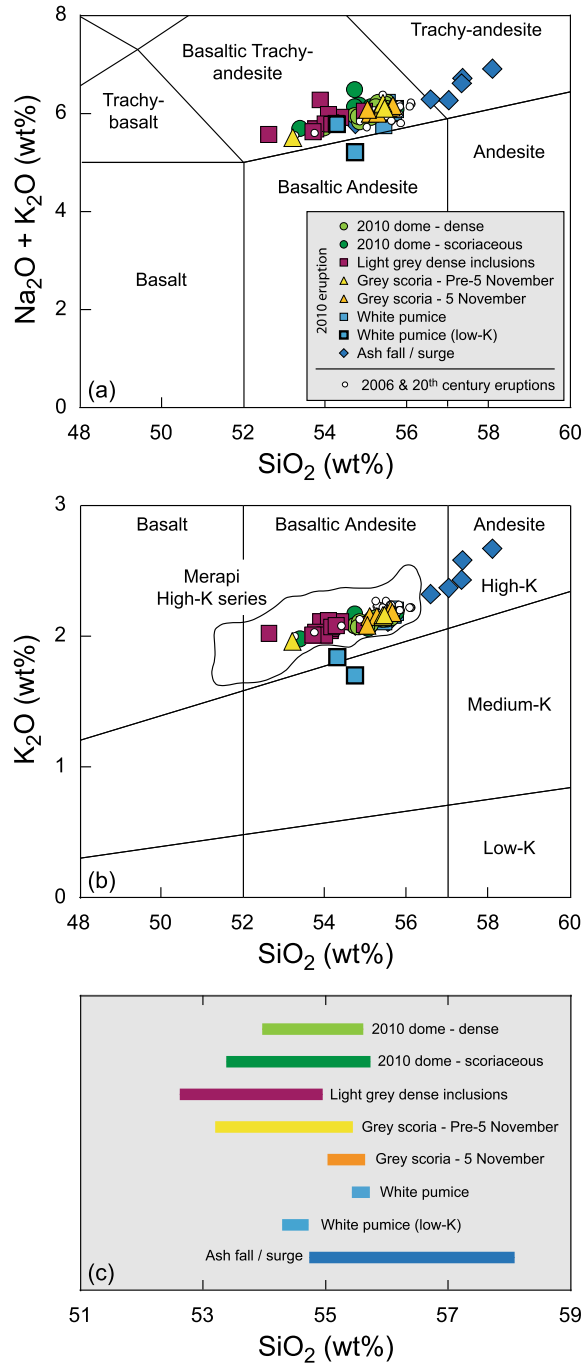

Fig. 12.21 **a** Total alkali versus SiO_2 (TAS) and **b** K_2O versus SiO_2 classification diagrams (Le Maitre et al. 2002) for the 2010 eruptive products. The dashed outline in **b** denotes the compositional field of the Merapi high-K series, as defined by Gertisser et al. (2012b). **c** SiO_2 range of the different lithologies erupted in 2010. All analyses are recalculated to 100 wt%, free of volatiles. *Data sources* 2010 eruption (Preece 2014; Preece et al. 2014); 2006 and twentieth century eruptions (Gertisser et al. 2012b; Preece et al. 2013)

lithologies possess a similar overall range of compositions, however white pumice microlites are generally more albitic and those from the light grey inclusions are predominantly alkali-rich.

Clinopyroxene is present as phenocrysts, microphenocrysts and microlites in all 2010 products, and orthopyroxene is a common microphenocryst and microlite phase. Crystals of anhedral to subhedral orthopyroxene are

Table 12.2 Selected whole-rock major element analyses of the 2010 eruptive products. Compiled from Preece (2014)

Sample	M11-80	M13-41	M11-130	M13-29	M13-23	M13-43	M11-85	M13-7
Type[a]	A	B	C	D	E	F	G	H
SiO_2	54.87	54.67	53.38	55.43	54.84	55.45	53.81	56.41
TiO_2	0.71	0.74	0.79	0.72	0.72	0.70	0.79	0.54
Al_2O_3	18.98	19.19	19.14	19.22	19.35	19.24	18.60	19.72
$Fe_2O_3^T$	7.41	8.03	8.48	7.76	7.77	7.62	8.33	6.01
MnO	0.19	0.19	0.20	0.19	0.19	0.19	0.18	0.14
MgO	2.31	2.50	2.80	2.37	2.38	2.33	2.99	1.63
CaO	7.86	8.15	8.70	7.88	8.03	7.84	8.18	7.16
Na_2O	3.89	4.04	3.62	3.94	3.99	4.04	3.49	4.08
K_2O	2.12	2.08	2.00	2.16	2.07	2.16	1.67	2.39
P_2O_5	0.32	0.31	0.30	0.30	0.32	0.30	0.28	0.30
LOI	0.02	0.40	-0.26	0.33	0.01	0.27	0.78	1.55
Total	98.68	100.30	99.15	100.30	99.67	100.14	99.10	99.93

[a] Sample type: A = 2010 dome—dense; B = 2010 dome—scoriaceous; C—Light grey dense inclusions; D = Grey scoria—pre-5 November; E = Grey scoria—5 November; F = White pumice; G = White pumice (low-K); H = Ash fall/surge

sometimes rimmed by clinopyroxene. Phenocrysts may be zoned, commonly with oscillatory or sectoral zoning (Costa et al. 2013; Li et al. 2021) or unzoned and often host silicate melt inclusions, as well as inclusions of magnetite, plagioclase and apatite. Clinopyroxene phenocrysts are classed as augite and diopside ($Wo_{39-50}En_{36-46}Fs_{10-19}$), following the scheme of Morimoto (1988) (Fig. 12.23b-I), with between 0.4 and 8.9 wt% Al_2O_3, although the majority contain between 1.5 and 2.5 wt% and have Mg# 61–85, with most between 75 and 85 (Mg# = 100 × Mg / (Mg + Fe^{2+}). Orthopyroxene phenocrysts are classed as enstatite ($Wo_{0.2-0.3}En_{57-70}Fs_{27-39}$) (Fig. 12.23b-I). Microphenocrysts and microlites generally have more variable compositions compared to the phenocrysts. They are usually augite and diopside ($Wo_{40-50}En_{35-45}Fs_{13-21}$) (Fig. 12.23b-II), with 0.8–7.6 wt% Al_2O_3 and Mg# 65–81, with most between Mg# 70–80. Less common pigeonite, and crystals with higher Fe content, classed as hedenbergite ($Wo_{49-50}En_{8-21}Fs_{29-41}$) and containing 1.2–2.6 wt% Al_2O_3 and Mg# 19–47, also occur (Fig. 12.23b-II). Hedenbergite crystals were exclusively found in the dome lava, near a calc-silicate xenolith and were bright green when viewed in plane-polarised light. Orthopyroxene microlites ($Wo_{0.5-9}En_{45-81}Fs_{16-53}$) are enstatite and ferrosilite (Fig. 12.23b-II). Orthopyroxene microphenocrysts and microlites contain between 0.2 and 3.6 wt% Al_2O_3 and have Mg# from 54 to 94, although the majority have Mg# ~65–75. The crystals with orthopyroxene cores and clinopyroxene rims plot within the same Wo-En-Fs space as the other pyroxene crystals.

Amphibole is present in all samples as phenocrysts (Fig. 12.23c-I) and microphenocrysts (Fig. 12.23c-II) but is absent as groundmass microlites. Amphibole is titanian magnesiohastingsite, following the classification of Leake et al. (1997), based on 23 oxygens with with Fe^{2+}/Fe^{3+} estimation assuming 13 cations except Ca, Na and K. Crystals may be homogeneous in composition or zoned, often with rims of higher Al_2O_3 and MgO, and lower SiO_2, K_2O and FeO compared to the cores (see also Costa et al. 2013). The overall range of Al_2O_3 content is 10.0–14.9 wt%, with Mg# ranging between 49 and 58, with a cluster at ~62–68. Of the crystals with Mg# >68, 70% are phenocrysts from the white pumice, with the rest being phenocrysts from the light grey inclusions. More than 55% of the crystals with Mg# <62 are dense dome

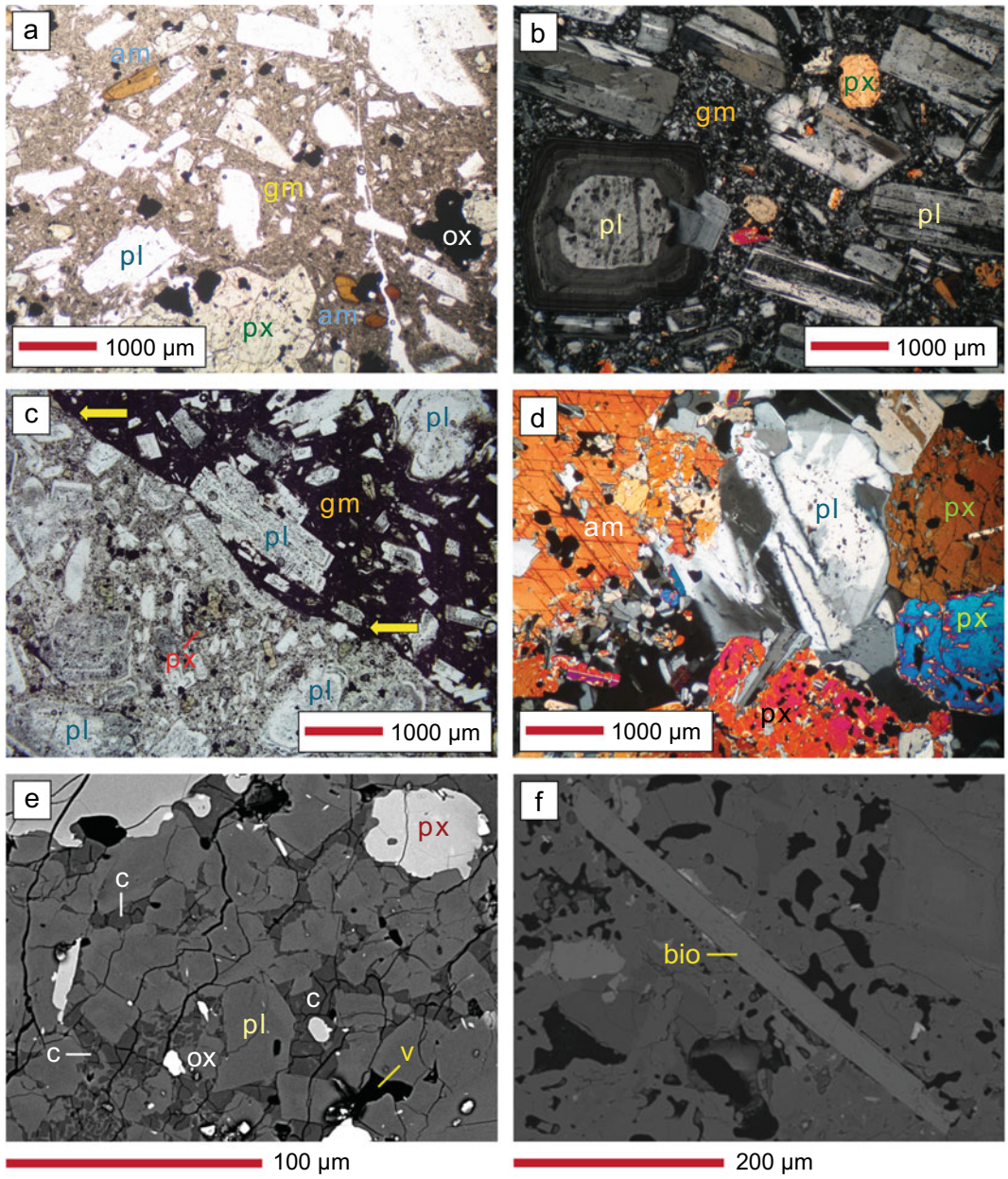

Fig. 12.22 Photomicrographs and backscattered electron (BSE) images of Merapi 2010 eruptive products. **a** Basaltic andesite of the 2010 lava dome, characterised by plagioclase, pyroxene (both clino- and orthopyroxene, Ti-magnetite and amphibole (both fresh and with breakdown rims) in a moderately crystalline groundmass (PPL). **b** Light-grey dense basaltic andesite inclusion containing complexly zoned plagioclase crystals, amphibole (rare and always with pronounced breakdown rims) and coarse grained, crystalline groundmass (X Nicols). **c** Contact relationship between light-grey dense inclusion (lower left) and 2010 dome lava (upper right) (X Nicols). **d** Coarse-grained plutonic xenolith (magmatic cumulate) consisting of plagioclase, clinopyroxene and amphibole (X Nicols). **e–f** BSE images of the light-grey dense inclusions in the 2010 lava dome: **e** Highly crystalline, micro-vesicular groundmass with plagioclase, pyroxene, Ti-magnetite and abundant cristobalite. **f** Late-stage biotite. Abbreviations used: am = amphibole, pl = plagioclase, px = pyroxene, ox = oxide (Ti-magnetite), c = cristobalite, bio = biotite, gm = groundmass, v = vesicles

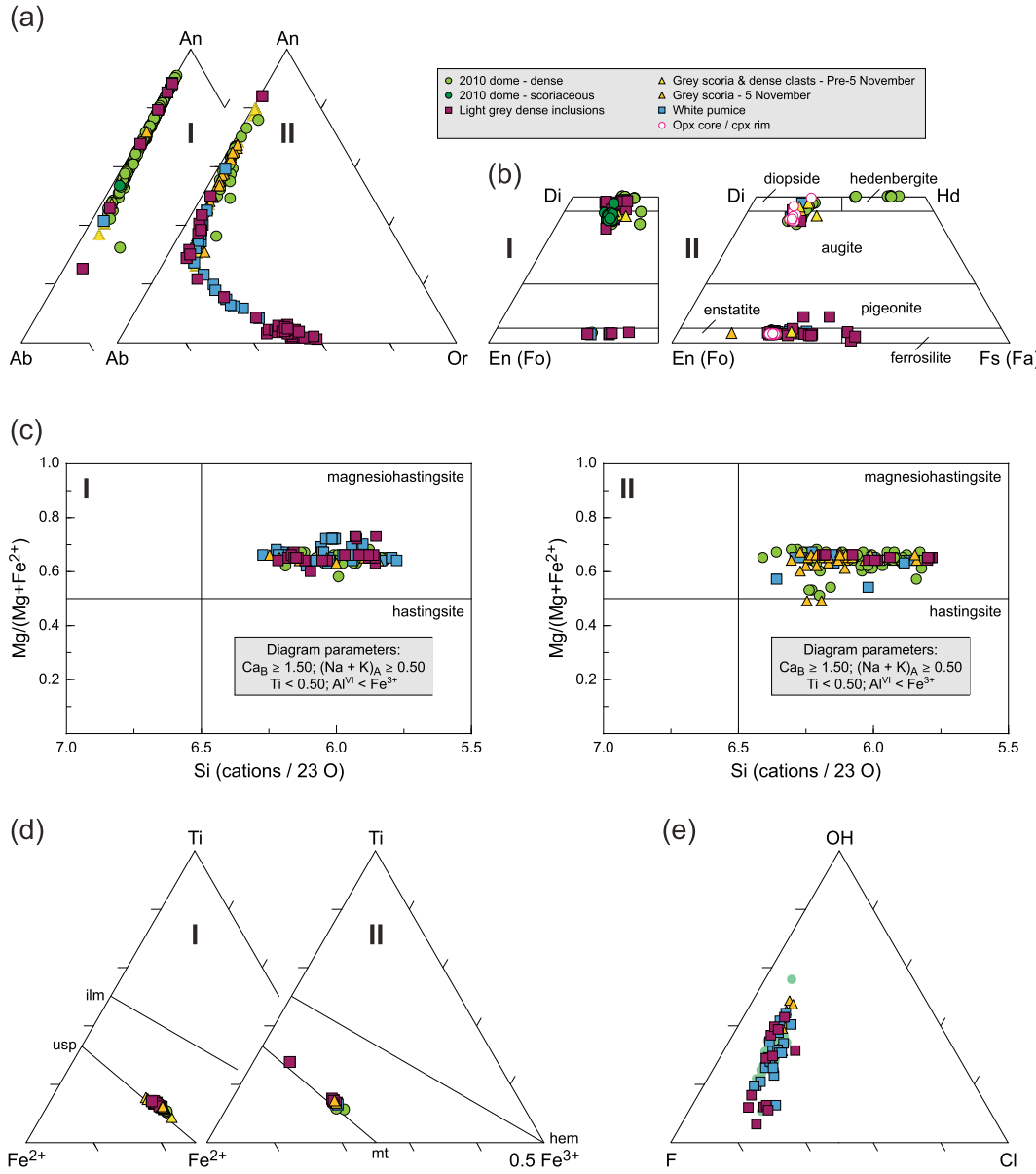

Fig. 12.23 Mineral compositions of phenocrysts, microphenocrysts and microlites from various 2010 eruptive products. **a** (I) Feldspar phenocrysts and microphenocrysts; (II) feldspar microlites. **b** (I) Pyroxene phenocrysts; (II) pyroxene microphenocrysts, microlites and crystals with opx cores/cpx rims. **c** (I) Amphibole phenocrysts; (II) amphibole microphenocrysts. **d** (I) Fe-Ti oxide microphenocrysts; (II) Fe-Ti oxide microlites. **e** Ternary OH-F-Cl plot of apatite compositions. *Data source* Preece (2014)

microphenocrysts. Amphiboles may be surrounded by breakdown reaction rims, composed of anhydrous minerals plagioclase, pyroxene (or olivine) and Fe-Ti oxides. However, amphiboles from 2010 frequently do not possess breakdown reaction rims.

Fe-Ti oxides are present in all samples as anhedral and irregularly shaped microphenocrysts (Fig. 12.23d-I) and microlites (Fig. 12.23d-II), as well as inclusions within clinopyroxene phenocrysts. All Fe-Ti oxides are titanomagnetite. Crystals range in ulvöspinel

content from 18–59 mol.%, although most range from ~22 to 35 mol.% (Fig. 12.23d). Titanomagnetite is often exsolved to various extents showing trellis-type exsolution, consisting of ilmenite lamellae parallel to the {111} planes of the titanomagnetite host (Buddington and Lindsley 1964; Haggerty 1993). Rare pyrrhotite inclusions have also been observed within magnetite, amphibole and clinopyroxene hosts.

Apatite crystals occur in trace amounts (<1 vol.%) as inclusions within clinopyroxene, plagioclase and amphibole phenocrysts or as microphenocrysts or groundmass microlites. Crystals are F-rich (2.8–5.4 wt% F, with the majority containing ~3–4 wt% F) and contain 0.6–1.4 wt% Cl (Fig. 12.23e). Data obtained by Li et al. (2021) also suggest the presence of apatite crystals with lower F contents (1.1–2.3 wt %), a similar range of Cl concentrations (0.4–1.2 wt%), and H_2O concentrations of 0.4–1.0 wt%. Some CO_2-rich apatite inclusions in amphibole, with concentrations up to 1.6 wt%, were also found.

The presence of biotite in the 2010 eruption products—a mineral that has not previously been observed at Merapi—was noted by Costa et al. (2013) and Preece (2014). Preece (2014) documented biotite within the light grey inclusions (Fig. 12.22f), alongside a crystalline silica phase, cristobalite. Biotite contains 0.5–3.8 wt% F, 0.1–0.3 wt% Cl, between 11.9 and 15.6 wt% FeO, with Mg# 63–70, and has been interpreted as a late-stage magmatic phase that crystallised from highly evolved residual melt resulting from extensive groundmass crystallisation in the light grey inclusions (Preece 2014). Cristobalite is observed to fill small vesicles and is pervasive within the groundmass, often with 'fish-scale' cracked morphology or a microbotryoidal texture (Fig. 12.22e).

12.5.3 Magma Storage and Magmatic Processes

The crystallisation depths of magma involved in the 2010 eruption were determined using multiple approaches, including thermobarometry, thermodynamic modelling, volatiles in melt inclusions, pumice glass and apatite crystals, experimental petrology and fluid inclusion barometry (Costa et al. 2013; Erdmann et al. 2014, 2016; Preece 2014; Preece et al. 2014; Drignon et al. 2016; Whitley et al. 2020; Li et al. 2021) that complemented geophysical investigations (Budi-Santoso et al. 2013; Saepuloh et al. 2013). Further insights into the pre-eruptive processes operating in the magma plumbing system were gleaned from mineral-scale elemental and oxygen isotopic variations (Borisova et al. 2013, 2016; Costa et al. 2013; Preece 2014; Preece et al. 2014; Erdmann et al. 2014) and major element, trace element and volatile concentrations in melt inclusions (Preece 2014; Preece et al. 2014) and apatite crystals (Li et al. 2021) that document a complex interplay of closed-system and open-system magmatic processes, including magma replenishment and mingling/mixing, assimilation of limestone and magmatic degassing. Bulk rock major element, trace element, and isotope (Sr, Nd, Pb, O, U-series) geochemistry have highlighted the similarity between the 2010 rock compositions and those of previous eruptions (Borisova et al. 2013; Preece 2014; Drignon et al. 2016; Preece et al. 2016; Handley et al. 2018), suggesting that similar processes and magma types drive eruptions at Merapi and that most Merapi magmas are potentially capable of producing explosive eruptions (Costa et al. 2013). Groundmass textures, glass and microlite compositions of the 2010 eruptive products (Preece 2014; Drignon et al. 2016; Preece et al. 2016) record the tapping of magma from depths of several kilometres, the final stages of magma ascent towards the surface, and the processes closest to the onset of and during eruption, as described in Preece et al. (2023, Chap. 9).

Based on application of different geothermobarometry and MELTS modelling, Costa et al. (2013) proposed at least three crystallisation zones at depths of (1) 30 ± 3 km, as evidenced by some amphibole compositions and high-Al clinopyroxene as well as by the presence of H_2O- and CO_2-rich apatite in amphibole and geobarometrical calculations that indicate comparable

crystallisation depths (Li et al. 2021), (2) 13 ± 2 km, where other amphiboles, high-Al clinopyroxene and high-An plagioclase crystallised, with very An-rich plagioclase linked to assimilation of limestone or, alternatively, to crystallisation from hydrous mafic magma (Preece 2014; Borisova et al. 2016), and (3) less than 10 km, where extensive crystallisation produced low-Al clinopyroxene, orthopyroxene and more Ab-rich plagioclase. Erdmann et al. (2014) concluded that amphibole crystallised at pressures of 200–800 MPa, corresponding to depths between ~9 and 28 km, assuming crustal densities of 2.242 and 2.9 g/cm^3 at depths above and below 10 km (Widiyantoro et al. 2018). Preece et al. (2014) presented geobarometrical calculations that show that clinopyroxene crystallised at depths of up to ~20 km, with the greatest depths associated with phenocrysts from white pumice. This is consistent with results from amphibole barometry (Preece 2014), which also indicated that the greatest amphibole crystallisation depths are from white pumice samples. Preece et al. (2014) further suggested that melt inclusions equilibrated during shallower storage and/or ascent, at depths of ~0.6–9.7 km, based on H_2O and CO_2 contents (see also Li et al. 2021). H_2O concentrations range from up to 3.94 wt% in grey scoria and up to 3.91 wt% in white pumice to <3.62 wt% in dense dome clasts, while CO_2 concentrations are generally <200 ppm but reach up to 695 ppm and, in some cases, up to 3000 ppm in white pumice. The presence of an exsolved brine phase was proposed based on the occurrence of melt inclusions enriched in Li and B, that show uniform buffered Cl concentrations (Preece et al. 2014). In a subsequent study, Erdmann et al. (2016) presented phase equilibrium experiments to infer crystallisation at more than 100–200 (± 75) MPa in a shallow magma storage zone, corresponding to depths of more than 4.5 to ~9 (± 3) km. This is broadly consistent with results from pumice glass water concentration measurements (Drignon et al. 2016) that indicate tapping of magma from depths of several kilometres. Fluid inclusion barometry in calc-silicate xenoliths also record low pressures of less than ~100 MPa, indicating that the fluid inclusions formed at shallow crustal depths or re-equilibrated during ascent (Whitley et al. 2020).

Despite the variations in the published models, there is an emerging consensus of the existence of multiple distinct or more continuous interlinked magma storage and crystallisation zones throughout the entire crust beneath Merapi prior to the 2010 eruption. Deeper and mid-crustal crystallisation were dominated by distinct types of amphiboles, high-Al clinopyroxene, and high-An plagioclase, while a more feldspar-dominated crystallisation regime existed at shallow crustal levels, where more Ab-rich plagioclase crystallised alongside low-Al clinopyroxene and, possibly, orthopyroxene. The shallow, uppermost crystallisation region at 10 km or less is thought to have consisted of a largely degassed and highly crystalline mush (Costa et al. 2013). This region is also located within the carbonate dominated upper crust beneath Merapi, where crustal carbonate assimilation plays an important role (Deegan et al. 2023, Chap. 10), although this process may extend to slightly deeper levels in the model of Costa et al. (2013). There have been suggestions that there were higher than usual rates of crustal carbonate assimilation and associated CO_2 addition to the volcanic system that may have contributed to the unusual explosivity of the 2010 eruption (Borisova et al. 2013; Costa et al. 2013), although U-series and radiogenic isotopic data (Handley et al. 2018) did not support such an interpretation. Multiple lines of evidence point towards interaction between degassed magma stored at shallower levels and hotter, deeper, more volatile-rich magma during the 2010 eruption (Surono et al. 2012; Costa et al. 2013; Preece 2014; Preece et al. 2014). In a general model, it may be envisaged that interaction between magma stored in various parts of the plumbing system plays a fundamental role in determining the eruptive behaviour of Merapi. Typical dome forming eruptions may predominantly be fed by the shallower crystal-rich or mush zones, in which magmas may have reacted intensively with carbonate country rock. Crystal mush rejuvenation may be triggered by reheating and remelting that result from small volumes of ascending hotter magma from depth that are partially or fully

stalled by the crystal-rich or mush zones that formed during previous intrusions into the shallow plumbing system (Costa et al. 2013). By contrast, a larger influx of deep magma that replenishes the shallower magma system at relatively short timescales and associated CO_2 fluxing (e.g. Caricchi et al. 2018) may be a controlling factor driving larger scale, explosive eruptions as in 2010. In such a scenario, the shallower crystal-rich magma system may get disrupted and eventually overwhelmed by the arrival of deep magma. This process may be capable of intensifying limestone assimilation (Costa et al. 2013), although there is little isotopic evidence for the latter when comparing the 2006 and 2010 eruptions (Handley et al. 2018). Subsequent processes include rapid magma ascent, accompanying closed-system degassing and, as inferred for the 2010 eruption, accumulation of ascending magma beneath a plugged conduit that builds up pressure in the uppermost conduit (Costa et al. 2013; Komorowski et al. 2013; Preece 2014; Preece et al. 2016). The light grey dense material in the 2010 dome rocks has been interpreted to originate from such a plug of cooled, rigid magma that resided at very shallow depth within the magmatic system and was partially reheated, fragmented and incorporated into the 2010 magma (Preece 2014; Preece et al. 2016, 2023, Chap. 9). If such a model is correct, magma replenishment and interaction with shallower crystal mush may exert important control on the continuum of eruption styles at Merapi that range from effusive, dome-forming eruptions to larger magnitude explosive eruptions.

12.5.4 Timescales of Magmatic Processes

An understanding of the timescales associated with the dynamic processes in the pre-and syn-eruptive 2010 magma system is fundamental to improved hazard assessment and interpretation of geophysical and geochemical monitoring signals. Based on Fe–Mg diffusion zoning in clinopyroxene, Costa et al. (2013) suggested that the inferred influx of hot and volatile-rich magma from depth into the shallower magma storage zones occurred up to 1.6–2.7 years before the eruption, while Borisova et al. (2016) presented ^{18}O diffusion data in plagioclase to propose a time span for plagioclase crystallisation prior to the 2010 eruption of up to 34 years. These results are broadly in line with those of a detailed study of U-series disequilibrium (Handley et al. 2018), where ^{226}Ra and ^{210}Pb excesses ($(^{226}Ra/^{230}Th)$ and $(^{210}Pb/^{226}Ra) > 1$) observed in plagioclase separates from the 2010 eruption indicate that a proportion of the plagioclase grew within the decades before the eruption. However, none of these processes, which may have significantly predated the eruption, left an obvious signal in the monitoring record and, in the latter cases, may partly record processes associated with previous eruptive events. At the time of eruption, the 2010 samples were depleted in ^{210}Po, a nuclide that partitions efficiently into an exsolving volatile phase and is almost completely lost during eruption, relative to ^{210}Pb ($(^{210}Po/^{210}Pb) < 1$), but variably degassed, with the degree of degassing strongly related to sample texture and eruption phase (Handley et al. 2018). ^{210}Po ingrowth calculations (Handley et al. 2018) suggested that initial intrusion into the shallower magma system occurred several weeks to a few months prior to the initial explosions on 26 October 2010, which broadly coincides with the increase of various monitoring parameters (see Fig. 12.1).

The 2010 samples show a wide range in initial $(^{210}Pb/^{226}Ra)$ activity ratios within a single eruption at Merapi, comparable to the range of ratios of the preceding eruption in 2006 and those reported for the time between 1981 and 1995 (Gauthier and Condomines 1999). They are largely characterised by ^{210}Pb deficits ($(^{210}Pb/^{226}Ra) < 1$) that have been interpreted to result from degassing of the intermediate nuclide ^{222}Rn over $\sim$ 0–3 years before eruption, a time span that is slightly less than for samples from the dome-forming 2006 eruption (Handley et al. 2018). A rock sample representing the onset of the 2010 eruption on 26 October (Stage 2) shows a significant ^{210}Pb deficit ($(^{210}Pb/^{226}Ra)_0 = 0.79$). This is followed by a change to near equilibrium $(^{210}Pb/^{226}Ra)_0$ values for samples

extruded during the rapid dome growth and destruction period between the 29 October to 4 November (stage 3) and emplaced in stage 4, which includes a sample of the light grey dense inclusions in the main 2010 lava dome. The white pumice sample erupted during the latest stages of the climactic phase of 5 November (stage 6) lies within uncertainty of the stage 4 emplaced samples with a ^{210}Pb deficit of 0.92. Samples from the climactic phase of the eruption therefore have smaller ^{210}Pb deficits than the analysed light grey dense crystalline inclusion ('plug') sample and the samples from the 2006 eruption, which also supports faster ascent and less time for degassing during the main phases of the 2010 eruption. The longer-term magma degassing processes described here, caused by changes in the subsurface conditions, may potentially be detectable through soil radon emission monitoring.

12.6 Eruption Effects, Impact and Recovery

The 2010 eruption had profound effects on the natural environment, built infrastructures and population, as well as all aspects of community livelihood (see also Lavigne et al. 2023, Chap. 2).

The morphology of the summit area of Merapi has seen continuous changes over the past years, decades and centuries. Explosive activity has produced craters and deep depressions, or breaches, at the top of the volcano or in the crater walls, which formed repeatedly by explosive activity or partial edifice collapses. Collapses have removed portions of the uppermost, often hydrothermally altered and weakened volcanic edifice, and have been promoted by dome growth and associated phenomena which may exert strain on the summit crater walls (e.g. Beauducel et al. 2000; Voight et al. 2000; Ratdomopurbo et al. 2013; Solikhin et al. 2015).

The 2010 eruption produced a large summit crater open to the SE (Fig. 12.24a), towards the headwaters of Kali Gendol, in an area previously occupied by the pre-2010 dome area and the remains of the 2006 lava dome, removing and incising lava domes and flows that were emplaced during the twentieth century (Solikhin et al. 2015). The initial explosions on 26 October produced a 200 m wide and 100 m deep crater with a horseshoe-shaped morphology, which was enlarged (350 × 400 m wide) during the 5 November paroxysm (Surono et al. 2012; Komorowski et al. 2013; Solikhin et al. 2015). In total, the summit area of Merapi lost some 10–19 × 10^6 m^3 of material (Kubanek et al. 2015; Solikhin et al. 2015). New lava domes grew rapidly inside the newly formed and enlarged crater. The earlier, pre-5 November dome was completely destroyed by laterally directed dome explosions and retrogressive gravitational collapse on 5 November (Komorowski et al. 2013), while the later lava extrusion on 6 November produced a dome ~200 m in diameter that, since then, has seen further morphological changes by subsequent lava extrusion and short explosive events (e.g. Darmawan et al. 2023, Chap. 15). The downslope extension of the crater, the Gendol breach (Fig. 12.24a), is a SE-NW trending summit scar that originally formed during the 1872 eruption (Ratdomopurbo et al. 2013) and opens the upper SE slope of Merapi towards Kali Gendol. The canyon of the Gendol breach was notably lengthened and deepened during the 2010 eruption, forming a major pathway for future dome related PDCs (Gertisser et al. 2011; Solikhin et al. 2015). Since 2010, the steep, hydrothermally altered and unstable crater and canyon walls have been subject to rockfalls and landslides, while the unconsolidated eruption deposits and the exposed hydrothermally altered wall rocks have continued to feed lahars (Solikhin et al. 2015).

The PDCs generated throughout the 2010 eruption were highly destructive, devastating an area of 22 km^2 on the densely populated southern flank of Merapi (Jenkins et al. 2013; Komorowski et al. 2013). The ground was scoured, and vegetation and soil stripped by PDCs down to 1300 m elevation (Solikhin et al. 2015). Trees were felled and uprooted, splintered, abraded on the upstream side and lightly charred up to distances of ~6 to 7 km by the passage of the high-energy PDC of 5 November. North of Kinahrejo, the orientation of

Fig. 12.24 Impact of the 2010 eruption. **a** Summit crater, open to the SE, formed during the 2010 eruption, with its downslope extension, the Gendol breach. **b** Ridges north of Kinahrejo with scoured soil and blown down trees. Tree orientation indicates flow direction from Kali Gendol towards Kinahrejo. **c** Remnants of house in Kinahrejo, destroyed by Stage 4 'blasts'. Walls remained partly standing as they were partially protected by local topography. **d** House destroyed by overbank deposits in Wukirsari near Bakalan, Lower K. Gendol. **e** Overturned and burnt car in Kinahrejo, covered by Stage 4 lapilli and blocks. **f** Bridge over Kali Opak on Merapi's south flank destroyed by lahars. For locations, see Figs. 12.1 and 12.14. *Photo credit* R. Gertisser, K. Preece

blown down trees indicates flow direction from Kali Gendol towards Kinahrejo (Fig. 12.24b). Unburnt vegetation frequently occurred at the base of the 5 November deposits (Komorowski et al. 2013). PDCs damaged or destroyed more than 2200 buildings along their flow paths up

to ~16 km from the source (Jenkins et al. 2013; Komorowski et al. 2013). About 150 buildings (and other objects) were damaged by PDCs associated with the early phases of the eruption; with most buildings destroyed by high-energy and overbank PDCs of 5 November (Jenkins et al. 2013) (Fig. 12.24c–e).

Using empirical damage data and calculations of material and structural resistance to lateral force, Jenkins et al. (2013) estimated dynamic pressures associated with the 5 November high-energy PDCs that exceeded 15 kPa at more than 6 km from the source and rapidly decreased towards the end of the PDC runout over a distance of less than 1 km. Temperatures of the high-energy PDCs were low, reaching ~200–300 °C, based on observed thermal damage to buildings and vegetation as well as medical observations (Jenkins et al. 2013; Komorowski et al. 2013; Baxter et al. 2017). This temperature range was subsequently confirmed by charcoal surface reflectance, which suggested a minimum temperature of 240–320 °C; a few charcoal fragments yielded temperatures up to 450 °C (Trolese et al. 2018). Charring temperatures were similar in proximal and distal high-energy PDC deposits, and significantly lower than those of the destroyed dome rock at source, indicating a rapid decrease in PDC temperature soon after its inception (Trolese et al. 2018).

Fatalities were caused over the entire length of the 2010 PDC runouts. Few people were killed directly by high-energy PDCs in proximal areas, due to the evacuation efforts by the Indonesian authorities (Surono et al. 2012; Komorowski et al. 2013). Most fatalities occurred more than 12 km from the volcano, as people were evacuating and caught in overbank PDCs and surges that spilled into villages after they were discharged from nearby Kali Gendol (Jenkins et al. 2013; Komorowski et al. 2013). At these distances, PDC dynamic pressures and temperatures were relatively low, causing little structural damage, apart from the village of Bakalan that was completely buried and destroyed by the overbank PDCs (e.g. Charbonnier et al. 2013). Fatalities occurred both outside and inside of buildings, partly because of building design that allowed PDCs to rapidly enter buildings (Jenkins et al. 2013; Komorowski et al. 2013).

At a greater distance from Merapi, the 2010 eruption led to major air traffic disruptions due to ash emissions (Picquout et al. 2013; Lavigne et al. 2023, Chap. 2). Adisucipto International Airport in Yogyakarta closed for a period of 15 days between 5 and 20 November, followed by a period of one month during which air traffic operations returned to pre-eruption levels. Other airports in Java, including Jakarta's Soekarno-Hatta International Airport were also affected by air traffic disturbances. Consequently, several airlines suspended their flights from and into Yogyakarta, while others adapted to the situation by transferring their flights to other airports. The Merapi crisis in 2010 revealed that, at the time, Indonesia had no suitable alternative means of transport to deal with airport closure during volcanic eruptions (Picquout et al. 2013).

Impact on the physical environment, built infrastructures and population continued for several years after the eruption (de Bélizal et al. 2013; Thouret et al. 2023, Chap. 17). Rain-induced lahars, including hyperconcentrated stream and debris flows, became a major hazard, with lahar occurrences in almost all major drainages. Lahar impact after the 2010 eruption was considerably larger than after previous eruptions due to the significantly larger volume of pyroclastic deposits (~36.3–80 × 10^6 m^3) on the flanks of the volcano. The first lahars associated with the 2010 eruption were syn-eruptive and hot, with 45 events recorded between 27 October and 3 December 2010. During the 2010–2011 rainy season, a total of 240 lahar occurrences were recorded (de Bélizal et al. 2013), notably in the Putih, Gendol, Boyong, Ladon and Apu river valleys, increasing to 429 events by March 2014. Lahar runouts exceeded 15 km and even reached Yogyakarta ~25 km south of Merapi on three occasions. Lahar filling of downstream river channels, followed by overbank flow into surrounding fields and villages, as well as riverbed and riverbank erosion, caused considerable damage. In total, 14 Sabo dams and 21 bridges were destroyed (Fig. 12.24f), affecting the road network on Merapi's southern and western flanks (de Bélizal et al. 2013). 860 houses were damaged

by burial with sediment, failure of walls and lahar infiltration into buildings, with the scale of damage related to building quality (de Bélizal et al. 2013; Jenkins et al. 2015). Weak masonry houses were destroyed by dilute lahars that travelled at low velocities (<3 m/s) and generated low dynamic pressures (<5 kPa), while stronger rubble stone buildings were able to resist higher lahar velocities (<6 m/s) and dynamic pressures (<20 kPa) (Jenkins et al. 2015). The number of direct fatalities remained very low, but more than 3000 people lost their home after the first rainy season following the eruption due to the damaging effects of lahars (Global Volcanism Program 2013).

Many areas on Merapi's south flank that were affected by PDCs have remained largely uninhabitable. Nearly 400,000 people were displaced from their homes as a result of the eruption (Mei et al. 2013; Lavigne et al. 2023, Chap. 2). After the eruption, temporary dwellings (Indon. = huntara) were constructed outside the danger zone, supported by the Indonesian government, NGOs and the private sector, among others. The largest of these settlements contained more than 1000 households (Maly and Nareswari 2015). Although some residents stayed in these temporary settlements, the launch of a housing reconstruction programme (Rekompak—REhabilitasi dan ReKOnstruksi Masyarakat dan Permukiman berbAsis Komunitas; Engl.: Community-Based Settlement Rehabilitation and Reconstruction) led to building of permanent homes, particularly in collective resettlement areas (Indon. = huntap). After completion in 2014, more than 80% of the 2000 new houses built within the framework of the Rekompak project in the most affected Cangkringan District, Slemen Regency were constructed in these collective resettlement areas (Maly and Nareswari 2015; Mei et al. 2016). The existing houses, infrastructures and facilities in two of these settlements, Huntap Kuwang and Huntap Plosokerep, were still in decent conditions, meeting the needs of the local community (Mei et al. 2016). While most residents appeared to be satisfied with their living conditions (Mei et al. 2016), further research is required to understand more fully understand the perception of residents in different settlements regarding their ability to complete or extend their homes, support of community livelihood and continued occupation of the sites (Maly and Nareswari 2015).

In the Kaliadem-Kinahrejo area, facilities and activities for attracting day-trippers and visitors to the area sprang up soon after the eruption and currently still exist there (see also Lavigne et al. 2023, Chap. 2). These include food stalls and souvenir shops, a small museum, displays of items damaged during the 2010 eruption, designated visitor sites, such as the bunker in Kaliadem where two people perished during the 2006 eruption, and activities including guided adventure tours across the area destroyed by the 2010 eruption (Fig. 12.25a–e). As after every eruption of Merapi, sand quarrying activities of PDC and lahar deposits have increased in the valleys around the volcano after the 2010 eruption, particularly in, but not limited to the Gendol valley (Fig. 12.25f). Such deposits have been a substantial natural resource that has supported the local economy and regional development (e.g. de Bélizal et al. 2011, 2013; Lavigne et al. 2023, Chap. 2). The Sleman District alone had mining tax revenues of 63 and 600 million IDR in 1999 and 2007, respectively (Ikhsan et al. 2010). At the same time, sand quarrying puts the people who mine the deposits at risk (de Bélizal et al. 2011), as demonstrated in 2016 and 2017, when several trucks were swept down Kali Bebeng on Merapi's south-west flank, and at least eight miners were killed, and eight others injured following a landslide. It also has negative environmental and ecological effects, and necessitates sediment disaster management efforts, together with regulated sustainable sediment resource management and measures to stabilise riverbeds to reduce riverbed degradation (Ikhsan et al. 2010). By contrast, riverbed exploitation by sand extraction may, at least initially, reduce the probability of lahar events and reduce the potential for PDCs to spill over valley margins due to increased channel capacity. This, however, is offset by morphological changes to the generally steep riverbanks that may allow PDCs to spread over wider areas and the potential hazards associated with the failure of Sabo dams, triggered by uncontrolled sand extraction near to such structures.

Fig. 12.25 Recovery after the 2010 eruption. **a** Food stalls and souvenir shops catering for visitors in Kaliadem in February 2011. **b** The bunker in Kaliadem, where two people died during the Merapi eruption in 2006, has attracted visitors ever since. **c** Display of a damaged minivan in Kinahrejo. **d**'Batu Alien ' (Alien Rock), one of the tourist attractions on Merapi's south flank following the 2010 eruption. **e** Adventure tour using off-road vehicles for tourists in Kaliadem. **f** Block and sand mining of the 2010 PDC and lahar deposits in Kali Gendol has turned into a profitable post-disaster business. For locations, see Figs. 12.1 and 12.14. *Photo credit* R. Gertisser, K. Preece

12.7 Managing the 2010 Volcanic Crisis

12.7.1 The Role of the National Disaster Management System in Indonesia

After the earthquake and tsunami disaster in Aceh in 2004, Indonesia considered it important to manage disasters with a new paradigm that prioritised risk management. Consequently, Law No. 24/2007 on Disaster Management was issued and, subsequently, the Indonesian National Board for Disaster Management (Badan Nasional Penanggulangan Bencana; BNPB) was formed based on Presidential Regulation No. 8/2008. Consisting of an organisational structure that includes a chairperson, a steering committee, and a disaster management implementer element, BNPB has the function of coordinating the implementation of disaster management in a planned, integrated, and comprehensive manner. As one of the steering elements in the National Disaster Management System, CVGHM under the Geological Agency of the Indonesian Ministry of Energy and Mineral Resources has been authorised to provide recommendations related to geological hazard mitigation at national, provincial and district/city level. Formally, BNPB has been a focal point of government agencies at the central level. Meanwhile, the disaster management focal point at the provincial and district/city level has been the Regional Disaster Management Agency. To strengthen the implementation of disaster management in Indonesia, forums for disaster risk reduction were formed at the national and local level. At a national level, a National Platform was formed, which consists of elements of civil society, the business world, universities, the media, and international institutions. At a local level, these included the Merapi Forum, the Yogyakarta Disaster Risk Reduction Forum, and the East Nusa Tenggara Disaster Risk Reduction Forum. A strategic step related to the 2010 Merapi eruption was the decision of BNPB to declare the eruption crisis as a national disaster because of its wide-ranging impact, covering both the Central Java Province and the Yogyakarta Special Region. This meant that the central government took responsibility for all impacts of the eruption.

12.7.2 Vulnerability Before the 2010 Eruption

In 2006, two disasters struck the Central Java Province and the Yogyakarta Special Region; the 27 May 2006 Bantul earthquake and the eruption of Merapi that peaked on 14 June 2006. Both disasters provided important lessons for the community and stakeholders in disaster management. For example, the public became more rational in understanding geological disasters and government officials were able to increase their knowledge and skills in disaster management. Participation of non-governmental organisations (NGOs) seemingly became more real and an important factor in disaster management. These aspects were important factors of strength when facing the threat of the impending 2010 eruption. During the 2006 eruption crisis, the status of activity was lowered from alert level IV to alert level III on 12 June 2006, two days before the peak of the eruption on 14 June, when a large PDC reached as far as 7 km in Kali Gendol (e.g. Charbonnier and Gertisser 2008), highlighting the challenges not only of raising but also of lowering alert levels related to volcanic activity. Coincidentally, the traditional leader, Mbah Marijan, whose house was located a few hundred metres west of the Gendol valley in Kinahrejo, survived and was not affected by the large 14 June PDC. However, Mbah Marijan's refusal to be evacuated during the 2006 eruption crisis, which attracted widespread media interest, critically influenced the peoples' perception of the incident and understanding of the volcano. Accordingly, inhabitants on Merapi's southern slopes, particularly in Kinahrejo, believed more in the supernatural power associated with the eruption than the scientists. This led to further challenges four years later, when faced with the 2010 eruption crisis.

With the issuance of Law No. 24/2007 on Disaster Management, there has been a strong legal basis in Indonesia to carry out disaster management, alongside the implementation of effective and sustainable planning to facilitate efforts to reduce disaster risk at Merapi. In these disaster risk reduction efforts, the adopted threat factor is routinely assumed to be a larger than predicted future eruption, based on the assessment of volcanic and related hazards. Moreover, to this day, the settlements on the slopes of Merapi are characterised by a high population density of 900–1900 inhabitants/km^2, with 60,000 inhabitants living in the most vulnerable disaster-prone area III (Indon.: Kawasan Rawan Bencana (KRB) III), which is located closest to the summit of Merapi and frequently affected by PDCs (CVGHM 2002, 2011). Inhabitants on the slopes of Merapi are socially, economically and culturally vulnerable (e.g. Mei and Lavigne 2012; Bakkour et al. 2015; Lavigne et al. 2015), and a strong bond between the volcanic environment and social life exists because Merapi, like other volcanoes, is regarded as a place full of blessings of natural resources, which encourages people to live near the volcano (e.g. Kelman and Mather 2008; Holmberg 2023, Chap. 3). Mystical beliefs (e.g. Schlehe 1996; Dove 2008) continue to be held by some people around Merapi, as shown by traditional ceremonies that take place at a certain time every year, even though they are considered as touristic events by some. Social, economic and cultural vulnerability of people living in disaster-prone areas have been important challenges or threat factors for risk reduction efforts, and mystical beliefs were, at times, an impediment for evacuations at critical points in time.

12.7.3 Disaster Risk Reduction Strategy

Successful volcanic disaster mitigation requires long-term hazard assessment, short-term prediction for early warning, and refugee management in times of crises. Appropriate early warning can only be achieved through various volcano monitoring data. Early warnings and recommendations issued by CVGHM must be understood by decision makers and the population, and implemented with concrete actions for disaster risk reduction. Therefore, the disaster risk reduction strategy before the 2010 eruption comprised four pillars: (1) Strengthening of the volcano monitoring system, (2) Formation of a disaster risk reduction (DRR) forum, (3) Strengthening of community capacity through disaster management training and information dissemination, and (4) Preparation of contingency plans for local governments based on hazard assessment as a threat scenario. This strategy continues to be applied up to the present time.

12.7.3.1 Strengthening of the Volcano Monitoring System During the 2010 Eruption Crisis

Before 2010, the Merapi volcano monitoring system consisted of seismic, deformation and geochemical monitoring, meeting the volcanic monitoring standards recommended by the International Association of Volcanology and Chemistry of the Earth's Interior (IAVCEI) (see Budi-Santoso et al. 2023, Chap. 13). In the face of the 2010 eruption, additional monitoring was carried out through the volcano observation posts around Merapi that had also been equipped with meteorological instruments to measure rainfall, wind speed, humidity and air temperature. Furthermore, visual monitoring was conducted using CCTV cameras installed at Gunung Plawangan, Kaliurang and Deles on the south to southeast slopes (see Budi-Santoso et al. 2023, Chap. 13).

The seismic monitoring system at Merapi in 2010 consisted of nine seismic stations (Fig. 12.1). These included four permanent Mark Products L-4 short-period stations (DEL, KLA, PLA, PUS) and five additional temporary broadband seismic stations. The latter comprised one Streckeisen STS-2 seismometer installed at station LBH, and four Güralp CMG-40 T seismometers installed prior to 2010 at stations GMR, GRW, PAS and WOR (Fig. 12.1), as part of the EU-funded MIAVITA (MItigate and Assess risk from Volcanic Impact on Terrain and

human Activities) project (Thierry et al. 2008; Surono et al. 2012; Budi-Santoso et al. 2013; Jousset et al. 2013b) This broadband seismic network operated from July 2009; station L56 (Fig. 12.1) was installed in September 2010. A broadband station installed ~40 km south of Merapi at Imogiri, used as a reference for regional seismic activity, was replaced prior to the 2010 eruption by a short-period seismic station (CRM), as part of the MIAVITA project (Surono et al. 2012; Budi-Santoso et al. 2013; Jousset et al. 2013b). All seismic data were sent in real-time to BPPTKG (Balai Penyelidikan dan Pengembangan Teknologi Kebencanaan Geologi) in Yogyakarta (Fig. 12.1) using wireless transmission. During the peak of the 2010 eruption, three of the broadband stations (GMR, PAS, L56) and three of the four short-period stations (DEL, KLA, PUS) were destroyed and, therefore, the remaining broadband stations were included in the routine monitoring at the time. The remaining short-period station (PLA) was saturated on 4–5 November and individual events were indistinguishable. Therefore, seismic activity recorded at the distal seismic station (CRM) was crucial during the peak of the eruption, illustrating the importance of both proximal and distal seismic stations in the volcano monitoring network of Merapi (Surono et al. 2012; Budi-Santoso et al. 2013; Jousset et al. 2013b).

Deformation monitoring at Merapi was conducted via temporal measurements using EDM, and real-time measurements, using a tiltmeter platform consisting of three electronic tiltmeter stations at the summit and data acquisition using digital telemetry (e.g. Surono et al. 2012). EDM was used to measure the slope distance between several benchmarks, located at the Kaliurang, Babadan, Jrakah and Selo volcano observation posts as well as Deles (Fig. 12.1), and fixed targets (reflectors) around the summit of Merapi (Budi-Santoso et al. 2013; Aisyah et al. 2018). The reflectors south of the summit used in 2010 were moved to a lower elevation of 2400–2600 m on the 1911 lava flow, following the destruction of reflectors installed near Geger Buaya during the 2006 eruption. During the main eruption phases, ground-based geodetic measurements were complemented by satellite data, providing insights into morphological changes at the summit, lava dome growth and PDC distribution, although cloud cover restricted data exploitation from optical satellite-based sensors (e.g. Surono et al. 2012; Pallister et al. 2013).

Geochemical monitoring prior to the 2010 eruption was carried out by regular measurements of gas composition from several fixed points of the solfatara in the Woro crater area. Gas samples were taken using the Giggenbach sampling method (Giggenbach 1975), followed by spectrophotometric and volumetrical analysis. In 2009, a mini-DOAS instrument was also installed through the MIAVITA collaboration to measure gas emissions remotely from the Babadan observation post, although measurements carried out during the 2010 eruption from Babadan as well as from Ketep and Yogyakarta were challenging (Surono et al. 2012). Ground-based gas monitoring during the 2010 eruption was complemented by satellite data, which were particularly useful for the provision of real-time SO_2 emission measurements and ash cloud dispersal (Surono et al. 2012).

12.7.3.2 Formation of a Disaster Risk Reduction Forum: The Merapi Forum

In order to implement disaster risk reduction measures, the strategy for Merapi has been to establish a Disaster Risk Reduction (DRR) forum, the so-called Merapi Forum (see also Lavigne et al. 2023, Chap. 2). Since its inception in 2006, the Merapi Forum has been a collaborative forum between CVHGM and four local governments, supported by local and international NGOs, including the Early Recovery Assistance United Nations Development Programme (ERA-UNDP) and the Center for Disaster Management Study at the Universitas Pembangunan Nasional Veteran Yogyakarta in the framework of disaster risk reduction at Merapi. The five objectives of the cooperation have been (1) the application of Merapi risk analysis and maps, (2) the development of an early warning system, (3) the construction of a radio and web communication

system, (4) the preparation of contingency plans in each district, and (5) the strengthening of community capacity through disaster management training programmes. Used for the development of an early warning system, sirens were installed successfully in four locations, namely at the Kaliurang, Ngepos, Babadan and Jrakah volcano observation posts, and sounded as an order for evacuation for residents who live in the disaster-prone areas of Merapi. This was in addition to sirens that have been used since at least the early 1990s to warn people in the fields or in river valleys of impending danger. As not all public communication equipment around Merapi was covered by the mobile phone network, radio communication, which had long been used to connect the Yogyakarta headquarters with the villages on the slopes of Merapi, was still required. In 2008, the Merapi Forum established a VHF radio communication network that could reach all disaster-prone areas simultaneously. Additionally, standard procedures for the delivery of information through radio communication were formulated as a reference for the delivery of information on Merapi hazards.

12.7.3.3 Strengthening of Community Capacity Through Disaster Management Training and Information Dissemination

To reduce the risk from a future eruption of Merapi as in 2010, a disaster management training programme, aiming at strengthening the capacity of the community to overcome the socio-cultural vulnerability on the slopes of Merapi, has been a top priority. Implementation of the programme has been two-fold; under normal circumstances, disaster management training is carried out, while during a volcanic crisis, dissemination is done directly in the community. Disaster management training targets comprise aspects of knowledge, awareness and behaviour of the community in order to be safe from disasters. Subjects covered include knowledge of the sources of threats, early warning systems, understanding maps of disaster-prone areas, and simulations of evacuation. In a volcanic crisis, dissemination is carried out for people living in disaster-prone areas, covering aspects such as the latest developments in the activity of Merapi, hazard estimation, and recommendations related to disaster risk reduction. Typically, a dissemination session lasts for about 2 h and is attended by 50–100 people.

After the volcanic earthquake swarm in October 2009 (Fig. 12.2), CVGHM held a disaster management training event on 16–17 December 2009 funded by ERA-UNDP. Among the 35 participants were the heads and community leaders of villages in disaster-prone areas in the Boyolali and Klaten regencies. Similar training events were held in the Magelang and Sleman districts on 22–23 December 2009. The trainees were chosen by the village heads and community leaders based on their involvement and responsibility for the community in case of an evacuation. Based on a survey of refugees during the 2010 eruption crisis, people received direct evacuation orders from the village head (54%), sirens (16%), radio/telephone communication equipment (19%) or neighbours (11%) (Mei et al. 2013).

With the beginning of the 2010 eruption and the shift to alert level II on 21 September 2010 (Fig. 12.2), dissemination of information in the disaster-prone area began. Between 29 September and 24 October 2010, people living in the most vulnerable areas, spread over 21 villages, were targeted. The last information dissemination event, which was attended by 35 residents, was held in Kinahrejo at the home of Mbah Marijan on 24 October 2010. The session failed to influence the participants to evacuate immediately, as they followed the orders of Mbah Marijan who refused to evacuate. Eventually they all fell victim to the first PDC at 17.02 WIB on 26 October 2010 (Fig. 12.2). In the aftermath of the eruption, Sri Sultan Hamengku Buwono X, the Sultan of the historic Yogyakarta Sultanate, appointed Mbah Marijan's son, Mas Asih, as Mbah Marijan's successor as caretaker of Merapi. This change may be regarded as the end of the era where a charismatic figure had been the mystical symbol of Merapi and the

beginning of an era in which the new caretaker is required to communicate with official institutions that observe the volcano's activity and in which the public is encouraged to accept science-based explanations rather than interpretations of dreams or irrational theories (Pajar Hatma 2012). The appointment of the new caretaker is symbolically interpreted as support for a modern mindset as opposed to support for a traditional mystical perspective.

12.7.3.4 Preparation of Contingency Plans

Contingency plans are important for local governments dealing with disasters in their regions and used to detect any gaps between the capacity and the magnitude of the threat, so that the appropriate strategy can be determined. The preparation of contingency plans for local governments has become a programme for the Merapi Forum involving various NGOs. Prior to the 2010 eruption crisis, contingency planning was carried out in four districts around Merapi (Sleman, Magelang, Klaten and Boyolali regencies) and completed in 2009. As a basis for the contingency plan, a scenario of a large eruption of Merapi directed towards the south was used, similar to the VEI 3 eruption in 1961. Following the guidelines, the eruption hazard scenario prepared on 8 June 2008 was based on (1) a maximum threat scenario to achieve optimal preparedness, (2) the history of Merapi eruptions, and (3) the experience and intuition of those involved in dealing with disasters at Merapi. In the completed scenario, the approximate runout distances and directions of the PDCs in the southern sector were estimated at 12 km in Kali Gendol, 10 km in Kali Woro, and 8 km in Kali Kuning and Kali Boyong. In addition, based on the history of the eruptions from 1872 to 2001, it was inferred that 90% of the PDCs followed the direction of the crater opening, which, since the 2006 eruption, was open to the south. Furthermore, it was estimated that 12,660 people in the Sleman Regency, 32,987 people in the Magelang Regency, 4420 people in the Klaten Regency, and 2540 people in the Boyolali Regency would have to be evacuated. When the 2010 eruption eventually happened, it caused 398 victims due to PDCs and evacuation of nearly 400,000 people, the largest ever evacuation at Merapi because of an eruption that is thought to have saved 10,000—20,000 lives (Surono et al. 2012).

12.7.4 International Collaboration

The role of international cooperation was important to reduce the disaster risk at Merapi in 2010. For example, within the framework of the EU-funded MIAVITA project (2008–2012), coordinated by BRGM (Bureau de Recherches Géologiques et Minières—Risks Division, France), several broadband seismic stations were installed at Merapi (Sect. 12.7.3.1) and a programme of disaster management training was implemented for residents in the village of Tlogolele (Boyolali Regency) in the disaster-prone area on 2–4 July 2009. Following the issue of alert level III on 21 October 2010 (Fig. 12.2), the World Organization of Volcano Observatories (WOVO) at Nanyang Technological University (Singapore), offered to aid hazard assessment by modelling PDCs using the Titan2D Geophysical Mass-Flow Simulation Software developed at the State University of New York at Buffalo, and analysed SO_2 exposure in the atmosphere based on OMNI satellite imagery. Close collaboration with the Volcano Disaster Assistance Program (VDAP) of the United States Geological Survey (USGS) began when the activity of Merapi entered a critical phase on 25 October 2010 and the alert level was raised to level IV (Fig. 12.2). A crucial role of this cooperation was the provision of satellite imagery information to monitor the growing lava dome following the initial eruptions on 26 October 2010. The rapid growth of the lava dome before the peak of the eruption on 5 November 2010, was an important piece of information that formed the basis for the decision to expand the danger area from 10 to 15 km and, subsequently, to 20 km from the summit of Merapi (Figs. 12.1 and 12.2). This decision was of strategic importance to reduce the possibility of casualties caused by PDCs. Collaboration with the Sakurajima Volcano Observatory (SVO),

Japan began on 9 November 2010 and included petrological analysis and prediction, installation of infrasonic stations to detect explosive eruptions, and sampling and analysis of volcanic ash.

12.7.5 Reflection and Lessons Learned

Mitigation of volcanic risk depends on the ability of short-term predictions for early warning, rapid evacuation of people from hazardous areas, and land-use planning to reduce the risk of impending eruptions. A fundamental question related to volcanic hazard assessment and risk reduction is the long-term estimation of volcanic activity, which is critical for preparing contingency plans, disaster preparedness plans and land use planning strategies (e.g. Blong 1984; Scott 1989; Tilling 1989; MIAVITA Team 2012; Martí Molist 2017).

The disaster risk reduction strategy for the 2010 Merapi eruption was implemented precisely and comprehensively. Strengthening of the monitoring systems, data analysis, and accurate short-term predictions allowed early warnings in a manageable time window for preparedness and evacuation during the critical 35-day-long period between 20 September 2010, when the alert level was raised to level II, and 25 October 2010, when the alert level was raised to the highest level (level IV) (Fig. 12.2).

A mid-term assessment, which was represented in the eruption hazard scenario, proved helpful in preparing contingency plans for each district around Merapi. As a minimum, local governments were able to assess the resources they have and the magnitude of the threats they might face. However, the 2010 eruption exceeded the estimated danger as described in the eruption hazard scenario, which was based on a VEI 3 eruption and PDCs travelling as far as 12 km towards Kali Gendol. With a VEI of 4, the 2010 eruption was significantly larger than anticipated and PDC reached distances of ~16 km in Kali Gendol.

Even though the early warning given was relatively accurate and the disaster risk reduction strategy before the eruption was considered appropriate, there were still many direct casualties (398) related to PDCs, total losses of >40 trillion IDR (>4.5 billion US$) due to damage to infrastructures, livestock, agriculture and housing, and nearly 400,000 refugees.

Several factors caused casualties by PDCs during the 2010 eruption, which occurred in two stages. At the immediate onset of the eruption on 26 October, as many as 35 casualties were caused when residents refused to be evacuated, even though the alert level was at the highest level (level IV). The refusal of people to evacuate was due to strong local beliefs, exemplified by Mbah Marijan's attitude as a local figure, and the fact that they had remained unharmed during the previous eruption in 2006, which affected the same area. Further victims occurred when the eruption peaked on 5 November 2010. During a 1.5-h-long period of continuous PDCs on 3 November, the danger zone was expanded to a radius of 15 km, and on 5 November, the danger zone was expanded further to a radius of 20 km. Based on information from the government of the Sleman Regency, some people did not believe that the PDCs could reach more than 10 km. Further casualties were caused by confusion among the people as to where to go following a sudden evacuation order.

Along Kali Gendol, several Sabo dams were built to control lahars and volcanic sediment, and to inhibit PDCs. However, when PDCs hit a Sabo dam, additional hazards may result from rapid valley infilling by pyroclastic material or detachment of the hot ash cloud from the denser basal avalanche of the current (e.g. Charbonnier and Gertisser 2008, 2011; Lube et al. 2011; Gertisser et al. 2012a). Several people were unaware that to avoid the PDCs, they had to move away from the riverbank. This resulted in 49 deaths on both sides of the Sabo dam in Bronggang, ~15 km south of Merapi (Fig. 12.1). Overall, the fast changes in threats, which led to rapid changes of the size of the danger zone, was the main cause of the large number of casualties. These sudden changes did not give the community and the government enough time to prepare all matters related to massive evacuations.

The main reason for the number of refugees reaching 400,000 people was the increased displacement after the expansion of the danger zone to a radius of 20 km on 5 November 2010, based on refugee development data from BNPB. On 6 November 2010, there were additional 100,000 refugees in the western sector, namely in the Magelang Regency, which were mainly due to ash fall that affected this area because of the prevailing winds at the time. In the Boyolali (north), Klaten (east) and Sleman regencies (south), the number of refugees increased by 60,000. Refugee numbers continued to increase sharply until they reached a peak of 399,403 people, spread over more than 600 refugee barracks on 14 November 2010. Unplanned refugees contributed to this increase due to panic that was triggered by news issued by spiritual figures through television media stating that Merapi would erupt even more severely, affecting areas as far as 35 km away from the volcano, and that the Palace of Yogyakarta (Kraton) would disappear. To address this issue, BNPB held a closed emergency meeting at the Center for Disaster Management and Operations for Mt. Merapi, Yogyakarta on 15 November 2010, which was attended by all stakeholders. On this occasion, BNPB reported that the seismic activity had declined since 5 November and that a larger eruption was unlikely based on the amount of tephra already produced and on a comparison with historical eruption records. This was key to reducing public panic and controlling evacuations.

With the implemented strategic approach, there was an unavoidable risk of loss, including damage to immovable infrastructures and settlement sites and ecological losses in disaster-prone areas. Therefore, to reduce the risk of an impending eruption of Merapi, the Geological Agency issued the several recommendations in its rehabilitation and reconstruction programme:

- A map of the hazardous areas around Merapi should be used as a reference for spatial planning policies based on disaster mitigation. Subsequently, the Ministry of Public Works proposed Merapi as a National Strategic Area (Indon.: Kawasan Strategis Nasional; KSN) to guide spatial planning, establishing Mount Merapi National Park through Presidential Regulation No. 70/2013. This step is regarded as a law enforcement map of the disaster-prone areas at Merapi that forms the basis for changing land use plans. When preparing detailed land use plans, local governments are required to refer to this Presidential Regulation.
- The area directly affected by the 2010 eruption was declared a restricted area for settlement. Utilisation of the area can be by cultivation such as plantations, agriculture, animal husbandry and tourism, as long as there are no accommodation facilities.
- People who were victims of the Merapi eruption in 2010, and whose homes were directly affected, had to be relocated to safer places. For people who still reside in parts of disaster-prone area (KRB) III that were not directly affected by the 2010 eruption, risk reduction efforts should be undertaken through social engineering (i.e. sustainable disaster management training) within a conceptual framework of living in harmony with Merapi.

12.8 Summary

The 2010 eruption of Merapi was the volcano's largest since 1872, differing markedly from other eruptions in the recent past. The eruption had clear precursors in the seismic, deformation and volcanic gas monitoring record. The earliest indications of renewed activity were observed about one year before the beginning of the eruption on 26 October 2010, demonstrated by a volcanic earthquake swarm and an increase in the rate of summit deformation. The 2010 eruption crisis lasted for about 3 months between September and November 2010. Early warning levels were gradually increased from alert level II on 20 September to alert level IV on 25 October, allowing about 35 days for mitigation measures to reduce disaster risk and save human lives. The runout distances of PDCs exceeded estimates

based on anticipated hazard scenarios, leading to crucial decisions to expand the danger area to a radius of 15 km on 3 November and to 20 km on 4 November 2010 before the climax of the eruption on 5 November, when PDCs propagated ~16 km down Kali Gendol. Despite the impact of the eruption that caused 398 casualties and considerable damage to infrastructures, it is estimated that the early warnings issued saved tens of thousands of lives. Apart from the remarkably long PDC runout, notable and in many respects unusual volcanic phenomena of the 2010 eruption included: (1) the lack of lava dome extrusion at the onset of the eruption, (2) the occurrence of powerful explosions that were directed laterally and focused to the south on 26 October and, particularly, during the paroxysmal phase on 5 November, when high-energy PDCs destroyed an area of up to 8.4 km from source on Merapi's south flank, (3) exceptionally high rates of lava dome extrusion and growth prior to and after the 5 November paroxysm, and (4) the generation of pumice-rich PDCs from collapse of short but sustained eruption columns. The 2010 eruption was driven by essentially the same basaltic andesite magma type as other recent Merapi eruptions. Multiple lines of evidence suggest that the exceptional magnitude of the eruption might have been caused by the arrival of deep, volatile-rich magma that disrupted and overwhelmed a shallower crystal-rich magma system, followed by rapid ascent, accompanying closed-system degassing and accumulation of ascending magma beneath a plugged conduit that builds up pressure in the uppermost conduit.

Acknowledgements The authors thank and respect Samsul Maarif, former Head of BNPB, Surono, former Head of the Center of Volcanology and Geological Hazard Mitigation (CVGHM; Indon.: Pusat Vulkanologi dan Mitigasi Bencana Geologi, PVMBG) and the Geological Agency, Ministry of Energy and Mineral Resources, and Raden Sukhyar, former Head of the Geological Agency, Ministry of Energy and Mineral Resources, for the management of the 2010 eruption crisis and the post-disaster rehabilitation and reconstruction phase. In addition, we gratefully acknowledge all staff members and volunteers of CVGHM, the Center for Research and Development of Geological Disaster Technology (Indon.: Balai Penyelidikan dan Pengembangan Teknologi Kebencanaan Geologi, BPPTKG), and those in the Indonesian disaster management agencies and forums for disaster risk reduction, who were involved in the management of the eruption crisis that saved many lives. We are also grateful for fruitful discussions on various aspects of the 2010 eruption with a large number of colleagues in Indonesia and elsewhere, many of whom have contributed to this book. Philippe Jousset and Franck Lavigne are thanked for their detailed and constructive formal reviews that gave substantial input into this work and helped clarify the ideas presented in this chapter.

References

Aisyah N, Iguchi M, Subandriyo BA, Hotta K, Sri Sumarti S (2018) Combination of a pressure source and block movement for ground deformation analysis at Merapi volcano prior to the eruptions in 2006 and 2010. J Volcanol Geotherm Res 357:239–253

Bakkour D, Enjolras G, Thouret J-C, Kast R, Mei ETW, Prihatminingtyas B (2015) The adaptive governance of natural disaster systems: insights from the 2010 mount Merapi eruption in Indonesia. Int J Disaster Risk Reduct 13:167–188

Baxter PJ, Jenkins S, Seswandhana R, Komorowski J-C, Dunn K, Purser D, Voight B, Shelley I (2017) Human survival in volcanic eruptions: thermal injuries in pyroclastic surges, their causes, prognosis and emergency management. Burns 43:1051–1069

Beauducel F, Cornet F-H, Suhanto E, Duquesnoy T, Kasser M (2000) Constraints on magma flux from displacements data at Merapi volcano, Java, Indonesia. J Geophys Res Solid Earth 105(B4):8193–8203

Belousov A, Voight B, Belousova M (2007) Directed blasts and blast-generated pyroclastic density currents: a comparison of the Bezymianny 1956, Mount St Helens 1980, and Soufrière Hills, Montserrat 1997 eruptions and deposits. Bull Volcanol 69:701–740

Belousov A, Belousova M, Hoblitt R, Patia H (2020) The 1951 eruption of Mount Lamington, Papua New Guinea: devastating directed blast triggered by small-scale edifice failure. J Volcanol Geotherm Res 401:106947

Bignami C, Ruch J, Chini M, Neri M, Buongiorno MF, Hidayati S, Sayudi DS, Surono (2013) Pyroclastic density current volume estimation after the 2010 Merapi volcano eruption using X-band SAR. J Volcanol Geotherm Res 261:236–243

Blong RJ (1984) Volcanic hazards: a source book on the effects of eruptions. Academic Press, Sydney and London, p 424

Borisova AY, Gurenko AA, Martel C, Kouzmanov K, Cathala A, Bohrson WA, Pratomo I, Sumarti S (2016) Oxygen isotope heterogeneity of arc magma recorded in plagioclase from the 2010 Merapi eruption (Central Java, Indonesia). Geochim Cosmochim Acta 190:13–34

Borisova AY, Martel C, Gouy S, Pratomo I, Sumarti S, Toutain JP, Bindeman IN, de Parseval P, Metaxian JP, Surono (2013) Highly explosive 2010 Merapi eruption: evidence for shallow level crustal assimilation and hybrid fluid. J Volcanol Geotherm Res 261:193–208

Botcharnikov RE, Behrens H, Holtz F, Koepke J, Sato H (2004) Sulfur and chlorine solubility in Mt. Unzen rhyodacitic melt at 850 °C and 200 MPa. Chem Geol 213:207–225

Buddington AF, Lindsley DH (1964) Iron-titanium oxide minerals and synthetic equivalents. J Petrol 5:310–357

Budi-Santoso A, Lesage P, Dwiyono S, Sumarti S, Subandriyo S, Jousset P, Metaxian JP (2013) Analysis of the seismic activity associated with the 2010 eruption of Merapi volcano, Java. J Volcanol Geotherm Res 261:153–170

Budi-Santoso A, Beauducel F, Nandaka IGMA, Humaida H, Costa F, Widiwijayanti C, Iguchi M, Métaxian J-P, Rudianto I, Rozin M, Sulistiyani, Nurdin I, Kelfoun K, Byrdina S, Pinel V, Fahmi AA, Laurin A, Rizal MH, Dahamna N (2023) The Merapi volcano monitoring system. In: Gertisser R, Troll VR, Walter TR, Nandaka IGMA, Ratdomopurbo A (eds) Merapi volcano—geology, eruptive activity, and monitoring of a high-risk volcano. Springer, Berlin, Heidelberg, pp 409–436

Caricchi L, Sheldrake TE, Blundy J (2018) Modulation of magmatic processes by CO_2 flushing. Earth Planet Sci Lett 491:160–171

Carr BB, Clarke AB, de' Michieli Vitturi M (2020). Volcanic conduit controls on effusive-explosive transitions and the 2010 eruption of Merapi volcano (Indonesia). J Volcanol Geotherm Res 392:106767

Carroll MR, Webster JD (1994) Solubilities of sulfur, noble gases, nitrogen, chlorine, and fluorine in magmas. Rev Mineral 30:231–280

Charbonnier SJ, Gertisser R (2008) Field observations and surface characteristics of pristine block-and-ash flow deposits from the 2006 eruption of Merapi volcano, Java, Indonesia. J Volcanol Geotherm Res 177:971–982

Charbonnier S, Gertisser R (2011) Deposit architecture and dynamics of the 2006 block-and-ash flows of Merapi volcano, Java, Indonesia. Sedimentology 58:1573–1612

Charbonnier SJ, Germa A, Connor CB, Gertisser R, Preece K, Komorowski J-C, Lavigne F, Dixon T, Connor L (2013) Evaluation of the impact of the 2010 pyroclastic density currents at Merapi volcano from high-resolution satellite imagery, field investigations and numerical simulations. J Volcanol Geotherm Res 261:295–315

Clarke AB, Voight B (2000) Pyroclastic current dynamic pressures from aerodynamics of tree or pole blowdown. J Volcanol Geotherm Res 100:395–412

Costa F, Andreastuti S, Bouvet de Maisonneuve C, Pallister JS (2013) Petrological insights into the storage conditions, and magmatic processes that yielded the centennial 2010 Merapi explosive eruption. J Volcanol Geotherm Res 261:209–235

Cronin SJ, Lube G, Dayudi DS, Sumarti S, Subrandiyo S, Surono (2013) Insights into the October-November 2010 Gunung Merapi eruption (Central Java, Indonesia) from the stratigraphy, volume and characteristics of its pyroclastic deposits. J Volcanol Geotherm Res 261:244–259

CVGHM (Center of Volcanology and Geological Hazard Mitigation) (2002) Merapi volcano hazard map. Bandung

CVGHM (Center of Volcanology and Geological Hazard Mitigation) (2011) Revised Merapi volcano hazard map. Bandung

Darmawan H, Putra R, Budi-Santoso A, Humaida H, Walter TR (2023) Morphology and instability of the Merapi lava dome monitored by unoccupied aircraft systems. In: Gertisser R, Troll VR, Walter TR, Nandaka IGMA, Ratdomopurbo A (eds) Merapi volcano—geology, eruptive activity, and monitoring of a high-risk volcano. Springer, Berlin, Heidelberg, pp 457–472

de Bélizal É, Lavigne F, Robin AK, Sri Hadmoko D, Cholik N, Thouret J-C, Sawudi DS, Muzani M, Sartohadi J, Vidal C (2013) Rain-triggered lahars following the 2010 eruption of Merapi volcano, Indonesia: a major risk. J Volcanol Geotherm Res 261:330–347

de Bélizal É, Lavigne F, Grancher D (2011) Quand l'aléa devient la ressource: l'activité d'extraction des matériaux volcaniques autour du volcan Merapi (Indonésie) dans la compréhension des risques locaux. Cybergeo: Eur J Geogr [online] 525. http://journals.openedition.org/cybergeo/23555

Deegan FM, Troll VR, Gertisser R, Freda C (2023) Magma-carbonate interaction at Merapi volcano, Indonesia. In: Gertisser R, Troll VR, Walter TR, Nandaka IGMA, Ratdomopurbo A (eds) Merapi volcano—geology, eruptive activity, and monitoring of a high-risk volcano. Springer, Berlin, Heidelberg, pp 291–321

Delmelle P, Stix J (2000) Volcanic gases. In: Sigurdsson H, Houghton BF, McNutt SR, Rymer H, Stix J (eds) Encyclopedia of volcanoes. Academic Press, pp 803–816

Dove MR (2008) Perception of volcanic eruption as agent of change on Merapi volcano, Central Java. J Volcanol Geotherm Res 172:329–337

Drignon MJ, Bechon T, Arbaret L, Burgisser A, Komorowski J-C, Martel C, Miller H, Yaputra R (2016) Preexplosive conduit conditions during the 2010 eruption of Merapi volcano (Java, Indonesia). Geophys Res Lett 43:11595–11602

Erdmann S, Martel C, Pichavant M, Kushnir A (2014) Amphibole as an archivist of magmatic crystallization conditions: problems, potential, and implications for inferring magma storage prior to the paroxysmal 2010 eruption of Mount Merapi, Indonesia. Contrib Mineral Petrol 167:1016

Erdmann S, Martel C, Pichavant M, Bourdier J-L, Champallier R, Komorowski J-C, Cholik N (2016) Constraints from phase equilibrium experiments on pre-eruptive storage conditions in mixed magma systems: a case study on crystal-rich basaltic andesites from Mount Merapi, Indonesia. J Petrol 57:535–560

Escher BG (1933) On a classification of central eruptions according to gas pressure of the magma and viscosity of the lava. Leidsche Geol Med 6:45–49

Gauthier PJ, Condomines M (1999) ^{210}Pb-^{226}Ra radioactive disequilibria in recent lavas and radon degassing: inferences on the magma chamber dynamics at Stromboli and Merapi volcanoes. Earth Planet Sci Lett 172:111–126

Gertisser R, Keller J (2003) Trace element and Sr, Nd, Pb and O isotope variations in medium-K and high-K volcanic rocks from Merapi Volcano, Central Java, Indonesia: evidence for the involvement of subducted sediments in Sunda Arc magma genesis. J Petrol 44:457–486

Gertisser R, Charbonnier SJ, Troll VR, Keller J, Preece K, Chadwick JP, Barclay J, Herd RA (2011) Merapi (Java, Indonesia): anatomy of a killer volcano. Geol Today 27:57–62

Gertisser R, Cassidy NJ, Charbonnier SJ, Nuzzo L, Preece K (2012a) Overbank block-and-ash flow deposits and the impact of valley-derived, unconfined flows on populated areas at Merapi volcano, Java, Indonesia. Nat Hazards 60:623–648

Gertisser R, Charbonnier SJ, Keller J, Quidelleur X (2012b) The geological evolution of Merapi volcano, Central Java, Indonesia. Bull Volcanol 74:1213–1233

Gertisser R, Troll VR, Nandaka IGMA (2023a) The scientific discovery of Merapi: from ancient Javanese sources to the 21st century. In: Gertisser R, Troll VR, Walter TR, Nandaka IGMA, Ratdomopurbo A (eds) Merapi volcano—geology, eruptive activity, and monitoring of a high-risk volcano. Springer, Berlin, Heidelberg, pp 1–44

Gertisser R, del Marmol M-A, Newhall C, Preece K, Charbonnier S, Andreastuti S, Handley H, Keller J (2023b) Geological history, chronology and magmatic evolution of Merapi. In: Gertisser R, Troll VR, Walter TR, Nandaka IGMA, Ratdomopurbo A (eds) Merapi volcano—geology, eruptive activity, and monitoring of a high-risk volcano. Springer, Berlin, Heidelberg, pp 137–193

Giggenbach WF (1975) A simple method for collecting and analysis of volcanic gas samples. Bull Volcanol 39:132–145

Global Volcanism Program (2013) Volcanoes of the world, v 4.9.4 (17 Mar 2021), Venzke E (ed) Smithsonian Institution. Downloaded 27 Apr 2021. https://doi.org/10.5479/si.GVP.VOTW4-2013

Grandjean JB (1931a) Korte mededeeling over de uitbarsting van den Merapi op 18 December 1930. De Mijningingenieur 12(1):4–6

Grandjean JB (1931b) De uitbartsting van den Merapi in 1930. De Mijningingenieur 12(4):47

Grandjean JB (1931c) Bijdrage tot de kennis der Gloedwolken van den Merapi van Midden-Java. De Mijningingenieur 12(12):20–25

Haggerty SE (1993) Oxide textures—A mini-atlas. In: Lindsley DH (ed) Oxide minerals: petrologic and magnetic significance. Rev Mineral 25:303–321

Handley HK, Reagan M, Gertisser R, Preece K, Berlo K, McGee LE, Barclay J, Herd R (2018) Timescales of magma ascent and degassing and the role of crustal assimilation at Merapi volcano (2006–2010), Indonesia: constraints from uranium-series and radiogenic isotopic compositions. Geochim Cosmochim Acta 222:34–52

Hidayat D, Voight B, Langston C, Ratdomopurbo A, Ebeling C (2000) Broadband seismic experiment at Merapi volcano, Java, Indonesia: very-long-period pulses embedded in multiphase earthquakes. J Volcanol Geotherm Res 100:215–231

Holmberg K (2023) Merapi and its dynamic 'disaster culture'. In: Gertisser R, Troll VR, Walter TR, Nandaka IGMA, Ratdomopurbo A (eds) Merapi volcano—geology, eruptive activity, and monitoring of a high-risk volcano. Springer, Berlin, Heidelberg, pp 67–87

Ikhsan J, Fujita M, Takebayashi H (2010) Sediment disaster and resource management in the Mount Merapi area, Indonesia. Int J Eros Control Eng 3:43–52

Jenkins S, Komorowski J-C, Baxter PJ, Spence R, Picquout A, Lavigne F, Surono (2013) The Merapi 2010 eruption: an interdisciplinary impact assessment methodology for studying pyroclastic density current dynamics. J Volcanol Geotherm Res 261:316–329

Jenkins S, Phillips JC, Price R, Feloy K, Baxter PJ, Hadmoko DS, de Bélizal E (2015) Developing building-damage scales for lahars: application to Merapi volcano, Indonesia. Bull Volcanol 77:75

Jousset P, Pallister P, Surono (2013a) The 2010 eruption of Merapi volcano. J Volcanol Geotherm Res 261:1–6

Jousset P, Budi-Santoso A, Jolly AD, Boichu M, Surono, Dwiyono S, Sumarti S, Hidayati S, Thierry P (2013b) Signs of magma ascent in LP and VLP seismic events and link to degassing: an example from the 2010 explosive eruption at Merapi volcano, Indonesia. J Volcanol Geotherm Res 261:171–192

Kelfoun K, Gueugneau V, Komorowski J-C, Aisyah N, Cholik N, Merciecca C (2017) Simulation of block-and-ash flows and ash-cloud surges of the 2010 eruption of Merapi volcano with a two-layer model. J Geophys Res Solid Earth 122:4277–4292

Kelman I, Mather TA (2008) Living with volcanoes: the sustainable livelihoods approach for volcano-related opportunities. J Volcanol Geotherm Res 172:189–198

Kemmerling GLL (1932) De controverse uitgeschoten gloedwolken (nuées ardentes d'explosion dirigée) of lawinen-gloedwolken (nuées ardentes d'avalanche). De Ingenieur 47:129–137

Paroxysmal dome explosion during the Merapi 2010 eruption: processes and facies relationships of associated high-energy pyroclastic density currents. J Volcanol Geotherm Res 261:260–294

Kubanek J, Westerhaus M, Schenk A, Aisyah N, Brotopuspito KS, Heck B (2015) Volumetric change quantification of the 2010 Merapi eruption using TanDEM-X InSAR. Remote Sens Environ 164: 16–25

Kushnir ARL, Martel C, Bourdier J-L, Heap M, Reuschlé T, Erdmann S, Komorowski J-C, Cholik N (2016) Probing permeability and microstructure: unravelling the role of a low-permeability dome on the explosivity of Merapi (Indonesia). J Volcanol Geotherm Res 316:56–71

Kushnir ARL, Martel C, Champallier R, Wadsworth FB (2017) Permeability evolution in variably glassy basaltic andesites measured under magmatic conditions. Geophys Res Lett 44:10262–10271

Lavigne F, Morin J, Surono M (2015) Atlas of Merapi volcano. Laboratoire de Géographie Physique, Meudon, France, 58 color plates. Online Publication (hal-03010922)

Lavigne F, Mei ETW, Morin J, Humaida H, Moatty A, de Bélizal E, Sri Hadmoko D, Grancher D, Picquout A (2023) Physical environment and human context at Merapi volcano: a complex balance between accessing livelihoods and coping with volcanic hazards. In: Gertisser R, Troll VR, Walter TR, Nandaka IGMA, Ratdomopurbo A (eds) Merapi volcano—geology, eruptive activity, and monitoring of a high-risk volcano. Springer, Berlin, Heidelberg, pp 45–66

Le Guern F, Gerlach TM, Nohl A (1982) Field gas chromatograph analyses of gases from a glowing dome at Merapi volcano, Java, Indonesia, 1977, 1978, 1979. J Volcanol Geotherm Res 14:223–245

Le Maitre RW (ed), Streckeisen A, Zanettin B, Le Bas MJ, Bonin B, Bateman P, Bellieni G, Dudek A, Efremova J, Keller J, Lameyre J, Sabine PA, Schmidt R, Sørensen H, Woolley AR (2002) Igneous rocks. A classification and glossary of terms. In: Recommendations of the International Union of Geological Sciences subcommission on the systematics of igneous rocks. University Press, Cambridge

Leake BE, Woolley AR, Arps CES, Birch WD, Gilbert MC, Grice JD, Hawthorne FC, Kato A, Kisch HJ, Krivovichev V, Linthout K, Laird J, Mandarino J, Maresch WV, Nickel EH, Rock NMS, Schumacher JC, Smith DC, Stephenson NCN, Ungaretti L, Whittaker EJW, Youzhi G (1997) Nomenclature of amphiboles: report of the subcommittee on amphiboles of the International Mineralogical Association Commission on new minerals and mineral names. Mineral Mag 61:295–321

Lerner GA, Jenkins SF, Charbonnier SJ, Komorowski J-C, Baxter PJ (2021) The hazards of unconfined pyroclastic density currents: a new synthesis and classification according to their deposits, dynamics, and thermal and impact characteristics. J Volcanol Geotherm Res 107429. https://doi.org/10.1016/j.jvolgeores.2021.107429

Li W, Costa F, Nagashima K (2021) Apatite crystals reveal melt volatile budgets and magma storage depths at Merapi volcano, Indonesia. J Petrol 62:egaa100

Lube G, Breard ECP, Jones J, Fullard L, Dufek J, Cronin SJ, Wang T (2019) Generation of air lubrication within pyroclastic density currents. Nat Geosci 12:381–386

Lube G, Cronin SJ, Thouret J-C, Surono (2011) Kinematic characteristics of pyroclastic density currents at Merapi and controls on their avulsion from natural and engineered channels. Geol Soc Am Bull 123:1127–1140

Maly E, Nareswari A (2015). Housing relocation after the 2010 eruption of Mt. Merapi, Indonesia. In: 7th i-Rec conference: reconstruction and recovery in urban contexts. London, 6–8 July 2015

Martí Molist J (2017) Assessing volcanic hazard: a review. Oxford Handbooks Online. https://doi.org/10.1093/oxfordhb/9780190699420.013.3

Mei ETW, Lavigne F (2013) Mass evacuation of the 2010 Merapi eruption. Int J Emerg Manag 9:298–311

Mei ETW, Lavigne F, Picquout A, de Bélizal E, Brunstein D, Grancher D, Sartohadi J, Cholik N, Vidal C (2013) Lessons learned from the 2010 evacuations at Merapi volcano. J Volcanol Geotherm Res 261:348–365

Mei ETW, Fajarwatia A, Hasanatia S, Saria IM (2016) Resettlement following the 2010 Merapi volcano eruption. Procedia Soc Behav Sci 227:361–369

Mei ETW, Lavigne F (2012) Pengungsian Penduduk Selama Erupsi Gunung Merapi 2010, dalam Buku Erupsi Gunung Merapi 2010 vol 2, Yogyakarta

MIAVITA Team (2012) Handbook for volcanic risk management—Prevention, crisis management, resilience. Orléans, France, 204 pp. https://reliefweb.int/report/world/handbook-volcanic-risk-management-prevention-crisis-management-resilience

Morimoto N (1988) Nomenclature of pyroxenes. Mineral Petrol 39:55–76

Neumann van Padang M (1933) De uitbarsting van den Merapi (Midden Java) in de jaren 1930–1931. Vulkanol Seismol Med 12:1–117

Pajar Hatma IJ (2012) Dinamika Pola Pikir Orang Jawa Di Tengah Arus Modernisasi. Humaniora 24:133–140

Pallister JS, Schneider DJ, Griswold JP, Keeler RH, Burton WC, Noyles C, Newhall CG, Ratdomopurbo A (2013) Merapi 2010 eruption—Chronology and extrusion rates monitored with satellite radar and used in eruption forecasting. J Volcanol Geotherm Res 261:144–152

Picquout A, Lavigne F, Mei ETW, Grancher D, Cholik N, Vidal CM, Hadmoko DS (2013) Air traffic disturbance due to the 2010 eruption of Merapi volcano. J Volcanol Geotherm Res 261:366–375

Preece K, Gertisser R, Barclay J, Berlo K, Herd RA, Facility EIM (2014) Pre- and syn-eruptive degassing and crystallisation processes of the 2010 and 2006 eruptions of Merapi volcano, Indonesia. Contrib Mineral Petrol 168:1061

Preece K, Gertisser R, Barclay J, Charbonnier SJ, Komorowski J-C, Herd RA (2016) Transitions between explosive and effusive phases during the cataclysmic 2010 eruption of Merapi volcano, Java, Indonesia. Bull Volcanol 78:54

Preece K, van der Zwan F, Hammer J, Gertisser R (2023) A textural perspective on the magmatic system and eruptive behaviour of Merapi volcano. In: Gertisser R, Troll VR, Walter TR, Nandaka IGMA, Ratdomopurbo A (eds) Merapi volcano—geology, eruptive activity, and monitoring of a high-risk volcano. Springer, Berlin, Heidelberg, pp 265–289

Preece K (2014) Transitions between effusive and explosive activity at Merapi volcano, Indonesia: a volcanological and petrological study of the 2006 and 2010 eruptions. Ph.D. thesis, University of East Anglia, Norwich, UK

Preece K, Barclay J, Gertisser R, Herd RA (2013) Textural and micro-petrological variations in the eruptive products of the 2006 dome-forming eruption of Merapi volcano, Indonesia: implications for subsurface processes. J Volcanol Geotherm Res 261:98–120

Ratdomopurbo A, Beauducel F, Subandriyo J, Nandaka IGMA, Newhall CG, Suharna, Sayudi DS, Suparwaka H, Sunarta (2013) Overview of the 2006 eruption of Mt. Merapi. J Volcanol Geotherm Res 261:87–97

Ratdomopurbo A, Poupinet G (2000) An overview of the seismicity of Merapi volcano (Java, Indonesia), 1983–1994. J Volcanol Geotherm Res 100:193–214

Ratdomopurbo A (1995) Etude sismologique du volcan Mérapi et formation du dôme de 1994. Ph.D. thesis, University of Joseph Fourier, Grenoble, France

Saepuloh A, Urai M, Aisyah N, Sunarta WC, Subandriyo JP (2013) Interpretation of ground surface changes prior to the 2010 large eruption of Merapi volcano using ALOS/PALSAR, ASTER TIR and gas emission data. J Volcanol Geotherm Res 261:130–143

Schlehe J (1996) Reinterpretations of mystical traditions. Explanations of a volcanic eruption in Java. Anthropos 91:391–409

Schwarzkopf LM, Schmincke H-U, Troll VR (2001) Pseudotachylite on impact marks of block surfaces in block-and-ash flows at Merapi volcano, Central Java, Indonesia. Int J Earth Sci 90:769–775

Scott WE (1989) Volcanic-hazards zonation and long-term forecasts. In: Tilling RI (ed) Volcanic hazards, vol 1. Short Courses in geology, pp 25–49

Shinohara H, Aiuppa A, Giudice G, Gurrieri S, Liuzzo M (2008) Variation of H_2O/CO_2 and CO_2/SO_2 ratios of volcanic gases discharged by continuous degassing of Mount Etna volcano, Italy. J Geophys Res Solid Earth 113:B09203

Shinohara H, Matsushima N, Kazahaya K, Ohwada M (2011) Magma-hydrothermal system interaction inferred from volcanic gas measurements obtained during 2003–2008 at Meakandake volcano, Hokkaido, Japan. Bull Volcanol 73:409–421

Siebert L, Simkin T, Kimberly P (2011) Volcanoes of the world. University of California Press, Berkeley

Siswowidjoyo S, Suryo I, Yokoyama I (1995) Magma eruption rates of Merapi volcano, Central Java, Indonesia during one century (1890–1992). Bull Volcanol 57:111–116

Solikhin A, Thouret J-C, Liew SC, Gupta A, Sayudi DS, Oehler J-F, Kassouk Z (2015) High spatial-resolution imagery helps map deposits of the large (VEI 4) 2010 Merapi volcano eruption and their impact. Bull Volcanol 77:20

Sparks RSJ, Barclay J, Calder ES, Herd RA, Luckett R, Norton GE, Pollard L, Robertson RA, Ritchie L, Voight B, Young SR, Woods AW (2002) Generation of a debris avalanche and violent pyroclastic density current: the Boxing Day eruption of 26 December 1997 at the Soufrière Hills volcano, Montserrat. In: Druitt T, Kokelaar BP (eds) The eruption of Soufrière Hills volcano, Montserrat, from 1995–1999. Geol Soc London Mem 21:409–434

Sumarti S, Suryono (1994) Chemistry model of Merapi volcano, Technical Report, The fifth field workshop on volcanic gases in Indonesian volcanoes, Volcanological Survey of Indonesia, Bandung, pp 96–111

Surono JP, Pallister J, Boichu M, Buongiorno MF, Budisantoso A, Costa F, Andreastuti S, Prata F, Schneider D, Clarisse L, Humaida H, Sumarti S, Bignami C, Griswold J, Carn S, Oppenheimer C, Lavigne F (2012) The 2010 explosive eruption of Java's Merapi volcano—A '100-year' event. J Volcanol Geotherm Res 241–242:121–135

Tanguy J-C (1994) The 1902–1905 eruptions of Montagne Pelée, Martinique: anatomy and retrospection. J Volcanol Geotherm Res 60:87–107

Tanguy J-C (2004) Rapid dome growth at Montagne Pelée during the early stages of the 1902–1905 eruption: a reconstruction from Lacroix's data. Bull Volcanol 66:615–621

Taylor GA (1958) The 1951 eruption of Mount Lamington, Papua. Austr Bur Mineral Res Geol Geophys 38:1–117

Thierry P, Jousset P, Le Cozannet G (2008) MIAVITA: mitigate and assess risk from volcanic impact on terrain and human activities. In: Abstract—IAVCEI General Assembly, 17–22 Aug 2008, Reykjavik, Iceland

Thouret J-C, Aisyah N, Jenkins SF, de Belizal E, Sulistiyani, Charbonnier S, Sayudi DS, Nandaka IGMA, Mainsant G, Solikhin A (2023) Merapi's lahars: characteristics, behaviour, monitoring, impact, hazard modelling and risk assessment. In: Gertisser R, Troll VR, Walter TR, Nandaka IGMA, Ratdomopurbo A (eds) Merapi volcano—geology, eruptive activity, and monitoring of a high-risk volcano. Springer, Berlin, Heidelberg, pp 501–552

Tilling RI (1989) Volcanic hazards and their mitigation: progress and problems. Rev Geophys 27:237–269

Trolese M, Giordano G, Komorowski J-C, Jenkins SF, Baxter PJ, Cholik N, Raditya P, Corrado S (2018) Very rapid cooling of the energetic pyroclastic density currents associated with the 5 November 2010 Merapi eruption (Indonesia). J Volcanol Geotherm Res 358:1–12

Troll VR, Deegan FM (2023) The magma plumbing system of Merapi: the petrological perspective. In: Gertisser R, Troll VR, Walter TR, Nandaka IGMA,

Ratdomopurbo A (eds) Merapi volcano—geology, eruptive activity, and monitoring of a high-risk volcano. Springer, Berlin, Heidelberg, pp 233–263

Voight B (1988) A method for prediction of volcanic eruptions. Nature 332:125–130

Voight B, Constantine EK, Siswowidjoyo S, Torley R (2000) Historical eruptions of Merapi volcano, Central Java, Indonesia, 1768–1998. J Volcanol Geotherm Res 100:69–138

Whitley S, Gertisser R, Halama R, Preece K, Troll VR, Deegan FM (2019) Crustal CO_2 contribution to subduction zone degassing recorded through calc-silicate xenoliths in arc lavas. Sci Rep 9:8803

Whitley S, Halama R, Gertisser R, Preece K, Deegan FM, Troll VR (2020). Magmatic and metasomatic effects of magma-carbonate interaction recorded in calc-silicate xenoliths from Merapi volcano (Indonesia). J Petrol 61:egaa048

Widiyantoro S, Ramdhan M, Métaxian J-P, Cummins PR, Martel C, Erdmann S, Nugraha AD, Budi-Santoso A, Laurin A, Fahmi AA (2018) Seismic imaging and petrology explain highly explosive eruptions of Merapi volcano, Indonesia. Sci Rep 8:13656